

Fast and Error-Correctable Quantum RAM

Francesco Cesa,^{1,2,3,4,*} Hannes Bernien,^{1,5,6} and Hannes Pichler^{1,2,†}

¹*Institute for Quantum Optics and Quantum Information of the Austrian Academy of Sciences, 6020 Innsbruck, Austria*

²*Institute for Theoretical Physics, University of Innsbruck, 6020 Innsbruck, Austria*

³*Department of Physics, University of Trieste, Strada Costiera 11, 34151 Trieste, Italy*

⁴*Istituto Nazionale di Fisica Nucleare, Trieste Section, Via Valerio 2, 34127 Trieste, Italy*

⁵*Institute for Experimental Physics, University of Innsbruck, 6020 Innsbruck, Austria*

⁶*Pritzker School of Molecular Engineering, University of Chicago, Chicago, IL 60637, USA*

Quantum devices can process data in a fundamentally different way than classical computers [1, 2]. To leverage this potential, many algorithms require the aid of a quantum Random Access Memory (QRAM), i.e. a module capable of efficiently loading datasets (both classical and quantum) onto the quantum processor [3]. However, a realization of this fundamental building block is still outstanding, since existing proposals [4–8] require prohibitively many resources for reliable implementations, or are not compatible with current architectures. Moreover, present approaches cannot be scaled-up, as they do not allow for efficient quantum error-correction. Here we develop a QRAM design, that enables fast and robust QRAM calls, naturally allows for fault-tolerant and error-corrected operation, and can be integrated on present hardware. Our proposal employs a special quantum resource state that is consumed during the QRAM call: we discuss how it can be assembled and processed efficiently in a dedicated module. Concretely, we provide detailed blueprints and quantitative estimations for modern neutral-atom processors [9–11], demonstrating that high-fidelity QRAM queries can be implemented at rates compatible with the fault-tolerant computational clock-time. Our work places a long missing, fundamental component of quantum computers within reach of currently available technology; this opens the door to algorithms featuring practical quantum advantage, including search or oracular problems [12–14], quantum chemistry [15] and machine learning [16].

Quantum computation (QC) promises significant algorithmic speedups for specific tasks [1, 2], fueling innovation across numerous modern technologies. Remarkable progress has been achieved in developing quantum processing units (QPUs), witnessed by increasing system sizes, improved performances, and the incorporation of quantum error-correction (QEC) [9–11, 17–28]. However, critical challenges remain: among these is the development of a quantum Random Access Memory (QRAM) [3]. This module is analogous to classical RAM, which enables fast import of data from a memory to the central processing unit (CPU). Specifically, when querying a memory location labeled by the address \mathbf{x} , the RAM responds by furnishing the corresponding databit $D_{\mathbf{x}}$. Analogously, a QRAM provides a fast quantum-mechanical interface between the QPU and datasets as in Fig. 1(a); a *quantum query* is therefore defined as

$$U_{\text{QRAM}} \left[\sum_{\mathbf{x}} \psi_{\mathbf{x}} |\mathbf{x}\rangle \otimes |0\rangle \right] = \sum_{\mathbf{x}} \psi_{\mathbf{x}} |\mathbf{x}\rangle \otimes |D_{\mathbf{x}}\rangle, \quad (1)$$

where $\psi_{\mathbf{x}}$ labels the amplitude of the computational basis state $|\mathbf{x}\rangle$ of the QPU register. The queried data $D_{\mathbf{x}}$ is written coherently onto a *bus* qubit that here is initialised in $|0\rangle$. While Eq. (1) describes a QRAM query to classical data, minimal modifications extend this to quantum memories [29]. Central to many foundational algorithms, QRAM queries are ubiquitously

present in the QC landscape, implementing e.g. ‘black-boxes’ in oracular paradigms and quantum search [12–14], and providing fast calls to complex multi-controlled gates [30, 31]; modern applications also include quantum chemistry [15, 32, 33], machine learning [16, 34] and quantum data centers [35]. More generally, a QRAM allows coherent access to pre-calculated (classical or quantum) lookup-tables, speeding up computations, e.g., in modern variations of Shor’s factoring algorithm [36].

So far, the realization of this primitive was obstructed by both theoretical and practical challenges, preventing the demonstration of many pioneering algorithms. To harness the power of QRAM, a query must be *fast* and *error-correctable*. Current approaches, e.g. the celebrated ‘bucket-brigade’ protocol [3], however necessitate to apply exponentially many non-Clifford gates *during* the query [37]; these operations are particularly hard to error-correct, demanding prohibitive space-time resources [1]. Moreover, existing proposal [4–8] are challenging to implement with present hardware: e.g., they require hybrid architectures where ‘quantum routers’ interface flying qubits (photons or phonons) with matter qubits [3, 6, 8]. Altogether, these outstanding problems not only hindered technological progress and raised debates on the feasibility of QRAMs, but also pin bold question marks on the potential of QC [38, 39].

Here, we present a novel QRAM design that is readily integrable in present large-scale processors. It allows for fast and robust quantum queries, and can be naturally combined with QEC. The key aspect is the separation of the QRAM subroutine in two parts. The first involves the preparation of a resource-state (RS) $|\Phi\rangle$, which is in-

* francesco.cesa@uibk.ac.at

† hannes.pichler@uibk.ac.at

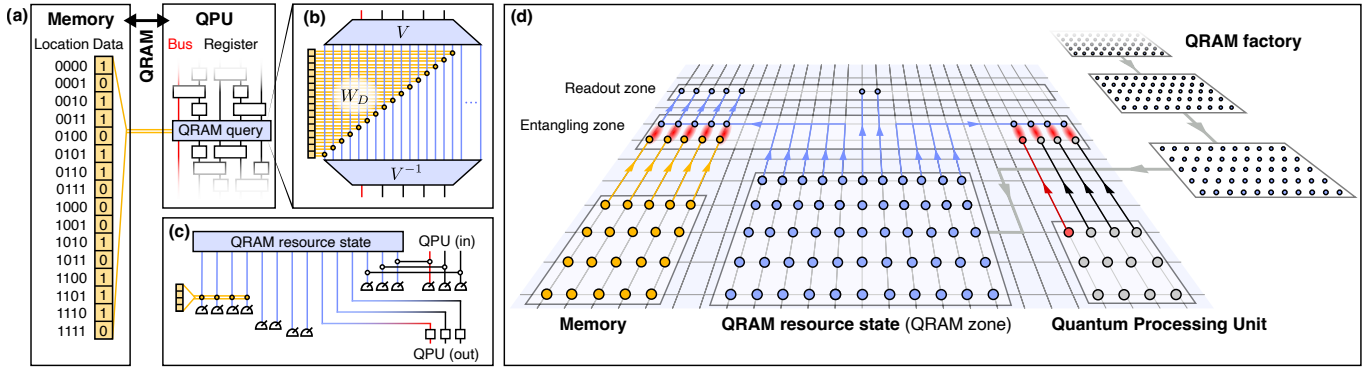


FIG. 1. **Quantum RAM.** (a) A memory stores N data bits $D_{\mathbf{x}} \in \{0, 1\}$ in locations $\mathbf{x} = (x_0, \dots, x_{\log N - 1})$. The QPU imports the data coherently according to *quantum* queries to the memory: an input state $|\psi\rangle = \sum_{\mathbf{x}} \psi_{\mathbf{x}} |\mathbf{x}\rangle$ plays the role of a quantum *address*, querying a superposition of data; the QRAM responds with the output state $\sum_{\mathbf{x}} \psi_{\mathbf{x}} |\mathbf{x}\rangle \otimes |D_{\mathbf{x}}\rangle$, with the data loaded on the bus qubit initialised in $|0\rangle$. (b) Unified sketch of fast and noise-resilient approaches according to Eq. (2). The operation V takes as input the address $|\psi\rangle$, and processes it together with $\mathcal{O}(N)$ ancillas, to provide a ‘one-hot encoded’ state which is interfaced with the memory by a *loading* operation $W_D = \otimes_{\mathbf{x}} Z_{\mathbf{x}}^{D_{\mathbf{x}}}$; finally, V^{-1} compresses back the state. (c) Our QRAM design answers to arbitrary queries with the aid of a resource-state (RS) $|\Phi\rangle$ on a set of ancillary qubits. We start by performing Bell measurements; then we load the data via single-qubit Pauli operations and measurements, retrieving the output on the unmeasured qubits. (d) We blueprint end-to-end implementations with neutral-atom processors, where physical qubits are encoded in single atoms trapped in optical tweezers. Coherent atom transport allows to inject the QRAM RS, and to interface the QPU with it. A parallel QRAM factory guarantees continuous supply of the RS via a fast and efficient generation protocol based on dynamical rearrangement. A classical memory can be stored either on classical hardware, or on atoms as in the figure (the latter configuration also allowing for quantum memories).

dependent of both the memory and the target task, and is assembled efficiently in advance at high rates; it is the resource ‘fueling’ the QRAM, and is serially assembled in a dedicated module - the QRAM factory. The second part, schematised in Fig. 1(c), implements the query by ‘consuming’ $|\Phi\rangle$ via Clifford operations and single-qubit Pauli measurements (SQPMs). This concept is inspired by measurement-based approaches to QC [40, 41] and the gate-teleportation paradigm (GT), which plays a foundational role in QEC [42]. While GT is typically only efficient for minimally non-Clifford tasks, like T-gate injection, here we exploit particular features of QRAM queries, to efficiently use GT for highly non-Clifford subroutines. Eventually, this yields a fast query protocol, which is entirely Clifford, and combines naturally with QEC. In addition, our design is intrinsically error-resilient, due to built-in mechanisms that automatically suppress faults; this results in an exponentially-enhanced fidelity, opening the door to near-term implementations.

Our QRAM approach can be implemented with any QC platform. We show that it integrates particularly well with neutral-atom arrays [9–11], where the ability to dynamically rearrange atoms [43] unlocks an efficient QRAM RS generation protocol. Moreover, atom-transport facilitates elegant QEC via transversal fault-tolerant operations [9], allowing to fully leverage the Cliffordness of our query subroutine. This motivates our design outlined in Fig. 1(d), which builds upon the ‘zoned’ architecture of modern neutral-atom processors [9–11], and complements it with a dedicated QRAM zone. The latter is continuously replenished by the parallel QRAM

factory, and supplies continuous queries to the memory. We provide quantitative analyses of this design, and show that both the query duration and the factory rate match the clock-time of the computation, thereby showcasing how our QRAM module can be readily integrated in present quantum computers.

Framework

Here, we highlight the key points of fast and noise-resilient (bucket-brigade-type) QRAMs [3] in a unified framework. We consider memories of size N , and QPU registers featuring $\log N$ qubits. In the main paradigm, Eq. (1) is executed in three steps as in Fig. 1(b),

$$U_{\text{QRAM}} = V^{-1} W_D V. \quad (2)$$

This can be read as follows: (i) A ‘one-hot encoding’ (OHE) [44, 45], discussed below, is applied via V ; (ii) The dataset D is loaded with W_D ; (iii) The OHE is inverted.

More precisely, V is a linear map that ‘expands’ the $\log N + 1$ register and bus qubits onto $2N - 1$ qubits as

$$V : |\mathbf{x}\rangle |0\rangle \xrightarrow{\text{one-hot}} |\text{OHE}(\mathbf{x})\rangle |\text{NOHE}(\mathbf{x})\rangle. \quad (3)$$

The first term, $|\text{OHE}(\mathbf{x})\rangle$, is a product state on N qubits: they are all in $|0\rangle$, except for a ‘pointer-qubit’, identified by \mathbf{x} , which is in the state $|+\rangle = (|0\rangle + |1\rangle)/\sqrt{2}$. In Fig. 2(b) we give an explicit example. The second factor, $|\text{NOHE}(\mathbf{x})\rangle$, is a $N - 1$ qubit state representing a ‘nested’ OHE of \mathbf{x} , ensuring reversibility in a noise-resilient way

(Methods). For $V|\mathbf{x}\rangle|1\rangle$ the output is similar, but the pointer qubit is flipped to $|-\rangle = (|0\rangle - |1\rangle)/\sqrt{2}$.

The loading acts on the first N qubits as $W_D = \bigotimes_{\mathbf{x}} Z_{\mathbf{x}}^{D_{\mathbf{x}}}$, leaving the last $N - 1$ qubits invariant; thus, during step (ii) the pointer is flipped as $|+\rangle \rightarrow |-\rangle$ if $D_{\mathbf{x}} = 1$ (since $Z|\pm\rangle = |\mp\rangle$).

Finally, V^{-1} inverts the OHE:

$$V^{-1}W_D|\text{OHE}(\mathbf{x})\rangle|\text{NOHE}(\mathbf{x})\rangle = |\mathbf{x}\rangle|D_{\mathbf{x}}\rangle, \quad (4)$$

retrieving the data on the QPU.

Following this recipe, in principle Eq. (1) can be realised with $\mathcal{O}(\log N)$ circuit-depth [3], and with a remarkable $\mathcal{O}(\text{polylog}N)$ infidelity scaling [37]. However, the crucial challenge is that V requires $\mathcal{O}(N)$ long-range non-Clifford gates on $\mathcal{O}(N)$ ancillary qubits. Executing and error-correcting them during a query incurs significant costs, obstructing efficiency and speed [46]. Moreover, when embedded on locally-connected processors, due to space-time constraints, typically the infidelity deteriorates to $\mathcal{O}(\text{poly}N)$, making noisy queries infeasible and demanding prohibitive resources for QEC.

Below we develop a novel approach to overcome these challenges. We show that, with the aid of a RS $|\Phi\rangle$, Eq. (2) can be implemented via Clifford operations, thereby allowing for efficient QEC. Furthermore, we present a method for preparing $|\Phi\rangle$ at high rates; for neutral-atom arrays, we show that this overcomes the mentioned constraints, leading to the desired $\mathcal{O}(\text{polylog}N)$ infidelity scaling.

Clifford QRAM query

Our construction is based on the observation that Eq. (2) can be generalised and rewritten as

$$U_{\text{QRAM}} = P_m^{-1}V^{-1}W_D(\mathbf{m})VP_m, \quad (5)$$

where P_m is an arbitrary Pauli operator (labeled by \mathbf{m}) acting on the QPU register. Here, $W_D(\mathbf{m}) = \pi_{\mathbf{m}}W_D\pi_{\mathbf{m}}^{-1}$, and $\pi_{\mathbf{m}}$ is a simple permutation of the OHE qubits. Importantly, this holds true for *any* choice of Pauli operator P_m . In our construction, \mathbf{m} will be intrinsically random. This rewriting allows us to design a modified query protocol comprising the following three Clifford steps.

Our step (i) is shown in Fig. 2(a): a protocol similar to GT [42, 47] applies VP_m in Eq. (5) to the input QPU state $|\psi\rangle$. As in standard GT, we employ the preassembled RS $|\Phi^{(1)}\rangle \equiv (\mathbb{1} \otimes V)|\Psi\rangle^{\otimes 1+\log N}$ where $|\Psi\rangle = \frac{1}{\sqrt{2}}(|00\rangle + |11\rangle)$. Performing $\log N$ Bell measurements (BMs) between the RS and the input, results in a state $VP_m|\psi\rangle$, where \mathbf{m} is random and determined by the BM's outcome. Crucially, this is now Clifford [48].

Step (ii) implements $W_D(\mathbf{m})$, which depends on the BM outcomes in step (i). This is achieved efficiently by a simple adaptation of W_D in classical processing. Indeed, as shown in Fig. 2(b), $\pi_{\mathbf{m}}$ is a highly structured permutation of the pointers, which we implement

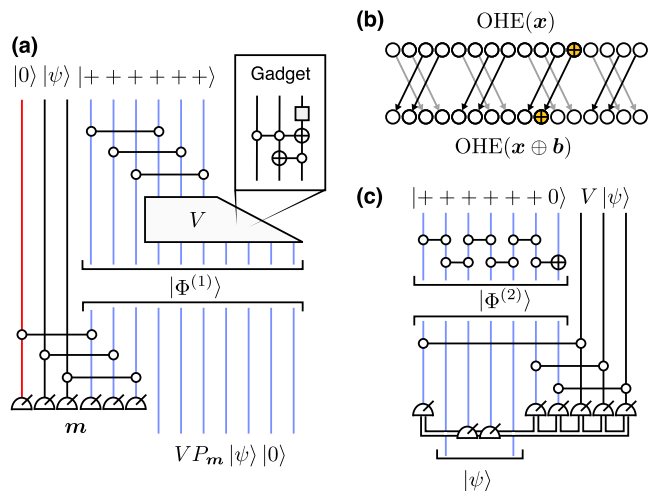


FIG. 2. (a) Gate-teleportation for the random OHE VP_m : we first prepare the resource-state (RS) $|\Phi^{(1)}\rangle$, and then apply Bell measurements (BMs) with the input $|\psi\rangle$. The box highlights the fundamental gadget used for V . (b) The OHE of a bit-string \mathbf{x} ; empty and yellow-crossed circles represent $|0\rangle$ and $|+\rangle$ respectively. For generalised OHEs VP_m , the locations are permuted. Here, $N = 16$, $\mathbf{x} = (1, 1, 0, 1)$ and $\mathbf{b} = (0, 1, 0, 0)$. (c) Clifford implementation of V^{-1} (for $N = 2$). We pre-assemble a stabiliser RS $|\Phi^{(2)}\rangle$ via a 1D Clifford circuit C . The input is then entangled with $|\Phi^{(2)}\rangle$; then, SQPMs enable the inversion. The first SQPMs are in the X basis; in the second layer of SQPMs we choose either the X or the Z basis depending on the previous outcomes.

as $W_D(\mathbf{m}) = \bigotimes_{\mathbf{x}} Z_{\mathbf{x}}^{D_{\mathbf{x} \oplus \mathbf{b}}}$, with \mathbf{b} determined by \mathbf{m} .

For step (iii), we again use a RS to realize $P_m^{-1}V^{-1}$ in Eq. (5) with Clifford operations. Since P_m is a Pauli operator, we only need to discuss V^{-1} . We first note that V can be constructed by iterating the circuit element (gadget) in Fig. 2(a). Crucially, even though this primitive is non-Clifford, in Fig. 2(c) we invert it with Clifford operations and SQPMs: this is possible because we only require inversion on the image of V , which is an exponentially smaller subspace [see Eq. (3) and Methods]. To efficiently integrate this inversion with the results above, we develop it within a measurement-based approach [40, 41]. Specifically, we find a *stabiliser* RS $|\Phi^{(2)}\rangle$ with the following property (Methods): after entangling any state $|\Xi\rangle = V|\psi\rangle$ with $|\Phi^{(2)}\rangle$ via BMs, $\mathcal{O}(\log N)$ layers of *adaptive* SQPMs extract the desired output $V^{-1}|\Xi\rangle$.

Combining these results, we thus implement Eq. (5) via Clifford operations, given the RS $|\Phi^{(1)}\rangle \otimes |\Phi^{(2)}\rangle$. Finally, we compress this in a unique RS $|\Phi\rangle$ using standard Clifford techniques (Methods). This RS is assembled prior to the query in the QRAM factory discussed below, and stored in the QRAM zone until a query is called.

The resulting compact query protocol is detailed in Fig. 3. This is very efficient especially under the viewpoint of QEC, as it only requires Clifford operations during the online computation. The query runtime $T_{\text{query}} \simeq 2\tau \log N$, corresponding to half the duration in previous

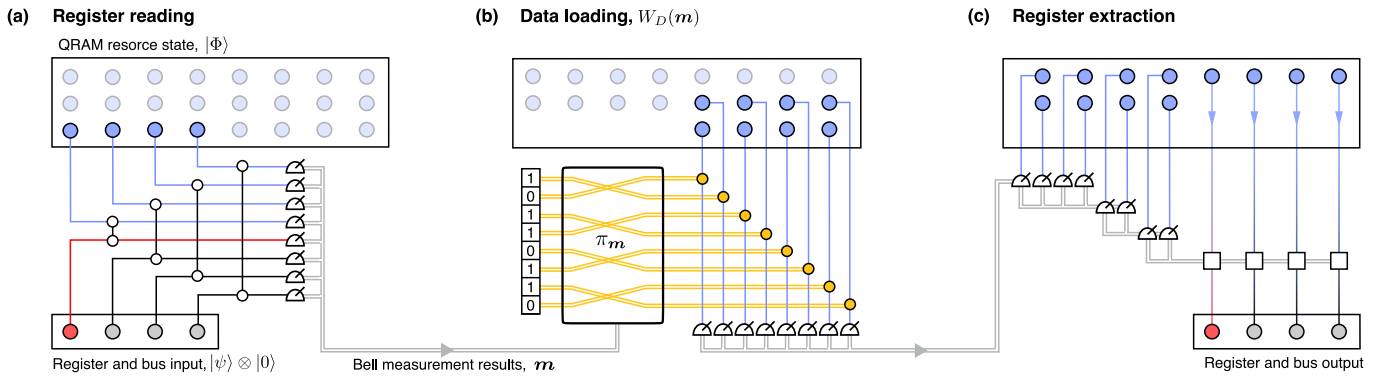


FIG. 3. **Clifford query.** (a) The QPU register is initially in the state $|\psi\rangle$ on $\log N$ qubits (grey), while the RS $|\Phi\rangle$ is stored on $\mathcal{O}(N)$ ancillas (blue); here we initialise the bus in $|0\rangle$ (red). In the first step, of depth $\mathcal{O}(1)$, we perform BMs between the QPU register and bus, and a subset of the RS qubits. The outcome of these measurements is denoted by \mathbf{m} and used in the next step. (b) In the second step, of depth $\mathcal{O}(1)$, the data (yellow) is loaded via conditional Clifford gates, on another subset of the QRAM ancillas. Depending on \mathbf{m} a permutation of the data according to the function f (see main text) is performed prior to the gate application to achieve the correct data loading operation, $W_D(\mathbf{m})$. The involved qubits are then measured in the X basis (bottom). (c) In the last step, of depth $\mathcal{O}(\log N)$, almost all the ancillary qubits, except $\log N + 1$, are measured in adaptive Pauli bases (X or Z); the answer to the query is retrieved on the remaining unmeasured qubits, after a final Pauli correction operation. Overall, the query is executed as Eq. (5) in $\mathcal{O}(\log N)$ depth, including $\log N$ BMs and $\mathcal{O}(N)$ SQPMs.

proposals [37], is dominated by the mid-circuit readout time τ , which also sets the computational clock-time due to the continuous syndrome extraction.

QRAM factory

We envision the assembly of $|\Phi\rangle$ in a dedicated QRAM factory, which continuously replenishes the QRAM zone after each query. In Fig. 4(a) we illustrate the factory scheme (see also Methods). It starts with the preparation of $\mathcal{O}(N)$ Bell pairs. This is followed by a reconfiguration of the system layout, that distributes the entanglement such that all subsequent operations can be realised in a *local* way with a circuit of depth $2 \log N$. These operations include $2N - \log N - 2$ Toffoli gates, which can be realised by the injection of $4 T$ -states per Toffoli gate [49].

An important quantity is the rate T_Φ of the QRAM factory, in particular in comparison with the query runtime T_{query} . In neutral-atom processors [9–11] this interplay is particularly favorable, as coherent dynamical rearrangement of physical atoms via optical tweezers [43] allows for a native implementation of the reconfiguration step [see Fig. 4(b)]. Specifically, in Methods we design a fast rearrangement subroutine, resulting in a factory runtime

$$T_\Phi \lesssim 3\sqrt{6}TN^{1/4} + 2\tau \log N; \quad (6)$$

here, T is the time required for moving an atom across the minimal trap distance, and again τ is the mid-circuit measurement time. Thus, the first term in Eq. (6) is related to the rearrangement, and the second one to the SQPMs. Considering current experiments [43], in our estimations we set $\tau \simeq 500\mu\text{s}$ and $T \simeq 33\mu\text{s}$. With these parameters, T_Φ is comparable to T_{query} , as the rearrangement time remains negligible up to $N \simeq 2^{24}$ (correspond-

ing to $\simeq 2\text{MB}$ of memory), which is much larger than current system sizes of single processors [50]. Quantitatively, even for 1kB of memory we find $T_{\text{query}} \simeq 13\text{ms}$ and a factory rate $1/T_\Phi \simeq 0.1\text{kHz}$, wherein only $\simeq 13\%$ of the time is spent on atom rearrangement. Since $T_\Phi \simeq T_{\text{query}}$, we can parallelise a query with the preparation of a new copy of $|\Phi\rangle$ for the next query, resulting in an efficient parallelised cycle, not adding substantial runtime.

Noise-resilience and error-correction

The impact of errors and decoherence has long been considered crucially problematic for QRAMs [37, 38, 46], not only for near-term implementations, but also for error-corrected, fault-tolerant (FT) processors. Importantly, our approach incorporates a built-in noise resilience, ensuring a favorable $\mathcal{O}(\log^\alpha N)$ error-scaling. Building upon the guidelines of the pivotal bucket-brigade proposal [3, 37], we achieve this via the nested OHE in Eq. (3), discussed in the Methods, which strongly constrains the error propagation. We certify this behavior in Fig. 4(c), where we calculate numerically the query fidelity F_{QRAM} for different realistic error models. In Figs. 4(d,e) we report the achievable performances given various two-qubit gate errors. To estimate the near-term potential (without QEC), we note that with error-rates $\varepsilon \sim 10^{-4}$, memories of size $N \gtrsim 512$ can be queried with fidelity above 50%. We remark that Z -biased error regimes feature a quadratic fidelity improvement, allowing to reach the 99% fidelity range for $N \simeq 512$. This is particularly relevant for neutral-atoms, where recent experiments [17, 51] have demonstrated conversion of two-qubit gate errors to Z -biased noise [52–54].

Concerning QEC, our design provides dramatic sim-

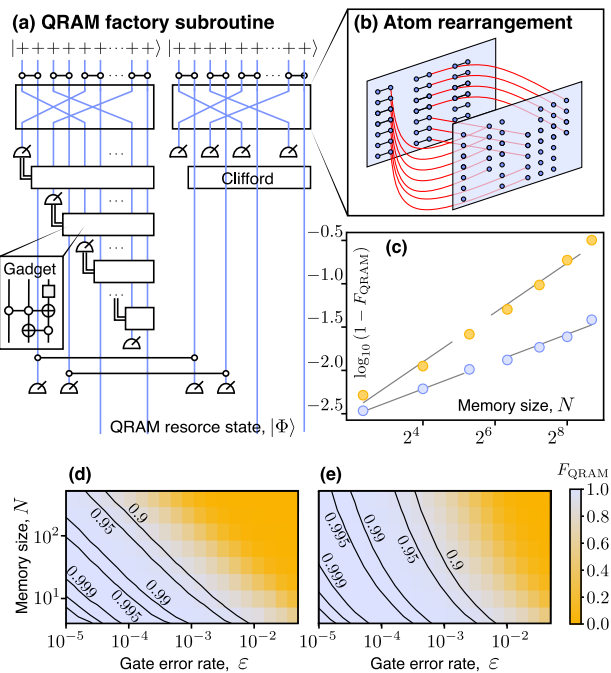


FIG. 4. (a) High-rate protocol for preparing $|\Phi\rangle$ in the QRAM factory. We first prepare $\mathcal{O}(N)$ Bell pairs, and then reconfigure the system layout via $\mathcal{O}(1)$ dynamical rearrangements. Next, we prepare the RSs $|\Phi^{(1)}\rangle$ (by iterating the gadget in the inset) and $|\Phi^{(2)}\rangle$ (via simple Clifford gates). Both, these subroutines also include adaptive Pauli gates and measurements. Finally, we perform BMs to merge the two in $|\Phi\rangle$, which is also achieved via local operations. (b) Specializing on neutral-atoms, we design a fast and efficient dynamical-rearrangement subroutine for the reconfiguration step, which only requires $\mathcal{O}(1)$ global atom motions. (c) Scaling of the query infidelity (defined in Methods); we consider a continuous depolarization model (yellow), as well as Z -biased noise (blue). The logarithmic plot highlights the favorable scaling: assuming $1 - F_{\text{QRAM}} \sim \log^\alpha N$, we extract the dominating exponents as $\alpha \simeq 3.8$ and $\alpha \simeq 1.9$ respectively. (d) Dependence of the query fidelity on the operational error for random Pauli errors, and (e) Z -biased noise.

plications, making FT QRAMs feasible on current processors. The first key is the noise-resilience above, which reduces exponentially the resources for QEC. The second key is that *all* operations in our query protocol are Clifford, allowing for FT *transversal* implementations in many important schemes, including the surface and CSS codes [1]. It follows that also a FT query proceeds via SQPMs only, by leveraging measurement-based QEC [55] e.g. within foliated [56] or fusion-based [54, 57] schemes. Similarly to Knill-type QEC [58], this can be understood by noting that in standard QEC codes, logical Pauli operators are transversal, and the parity-check observables are products of physical Pauli operators. Since our protocol is based on destructive SQPMs, even within error-corrected computations we can simply measure the physical qubits individually: the obtained results not only contain the logical measurement outcome, but also the

syndrome snapshots. Leveraging these facts together, the entire query can be executed by simply parallelising all the operations we would apply to physical qubits, to logical blocks. In practice, this is achieved elegantly with neutral atoms by physically interfacing the logical blocks via atom transport, as recently demonstrated [9, 10].

Discussion and outlook

Our results mark a major step forward in the development of a QRAM, by designing the first fast and error-correctable blueprint that can be integrated in current large-scale processors. Most importantly, our design is fully compatible with standard QEC, overcoming the crucial obstacles towards FT implementations of QRAM that have long concerned the community [37, 38].

Our proposed QRAM module is the result of an effective co-design, incorporating novel insights from quantum information as well as crucial inputs from modern atomic physics experiments. For instance, we have shown how generalised GT, in combination with measurement-based methods, allow to outsource the complexity of QRAM queries to an independent factory, where dynamical atom rearrangement is harnessed to allow for efficient operation. We elaborate more in depth on this synergy in Methods, where we present a detailed neutral-atom blueprint. We note that our protocol may be adapted to trapped-ion processors, which have also developed the ability to shuttle physical qubits [59]. Moreover, the general ideas behind our proposal can find application also in other platforms, including superconducting [24] or photonic [28] systems.

The deployment of a QRAM places many pioneering algorithms, whose end-to-end demonstration is still outstanding, in reach for present experiments. Paradigmatic examples include e.g. Grover search and oracle-based tasks [12–14]; demonstrating these algorithms would allow the assessment of the predicted advantage of QC in ‘black-box query models’ on real hardware [1]. More generally, QRAM benefits many quantum algorithms promising exponential speedups, with known applications ranging from factoring [36] to quantum chemistry [15, 32, 33], matrix inversion and quantum machine learning [16, 34]. Exploiting queries to a QRAM for such tasks will be possible on fault-tolerant processors by leveraging our manifestly error-correctable design in combination with recently demonstrated progresses in experimental QEC [9, 10, 22–27]. However, owing to its built-in noise-resilience, our QRAM prototype could be successfully employed even without QEC, e.g., for small-scale quantum chemistry algorithms [15], on noisy intermediate-sized quantum devices [60].

ACKNOWLEDGEMENTS

We thank Dolev Bluvstein, Hans Briegel, Vittorio Giovannetti, Mikhail Lukin and Peter Zoller for valuable discussions, and Gabriele Calliari for precious support with the numerical simulations. This work is supported by the ERC Starting grant QARA (Grant No. 101041435), the Horizon Europe programme

HORIZON-CL4-2022-QUANTUM02-SGA via the project 101113690 (PASQuanS2.1) and by the Austrian Science Fund (FWF) (Grant No. DOI 10.55776/COE1). HB gratefully acknowledges funding from the Air Force Office of Scientific Research (Grant No. FA9550-21-1-0209), the Office of Naval Research (Grant No. N00014-23-1-2540), and the Army Research Office (Grant no. W911NF2410388).

-
- [1] M. A. Nielsen and I. L. Chuang, *Quantum computation and quantum information* (Cambridge university press, 2010).
- [2] A. M. Dalgell, S. McArdle, M. Berta, P. Bienias, C.-F. Chen, A. Gilyén, C. T. Hann, M. J. Kastoryano, E. T. Khabiboulline, A. Kubica, G. Salton, S. Wang, and F. G. S. L. Brandão, (2023), [arXiv:2310.03011 \[quant-ph\]](https://arxiv.org/abs/2310.03011).
- [3] V. Giovannetti, S. Lloyd, and L. Maccone, *Phys. Rev. Lett.* **100**, 160501 (2008).
- [4] V. Giovannetti, S. Lloyd, and L. Maccone, *Phys. Rev. A* **78**, 052310 (2008).
- [5] C. T. Hann, C.-L. Zou, Y. Zhang, Y. Chu, R. J. Schoelkopf, S. M. Girvin, and L. Jiang, *Phys. Rev. Lett.* **123**, 250501 (2019).
- [6] K. C. Chen, W. Dai, C. Errando-Herranz, S. Lloyd, and D. Englund, *PRX Quantum* **2**, 030319 (2021).
- [7] D. Weiss, S. Puri, and S. Girvin, *PRX Quantum* **5**, 020312 (2024).
- [8] Z. Wang, H. Qiao, A. N. Cleland, and L. Jiang, (2024), [arXiv:2411.00719 \[quant-ph\]](https://arxiv.org/abs/2411.00719).
- [9] D. Bluvstein, S. J. Evered, A. A. Geim, S. H. Li, H. Zhou, T. Manovitz, S. Ebadi, M. Cain, M. Kalinowski, D. Hangleiter, J. P. Bonilla Ataides, N. Maskara, I. Cong, X. Gao, P. Sales Rodriguez, T. Karolyshyn, G. Semeghini, M. J. Gullans, M. Greiner, V. Vuletić, and M. D. Lukin, *Nature* **626**, 58 (2023).
- [10] B. W. Reichardt, A. Paetznick, D. Aasen, I. Basov, J. M. Bello-Rivas, P. Bonderson, R. Chao, W. van Dam, M. B. Hastings, A. Paz, M. P. da Silva, A. Sundaram, K. M. Svore, A. Vashillo, Z. Wang, M. Zanner, W. B. Cairncross, C.-A. Chen, D. Crow, H. Kim, J. M. Kindem, J. King, M. McDonald, M. A. Norcia, A. Ryou, M. Stone, L. Wadleigh, K. Barnes, P. Battaglino, T. C. Bohdanowicz, G. Booth, A. Brown, M. O. Brown, K. Cassella, R. Coxe, J. M. Epstein, M. Feldkamp, C. Griger, E. Halperin, A. Heinz, F. Hummel, M. Jaffe, A. M. W. Jones, E. Kapit, K. Kotru, J. Lauigan, M. Li, J. Marjanovic, E. Megidish, M. Meredith, R. Morshead, J. A. Muniz, S. Narayanaswami, C. Nishiguchi, T. Paule, K. A. Pawlak, K. L. Pudenz, D. R. Pérez, J. Simon, A. Smull, D. Stack, M. Urbanek, R. J. M. van de Veerdonk, Z. Vendeiro, R. T. Weverka, T. Wilkason, T.-Y. Wu, X. Xie, E. Zaly-Geller, X. Zhang, and B. J. Bloom, (2024), [arXiv:2411.11822 \[quant-ph\]](https://arxiv.org/abs/2411.11822).
- [11] A. G. Radnaev, W. C. Chung, D. C. Cole, D. Mason, T. G. Ballance, M. J. Bedalov, D. A. Belknap, M. R. Berman, M. Blakely, I. L. Bloomfield, P. D. Buttler, C. Campbell, A. Chopinaud, E. Copenhagen, M. K. Dawes, S. Y. Eubanks, A. J. Friss, D. M. Garcia, J. Gilbert, M. Gillette, P. Goiporia, P. Gokhale, J. Goldwin, D. Goodwin, T. M. Graham, C. Guttormsson, G. T. Hickman, L. Hurlley, M. Iliev, E. B. Jones, R. A. Jones, K. W. Kuper, T. B. Lewis, M. T. Lichtman, F. Majdeteimouri, J. J. Mason, J. K. McMaster, J. A. Miles, P. T. Mitchell, J. D. Murphree, N. A. Neff-Mallon, T. Oh, V. Omole, C. P. Simon, N. Pederson, M. A. Perlin, A. Reiter, R. Rines, P. Romlow, A. M. Scott, D. Stiefvater, J. R. Tanner, A. K. Tucker, I. V. Vinogradov, M. L. Warter, M. Yeo, M. Saffman, and T. W. Noel, (2025), [arXiv:2408.08288 \[quant-ph\]](https://arxiv.org/abs/2408.08288).
- [12] D. Deutsch and R. Jozsa, *Proceedings of the Royal Society of London. Series A: Mathematical and Physical Sciences* **439**, 553 (1992).
- [13] E. Bernstein and U. Vazirani, in *Proceedings of the twenty-fifth annual ACM symposium on Theory of computing* (1993) pp. 11–20.
- [14] L. K. Grover, in *Proceedings of the twenty-eighth annual ACM symposium on Theory of computing* (1996) pp. 212–219.
- [15] Y. Cao, J. Romero, J. P. Olson, M. Degroote, P. D. Johnson, M. Kieferová, I. D. Kivlichan, T. Menke, B. Peropadre, N. P. D. Sawaya, S. Sim, L. Veis, and A. Aspuru-Guzik, *Chemical Reviews* **119**, 10856–10915 (2019).
- [16] J. Biamonte, P. Wittek, N. Pancotti, P. Rebentrost, N. Wiebe, and S. Lloyd, *Nature* **549**, 195 (2017).
- [17] S. Ma, G. Liu, P. Peng, B. Zhang, S. Jandura, J. Claes, A. P. Burgers, G. Pupillo, S. Puri, and J. D. Thompson, *Nature* **622**, 279 (2023).
- [18] R. Finkelstein, R. B.-S. Tsai, X. Sun, P. Scholl, S. Dirckci, T. Gefen, J. Choi, A. L. Shaw, and M. Endres, *Nature* **634**, 321–327 (2024).
- [19] A. Cao, W. J. Eckner, T. Lukin Yelin, A. W. Young, S. Jandura, L. Yan, K. Kim, G. Pupillo, J. Ye, N. Darkwah Oppong, and A. M. Kaufman, *Nature* **634**, 315–320 (2024).
- [20] S. A. Moses, C. H. Baldwin, M. S. Allman, R. Ancona, L. Ascarrunz, C. Barnes, J. Bartolotta, B. Bjork, P. Blanchard, M. Bohn, J. G. Bohnet, N. C. Brown, N. Q. Burdick, W. C. Burton, S. L. Campbell, J. P. Campora, C. Carron, J. Chambers, J. W. Chan, Y. H. Chen, A. Chernoguzov, E. Chertkov, J. Colina, J. P. Curtis, R. Daniel, M. DeCross, D. Deen, C. Delaney, J. M. Dreiling, C. T. Ertsgaard, J. Esposito, B. Estey, M. Fabrikant, C. Figgatt, C. Foltz, M. Foss-Feig, D. Francois, J. P. Gaebler, T. M. Gatterman, C. N. Gilbreth, J. Giles, E. Glynn, A. Hall, A. M. Hankin, A. Hansen, D. Hayes, B. Higashi, I. M. Hoffman, B. Horning, J. J. Hout, R. Jacobs, J. Johansen, L. Jones, J. Karcz, T. Klein, P. Lauria, P. Lee, D. Liefer, S. T. Lu, D. Luchetti, C. Lytle, A. Malm, M. Matheny, B. Mathewson, K. Mayer, D. B. Miller, M. Mills, B. Neyenhuis, L. Nugent, S. Olson, J. Parks, G. N. Price, Z. Price,

- M. Pugh, A. Ransford, A. P. Reed, C. Roman, M. Rowe, C. Ryan-Anderson, S. Sanders, J. Sedlacek, P. Shevchuk, P. Siegfried, T. Skripka, B. Spaun, R. T. Sprenkle, R. P. Stutz, M. Swallows, R. I. Tobey, A. Tran, T. Tran, E. Vogt, C. Volin, J. Walker, A. M. Zolot, and J. M. Pino, *Phys. Rev. X* **13**, 041052 (2023).
- [21] J. F. Marques, B. M. Varbanov, M. S. Moreira, H. Ali, N. Muthusubramanian, C. Zachariadis, F. Battistel, M. Beekman, N. Haider, W. Vlothuizen, A. Bruno, B. M. Terhal, and L. DiCarlo, *Nature Physics* **18**, 80 (2021).
- [22] S. Krinner, N. Lacroix, A. Remm, A. Di Paolo, E. Genois, C. Leroux, C. Hellings, S. Lazar, F. Swiadek, J. Herrmann, G. J. Norris, C. K. Andersen, M. Müller, A. Blais, C. Eichler, and A. Wallraff, *Nature* **605**, 669 (2022).
- [23] Google and Collaborators, *Nature* **614**, 676 (2023).
- [24] Google and Collaborators, *Nature* **638**, 920 (2025).
- [25] L. Egan, D. M. Debroy, C. Noel, A. Risinger, D. Zhu, D. Biswas, M. Newman, M. Li, K. R. Brown, M. Cetina, and C. Monroe, *Nature* **598**, 281 (2021).
- [26] L. Postler, S. Heussen, I. Pogorelov, M. Rispler, T. Feldker, M. Meth, C. D. Marciniak, R. Stricker, M. Ringbauer, R. Blatt, P. Schindler, M. Müller, and T. Monz, *Nature* **605**, 675 (2022).
- [27] A. Paetznick, M. P. da Silva, C. Ryan-Anderson, J. M. Bello-Rivas, J. P. C. III, A. Chernoguzov, J. M. Dreiling, C. Foltz, F. Frachon, J. P. Gaebler, T. M. Gatterman, L. Grans-Samuelsson, D. Gresh, D. Hayes, N. Hewitt, C. Holliman, C. V. Horst, J. Johansen, D. Lucchetti, Y. Matsuoka, M. Mills, S. A. Moses, B. Neyenhuis, A. Paz, J. Pino, P. Siegfried, A. Sundaram, D. Tom, S. J. Wernli, M. Zanner, R. P. Stutz, and K. M. Svore, (2024), [arXiv:2404.02280](https://arxiv.org/abs/2404.02280) [quant-ph].
- [28] Xanadu and Collaborators, *Nature* **638**, 912 (2025).
- [29] See Supplemental Material.
- [30] P. A. Ivanov, E. S. Kyoseva, and N. V. Vitanov, *Phys. Rev. A* **74**, 022323 (2006).
- [31] G. H. Low, V. Kliuchnikov, and L. Schaeffer, *Quantum* **8**, 1375 (2024).
- [32] D. W. Berry, A. M. Childs, R. Cleve, R. Kothari, and R. D. Somma, *Phys. Rev. Lett.* **114**, 090502 (2015).
- [33] R. Babbush, C. Gidney, D. W. Berry, N. Wiebe, J. McClean, A. Paler, A. Fowler, and H. Neven, *Phys. Rev. X* **8**, 041015 (2018).
- [34] A. W. Harrow, A. Hassidim, and S. Lloyd, *Phys. Rev. Lett.* **103**, 150502 (2009).
- [35] J. Liu, C. T. Hann, and L. Jiang, *Phys. Rev. A* **108**, 032610 (2023).
- [36] C. Gidney and M. Ekerå, *Quantum* **5**, 433 (2021).
- [37] C. T. Hann, G. Lee, S. Girvin, and L. Jiang, *PRX Quantum* **2**, 020311 (2021).
- [38] S. Aaronson, *Nature Physics* **11**, 291 (2015).
- [39] S. Jaques and A. G. Rattew, (2023), [arXiv:2305.10310](https://arxiv.org/abs/2305.10310) [quant-ph].
- [40] R. Raussendorf and H. J. Briegel, *Phys. Rev. Lett.* **86**, 5188 (2001).
- [41] H. J. Briegel, D. E. Browne, W. Dür, R. Raussendorf, and M. Van den Nest, *Nature Physics* **5**, 19 (2009).
- [42] D. Gottesman and I. L. Chuang, *Nature* **402**, 390 (1999).
- [43] D. Bluvstein, H. Levine, G. Semeghini, T. T. Wang, S. Ebadi, M. Kalinowski, A. Keesling, N. Maskara, H. Pichler, M. Greiner, V. Vuletić, and M. D. Lukin, *Nature* **604**, 451 (2022).
- [44] D. Harris and S. Harris, *Digital Design and Computer Architecture*, 2nd ed. (Morgan Kaufmann, San Francisco, Calif., 2012) p. 129.
- [45] Y. Bengio, I. Goodfellow, and A. Courville, *Deep learning*, Vol. 1 (MIT press Cambridge, MA, USA, 2017).
- [46] O. Di Matteo, V. Gheorghiu, and M. Mosca, *IEEE Transactions on Quantum Engineering* **1**, 1 (2020).
- [47] M. A. Nielsen and I. L. Chuang, *Phys. Rev. Lett.* **79**, 321 (1997).
- [48] We note that this contrasts with typical GT, where typically highly non-Clifford byproducts must be applied to make the protocol deterministic (see Methods).
- [49] C. Jones, *Phys. Rev. A* **87**, 022328 (2013).
- [50] H. J. Manetsch, G. Nomura, E. Bataille, K. H. Leung, X. Lv, and M. Endres, (2024), [arXiv:2403.12021](https://arxiv.org/abs/2403.12021) [quant-ph].
- [51] P. Scholl, A. L. Shaw, R. B.-S. Tsai, R. Finkelstein, J. Choi, and M. Endres, *Nature* **622**, 273–278 (2023).
- [52] I. Cong, H. Levine, A. Keesling, D. Bluvstein, S.-T. Wang, and M. D. Lukin, *Phys. Rev. X* **12**, 021049 (2022).
- [53] Y. Wu, S. Kolkowitz, S. Puri, and J. D. Thompson, *Nature Communications* **13**, 4657 (2022).
- [54] K. Sahay, J. Jin, J. Claes, J. D. Thompson, and S. Puri, *Phys. Rev. X* **13**, 041013 (2023).
- [55] R. Raussendorf, J. Harrington, and K. Goyal, *Annals of Physics* **321**, 2242–2270 (2006).
- [56] A. Bolt, G. Duclos-Cianci, D. Poulin, and T. M. Stace, *Phys. Rev. Lett.* **117**, 070501 (2016).
- [57] K. Sahay, J. Claes, and S. Puri, *Phys. Rev. Lett.* **131**, 120604 (2023).
- [58] E. Knill, *Nature* **434**, 39 (2005).
- [59] J. M. Pino, J. M. Dreiling, C. Figgatt, J. P. Gaebler, S. A. Moses, M. S. Allman, C. H. Baldwin, M. Foss-Feig, D. Hayes, K. Mayer, C. Ryan-Anderson, and B. Neyenhuis, *Nature* **592**, 209 (2021).
- [60] J. Preskill, *Quantum* **2**, 79 (2018).
- [61] D. Gottesman, *Phys. Rev. A* **57**, 127 (1998).
- [62] B. Eastin and E. Knill, *Phys. Rev. Lett.* **102**, 110502 (2009).
- [63] A. R. Calderbank and P. W. Shor, *Phys. Rev. A* **54**, 1098 (1996).
- [64] A. Steane, *Proc. R. Soc. Lond. A* **452**, 2551 (1996).
- [65] H. Bombin and M. A. Martin-Delgado, *Phys. Rev. Lett.* **97**, 180501 (2006).
- [66] A. Kitaev, *Annals of Physics* **303**, 2–30 (2003).
- [67] B. Eastin, *Phys. Rev. A* **87**, 032321 (2013).
- [68] J. Haah and M. B. Hastings, *Quantum* **2**, 71 (2018).
- [69] S. Bravyi and A. Kitaev, *Phys. Rev. A* **71**, 022316 (2005).
- [70] S. Bravyi and J. Haah, *Phys. Rev. A* **86**, 052329 (2012).
- [71] P. W. Shor, in *Proceedings of 37th conference on foundations of computer science (IEEE, 1996)* pp. 56–65.
- [72] S. J. Evered, D. Bluvstein, M. Kalinowski, S. Ebadi, T. Manovitz, H. Zhou, S. H. Li, A. A. Geim, T. T. Wang, N. Maskara, H. Levine, G. Semeghini, M. Greiner, V. Vuletić, and M. D. Lukin, *Nature* **622**, 268 (2023).
- [73] K. Singh, C. E. Bradley, S. Anand, V. Ramesh, R. White, and H. Bernien, *Science* **380**, 1265 (2023).
- [74] M. A. Norcia, W. B. Cairncross, K. Barnes, P. Battaglino, A. Brown, M. O. Brown, K. Cassella, C.-A. Chen, R. Coxe, D. Crow, J. Epstein, C. Griger, A. M. W. Jones, H. Kim, J. M. Kindem, J. King, S. S. Kondov, K. Kotru, J. Lauigan, M. Li, M. Lu, E. Megidish, J. Marjanovic, M. McDonald, T. Mittiga, J. A. Muniz, S. Narayanaswami, C. Nishiguchi, R. Notermans, T. Paule, K. A. Pawlak, L. S. Peng, A. Ryou, A. Smull, D. Stack, M. Stone, A. Sucić,

- M. Urbanek, R. J. M. van de Veerdonk, Z. Vendeiro, T. Wilkason, T.-Y. Wu, X. Xie, X. Zhang, and B. J. Bloom, *Phys. Rev. X* **13**, 041034 (2023).
- [75] J. W. Lis, A. Senoo, W. F. McGrew, F. Rönchen, A. Jenkins, and A. M. Kaufman, *Phys. Rev. X* **13**, 041035 (2023).
- [76] T. M. Graham, L. Phuttitarn, R. Chinnarasu, Y. Song, C. Poole, K. Jooya, J. Scott, A. Scott, P. Eichler, and M. Saffman, *Phys. Rev. X* **13**, 041051 (2023).
- [77] D. B. Tan, D. Bluvstein, M. D. Lukin, and J. Cong, *Quantum* **8**, 1281 (2024).

METHODS

Nested one-hot encoding

Let $\mathbf{x} = (x_0, \dots, x_{\log N - 1}) \in \{0, 1\}^{\log N}$ be a classical address, and for $K < \log N$ define the 2^K -bit string $\mathbf{ohe}^{(K)}(\mathbf{x})$ such that for $\alpha = 0, \dots, 2^K - 1$ the components read $\mathbf{ohe}_\alpha^{(K)}(\mathbf{x}) = x_K \delta_{\alpha, \mu(x_0, \dots, x_{K-1})}$, where for any bitstring \mathbf{z} we set $\mu(\mathbf{z}) = \sum_j x_j 2^j$. For instance, if $\mathbf{x} = (0, 1, 1, x_3, x_4, \dots)$, then $\mathbf{ohe}^{(3)}(\mathbf{x}) = (0, 0, 0, 0, 0, 0, x_3, 0)$. Then, the nested one-hot encoding (NOHE) of \mathbf{x} is defined as

$$\text{NOHE}(\mathbf{x}) = \left(\mathbf{ohe}^{(0)}(\mathbf{x}), \dots, \mathbf{ohe}^{(\log N - 1)}(\mathbf{x}) \right); \quad (7)$$

it thus comprises $N - 1$ bits.

We generalize this to the quantum domain by linearity: for any $\log N$ qubit state $|\psi\rangle = \sum_{\mathbf{x}} \psi_{\mathbf{x}} |\mathbf{x}\rangle$ we set $|\text{NOHE}(\psi)\rangle \equiv \sum_{\mathbf{x}} \psi_{\mathbf{x}} |\text{NOHE}(\mathbf{x})\rangle$. We will refer to this operation via a map $U_{\text{NOHE}}^{(N)}$, defined such that

$$U_{\text{NOHE}}^{(N)} |\psi\rangle = |\text{NOHE}(\psi)\rangle \quad (8)$$

for an arbitrary state $|\psi\rangle$. It can be implemented by iterating the application of a simple primitive:

$$U_{\text{NOHE}}^{(N)} = \left[\prod_{K=0}^{\log N - 2} \prod_{J=K+1}^{\log N - 1} \overline{CS}(K|J) \right] \left[\prod_{K=2}^{\log N - 1} S_{K, 2^{K-1}} \right]. \quad (9)$$

Therein, $S_{b,c}$ implements a swap of the qubits $b \leftrightarrow c$, i.e. $S_{b,c} |\psi_b\rangle \otimes |\phi_c\rangle = |\phi_b\rangle \otimes |\psi_c\rangle$, and $CS(a|b, c) = |0\rangle_a \langle 0| \otimes \mathbb{1}_{b,c} + |1\rangle_a \langle 1| \otimes S_{b,c}$ is the Friedkin gate (controlled-swap); moreover, for $K < J$ we set

$$\overline{CS}(K|J) = \prod_{\alpha=2^{K-1}}^{2(2^K-1)} CS(\alpha|\alpha + 2^J - 2^K, \alpha + 2^J). \quad (10)$$

Here, we label the string of $N - 1$ qubits via $\alpha = 0, 1, \dots, N - 2$; moreover, we use the ordering convention that $\prod_{k=k_{\min}}^{k_{\max}} U_k = U_{k_{\max}} U_{k_{\max}-1} \dots U_{k_{\min}}$. This decomposition can be further simplified by realising that the Friedkin gate is always applied with one of the targets in the $|0\rangle$ state; this allows to substitute it

with the ‘gadget’ in Fig. 5(d), consisting of a Toffoli and a controlled-not gate. Altogether, this results in the circuit decomposition shown in Fig. 5(a) for the explicit example of $N = 8$. In the SM we show that the circuit depth of $U_{\text{NOHE}}^{(N)}$ is $T_f = 2 \log N - 3$ with this recipe.

Bus qubit. In Eq. (3) we introduce a ‘bus qubit’ and define the operation

$$V = U_{\text{NOHE}}^{(2N)} H_{\text{bus}}. \quad (11)$$

The output in Eq. (3) thus reads $V |\mathbf{x}\rangle |0\rangle = |\text{NOHE}(\mathbf{x}, +)\rangle = |\text{NOHE}(\mathbf{x})\rangle |\text{OHE}(\mathbf{x})\rangle$ where

$$|\text{OHE}(\mathbf{x})\rangle = \frac{|0\rangle^{\otimes N} + |\mathbf{ohe}(\mathbf{x})\rangle}{\sqrt{2}}. \quad (12)$$

This state is factorized, and represents a computational state in the original Hilbert space via the physical location of the pointer $|+\rangle$: if e.g. $\mathbf{x} = (0, 1, 0)$, then $|\text{OHE}(\mathbf{x})\rangle = |0, 0, +, 0, 0, 0, 0, 0\rangle$. The term $|\text{NOHE}(\mathbf{x})\rangle$ can be understood as a byproduct of the circuit, which also ensures reversibility (note that $\langle \text{OHE}(\mathbf{x}) | \text{OHE}(\mathbf{y}) \rangle = (1 + \delta_{\mathbf{x}, \mathbf{y}}) / 2$). Fig. 5(f) illustrates this concept. In Eq. (3) we have exchanged the order of $\text{NOHE}(\mathbf{x})$ and $\text{OHE}(\mathbf{x})$ for simplicity; here we follow the order above.

Rewriting the QRAM operation

Eq. (5) builds upon three main observations. Let $P_{\mathbf{m}} = X^{\otimes \mathbf{b}} Z^{\otimes \mathbf{a}}$ be a generic Pauli operator acting on the QPU register; here, $\mathbf{m} = (\mathbf{a}, \mathbf{b}) \in \{0, 1\}^{2 \log N}$ and we set e.g. $Z^{\otimes \mathbf{a}} \equiv \bigotimes_i Z_i^{a_i}$. We emphasize that $P_{\mathbf{m}}$ only acts on the QPU register, and *not* on the bus qubit.

The first observation is that

$$V X^{\otimes \mathbf{b}} = U_{\mathbf{m}} \otimes \pi_{\mathbf{m}} V. \quad (13)$$

Therein, $U_{\mathbf{m}}$ and $\pi_{\mathbf{m}}$ act respectively on the first $N - 1$ and on the last N output qubits: $U_{\mathbf{m}} \otimes \pi_{\mathbf{m}} V |\mathbf{x}, 0\rangle = U_{\mathbf{m}} |\text{NOHE}(\mathbf{x})\rangle \otimes \pi_{\mathbf{m}} |\text{OHE}(\mathbf{x})\rangle$. More precisely, $U_{\mathbf{m}}$ is a complicated, deeply non-Clifford byproduct operator; however, $\pi_{\mathbf{m}}$ instead is a very simple permutation of the N OHE output qubits. This follows directly from the concept of OHE: since Pauli X operators permute the computational basis states, if then a OHE is applied, this permutation in the Hilbert space results in a physical permutation of the pointer qubits. For concreteness, let $\mathbf{x} = (0, 1, 1)$, and $\mathbf{b} = (0, 0, 1)$; then, $V |\mathbf{x}, 0\rangle = |0, 0, 0, 0, 0, 0, +, 0\rangle$, while $V X^{\otimes \mathbf{b}} |\mathbf{x}, 0\rangle = |0, 0, +, 0, 0, 0, 0, 0\rangle = \pi_{\mathbf{m}} |0, 0, 0, 0, 0, 0, +, 0\rangle$.

The second observation is that

$$U_{\text{QRAM}} Z^{\otimes \mathbf{a}} = Z^{\otimes \mathbf{a}} U_{\text{QRAM}}. \quad (14)$$

For this, note that U_{QRAM} is a multiple-controlled gate, where the $\log N$ register qubits simply act as controls; thus, U_{QRAM} commutes with any gate which is diagonal

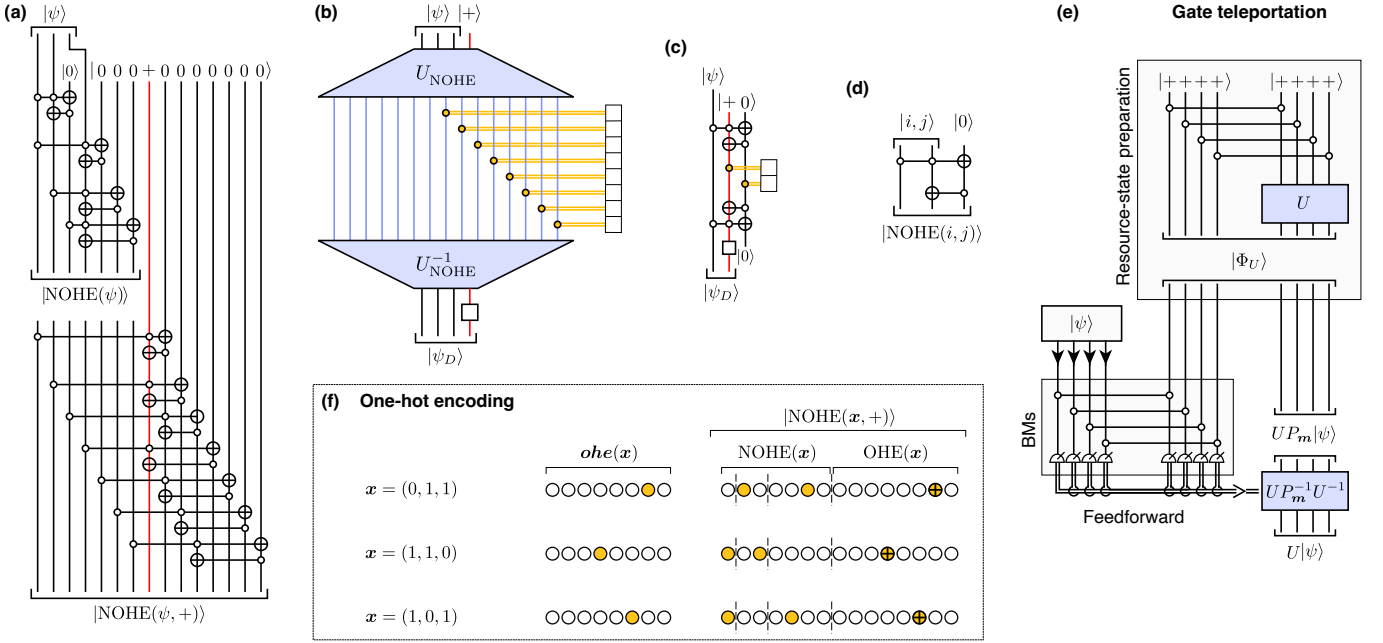


FIG. 5. **Nested one-hot encoding, quantum RAM and gate teleportation.** (a) Circuit decomposition for realising a NOHE (here we display directly $U_{\text{NOHE}}^{(2N)}$ for $N = 8$). The standard state $|\text{NOHE}(\psi)\rangle$ is obtained by applying the circuit in the top-left part; by adding a *bus* qubit in the $|+\rangle$ state and iterating the same procedure, we obtain $|\text{NOHE}(\psi, +)\rangle = V|\psi, 0\rangle$. (b) An example of QRAM model based on a NOHE; the red lines are classically-controlled Z gates, conditioned on the memory elements being $D_x = 1$. (c) Explicit QRAM model for $N = 2$, where the address is a single qubit. (d) Minimal gadget for the circuit decomposition of U_{NOHE} : a Toffoli gate followed by a controlled-not. (e) Depiction of standard gate teleportation (GT) for realising an arbitrary gate U : First, a RS $|\Phi_U\rangle$ is prepared; Second, Bell measurements (BMs) are applied between the input and part of the RS qubits; Third, feedforward of the BM outcomes regulates the application of a byproduct operation $UP_m U^{-1}$, where P_m is a Pauli operator. (f) Explicit depiction of the various variations of one-hot encoding, on the example of $N = 8$. Here empty or red-colored circles represent the $|0\rangle$ or the $|1\rangle$ state respectively; red-colored circles with a black cross represent the $|+\rangle$ state.

in the QPU computational basis - such as $Z^{\otimes a}$.

The third observation is that since by definition W_D only acts on the N OHE qubits, then $W_D U_m = U_m W_D$.

Finally, Eq. (5) follows straightforwardly by merging these three facts, and by defining $W_D(\mathbf{m}) = \pi_m W_D \pi_m^{-1}$. In summary, the QRAM operation is rewritten as

$$U_{\text{QRAM}} = [P_m V] [\pi_m W_D \pi_m^{-1}] [V P_m], \quad (15)$$

where we highlighted the modified versions of steps (i-iii). Importantly, this holds true for *any* Pauli operator P_m acting on the QPU register. In our construction, this is intrinsically random, as we discuss below.

Clifford generalised NOHE via gate-teleportation

For realising U_{QRAM} in Eq. (1) according to the recipe in Eq. (15), step (i) requires to apply $V P_m$ to the input state $|\psi\rangle |0\rangle$, where $|\psi\rangle$ is the QPU register state and P_m is a (arbitrary, not yet defined) Pauli operator acting on it. We realize $V P_m$ with a Clifford procedure, during which P_m is determined randomly. Similarly to the gate-teleportation (GT) paradigm [42, 47], illustrated in

Fig. 5(e), we use the pre-assembled resource-state (RS)

$$|\Phi^{(1)}\rangle = \frac{1}{N} \sum_{\mathbf{y}, \mathbf{z}} (-)^{\mathbf{y} \cdot \mathbf{z}} |y\rangle_{\mathcal{I}} \otimes |\text{NOHE}(\mathbf{z}, +)\rangle_{\mathcal{D}}; \quad (16)$$

where \mathcal{I} and \mathcal{D} feature $\log N$ and $2N - 1$ qubits.

Initially the state of the QPU register is $|\psi\rangle$, supported on qubits \mathcal{R} ; the bus qubit, in principle initialized in $|0\rangle$, does not need to be provided as input. Then, we simply implement BMs between \mathcal{R} and \mathcal{I} , collecting the outcomes \mathbf{m} ; this directly leaves us with the state $V P_m |\psi\rangle |0\rangle$ on the unmeasured qubits \mathcal{D} . We explicit in the SM the simple relation between \mathbf{m} and P_m .

Efficient adaptive loading

Step (ii) for implementing U_{QRAM} according to Eq. (15) requires to efficiently implement the loading operation $W_D(\mathbf{m})$. Importantly, in our protocol \mathbf{m} is not known prior to the start of the query, as it is only determined by the random BM outcomes during step (i). Here, we discuss how the loading can always be implemented efficiently for any obtained \mathbf{m} .

Let now $l \in \mathcal{L} = \{0, 1, \dots, N - 1\}$ label the qubits

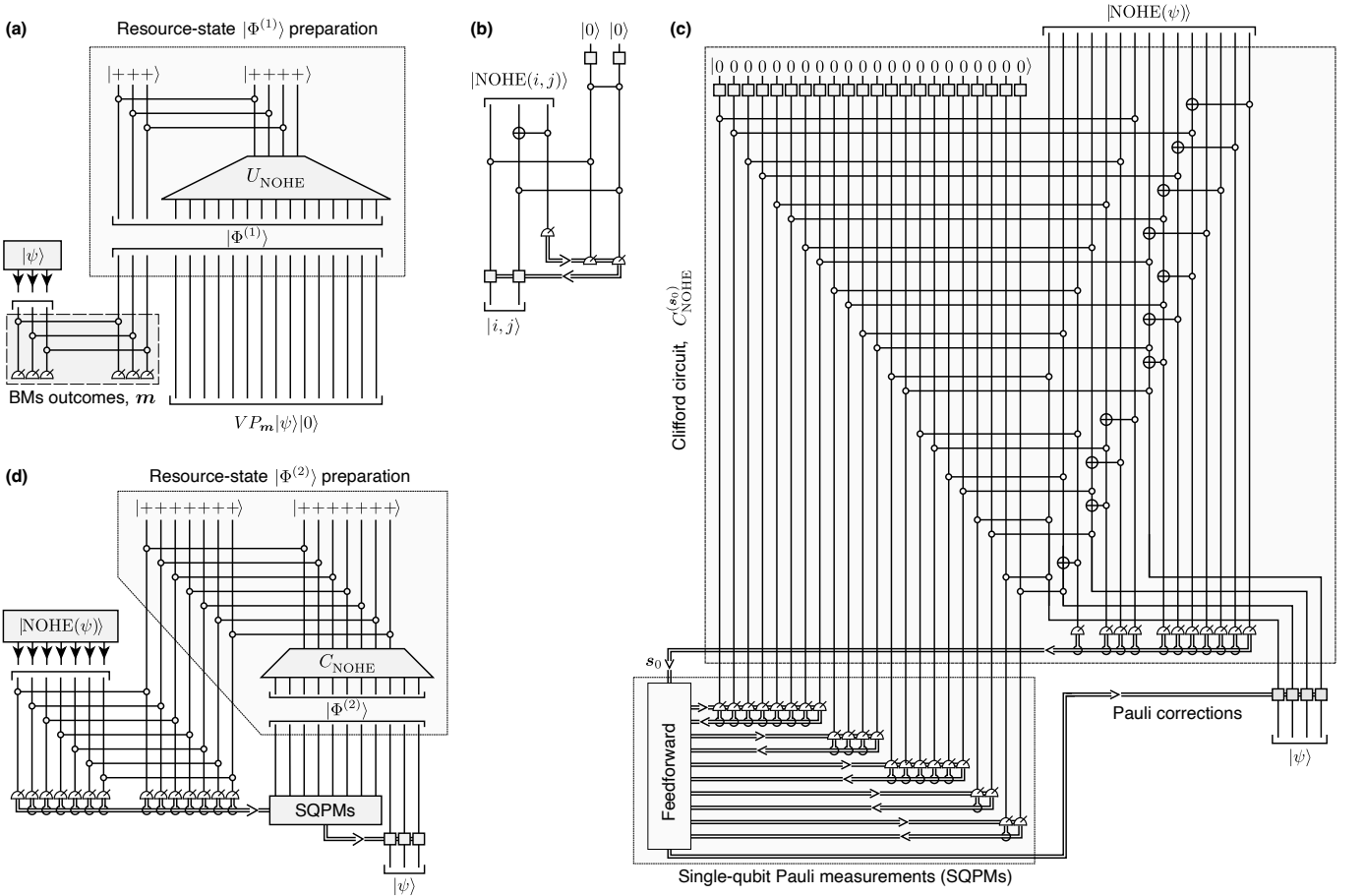


FIG. 6. **Clifford implementation of NOHE, and its Clifford inversion.** (a) Gate-teleportation (GT) implementation of $U_{\text{NOHE}}P_m$, where P_m is a random Pauli operator revealed by the outcomes of the Bell measurements (BMs). (b) Although the basic operation $|i, j\rangle \rightarrow |\text{NOHE}(i, j)\rangle$ is non-Clifford, it can be inverted with a Clifford circuit. Therein, the first measurement is in the X basis, while the second two are either in the X or in the Z basis, depending on the previous outcome; the last layer of gates single-qubit gates is of the form $Z^\alpha \otimes Z^\beta$, with α, β determined by the previous measurement outcomes. (c) Generic circuit for the Clifford inversion of the NOHE. This is composed by two parts: the first is a circuit C_{NOHE} featuring deterministic operations (a series of Clifford two-qubit gates followed by a set of measurements in the X basis); the second part is a sequence of *adaptive* Pauli measurements, where each qubit is measured either in the X or in the Z basis. (d) Resource-state protocol for inverting U_{NOHE} .

$W_D(\mathbf{m})$ has to be applied to. At an abstract level it is sufficient to proceed as follows. Given \mathbf{m} , for each qubit l we compute the string $\mathbf{x} = \mathbf{b} \oplus \mu^{-1}(l)$; then, we apply a Z gate to l if $D_{\mathbf{x}} = 1$. This is executed in parallel on all qubits \mathcal{L} , allowing for a $\mathcal{O}(1)$ implementation. Crucially, as we show below, we do not need the classical control software to ‘lookup’ the memory.

We model the controls on \mathcal{L} as follows. To each l , we associate one ‘control bit’ $B_l \in \{0, 1\}$, and one ‘control device’ \mathcal{C}_l pointing at l ; when \mathcal{C}_l is triggered, it only looks up B_l , and applies a Z gate to l if $B_l = 1$. All the control devices can be triggered in parallel. In addition, the classical memory is coupled to a network of swaps, which are controlled by only $\log N$ external control bits $\mathcal{B}_0, \mathcal{B}_1, \dots, \mathcal{B}_{\log N-1}$; note that each \mathcal{B}_K controls $N/2$ swaps simultaneously. When $W_D(\mathbf{m})$ is called, we have already registered $\mathbf{m} = (\mathbf{a}, \mathbf{b})$ on classical memory; we thus straightforwardly set $\mathcal{B}_K = b_K$. Next, we activate

the circuit of swaps; this sets the control bits to exactly $B_l = D_{\mathbf{b} \oplus \mu^{-1}(l)}$. Finally, we trigger all the controls \mathcal{C}_l in parallel, resulting in the implementation of $W_D(\mathbf{m})$. Thus, the desired loading is executed without any ‘reading’ of the memory by classical hardware.

Clifford NOHE inversion

Step (iii) of the recipe in Eq. (15) requires to implement $P_m^{-1}V^{-1}$. The last term, P_m^{-1} , is a Pauli operation that can be implemented straightforwardly at the end. Recalling that $V^{-1} = H_{\text{bus}}U_{\text{NOHE}}^{-1}$ and noting that also H_{bus} is Clifford, the only complex part remains the inversion U_{NOHE}^{-1} . In principle, this is deeply non-Clifford, as it is the inverse of the non-Clifford circuit in Eq. (9). However, below we show that if we regard instead

U_{NOHE} as an isometry from $\log N$ to $N - 1$ qubits, and only consider its inversion on the image $U_{\text{NOHE}}^{(N)}(\mathcal{H}^{\log N})$ in the codomain, where $\mathcal{H}^{(n)} \sim \mathbb{C}^{2^n}$ is the Hilber space of n qubits, then we can invert it via Clifford operations only.

Inverting a minimal NOHE. To illustrate the main idea, we first elaborate on the example of $N = 4$; according to Eq. (11), this aids U_{QRAM} on a memory featuring 2 databits. Then, from Eq (9) the NOHE can be written as the isometry $U_{\text{NOHE}}^{(4)} \equiv \sum_{i,j} |i, j \oplus ij, ij\rangle \langle i, j|$. For inverting it, we need to implement the right-inverse $G \equiv \sum_{i,j,k} |i, j \oplus k\rangle \langle i, j, k|$, such that $GU_{\text{NOHE}} = \mathbb{1}$ is the identity on $\mathcal{H}^{(2)}$. Due to the manifest non-reversibility of G , it cannot be implemented via unitary operations; however, we now outline a protocol to execute G on the image of U_{NOHE} by introducing measurements. Crucially, this will only involve Clifford resources: specifically, simple Clifford gates, SQPMs, Pauli operations and a stabilizer RS. To this end, let us first consider a generic three-qubit input state $|\chi\rangle = \sum_{i,j,k} \chi_{i,j,k} |i, j, k\rangle$. Our goal is to construct the state $G|\chi\rangle = \sum_{i,j,k} \chi_{i,j,k} |i, j \oplus k\rangle$, under the assumption that $|\chi\rangle \in U_{\text{NOHE}}(\mathcal{H}^{(2)})$. For this, we proceed as in Fig. 6(b): (a) We implement a controlled-not gate between the third and the second qubit; (b) We entangle the first and second qubit with an ancillary Bell pair via controlled-phase gates; (c) We measure the third input qubit in the X basis, collecting the outcome $s_0 \in \{0, 1\}$; (d) We measure the ancillas in a single-qubit Pauli basis, choosing either the Z (if $s_0 = 0$) or the X basis (if $s_0 = 1$), and we collect the outcomes $\mathbf{s}_1 = (\alpha, \beta) \in \{0, 1\}^2$; (e) We finally apply single-qubit Pauli gates on the original qubits, depending on (s_0, \mathbf{s}_1) .

Explicitly, the conditional state after the X basis measurement in step (c) reads

$$|\chi|_{s_0} = \sum_{a,b} (-)^{a,b} |a, b\rangle \otimes \sum_{i,j,k} (-)^{ai+b(j+k)+s_0k} \chi_{i,j \oplus k,k} |i, j\rangle; \quad (17)$$

here the ancillary qubits are written to the left of the tensor product. Next, we implement step (d). If we measured $s_0 = 0$, we measure in the Z basis; the system is then projected to

$$|\chi|_{s_0=0, \mathbf{s}_1} = Z^\alpha \otimes Z^\beta \sum_{i,j,k} \chi_{i,j,k} |i, j \oplus k\rangle. \quad (18)$$

Thus, in step (v) we simply need to apply the Pauli correction $Z^\alpha \otimes Z^\beta$ to cancel the byproduct and retrieve our target output $G|\chi\rangle$. Differently, if $s_0 = 1$ we measure in the X basis; now the conditional state is

$$|\chi|_{s_0=1, \mathbf{s}_1} = Z^\beta \otimes Z^\alpha \sum_{i,j,k} (-)^{i(j+k)+k} \chi_{i,j,k} |i, j \oplus k\rangle, \quad (19)$$

which for general inputs $|\chi\rangle$ is not trivially connected to the target output. However, recall now that $|\chi\rangle \in$

$U_{\text{NOHE}}(\mathcal{H}^{(2)})$. This subspace is characterised by the projector

$$\mathbb{P} = \sum_{i,j,k} \delta_{ij,0} \delta_{k,ik} |i, j, k\rangle \langle i, j, k|. \quad (20)$$

Crucially, if $|\chi\rangle$ is stabilised by this projector, i.e. $\mathbb{P}|\chi\rangle = |\chi\rangle$, then on all its non-vanishing components we get $(ij + ik + k) \equiv 0 \pmod{2}$, meaning that the phases in the equation above are all equal. Thus, if the input is from the subspace of interest, again we can retrieve the desired output by simply applying the Pauli correction $Z^\beta \otimes Z^\alpha$. In both cases, we deterministically apply G , under the assumption that $|\chi\rangle = |\text{NOHE}(\psi)\rangle$ for some $\psi \in \mathcal{H}^{(2)}$.

General case. For larger N , recall that U_{NOHE} can be implemented by iterating the same isometry G introduced above as in Fig. 5(a), eventually resulting in a larger isometry from $\log N$ qubits to $N - 1$ qubits. Since the basic building-block is the same, it can be inverted by iterating the inversion procedure outlined for $N = 4$. This is shown explicitly for $N = 16$ in Fig. 6(c). The circuit therein can be understood by comparison with the circuit for realising U_{NOHE} in Fig. 5(a): we invert it by applying the destructive protocol in Fig. 6(b) in place of the direct (non-Clifford) unitary inversion of the gadget in Fig. 5(d).

Note that in Fig. 6(c) we *first* execute all the unitary gates, and *then* all the SQPMs. This is allowed since only Clifford operations are involved, implying that we do not need to physically implement the adaptive Pauli corrections - that is, the byproducts of the form $Z^\alpha \otimes Z^\beta$ in Eqs. (18) and (19). Instead, byproducts can be propagated through the circuit up to the point of a SQPM, where they are accounted for by adequately interpreting the measurement outcomes.

This eliminates the need for mid-circuit adaptive gates, thereby separating the circuit in two parts, as highlighted in Fig. 6(c): the first part C_{NOHE} contains the Clifford operations and Pauli measurements that are *pre-determined*; the second part contains *adaptive* SQPMs on the ancillas, where the measurement bases are chosen depending on previous measurement outcomes. Since these outcomes are probabilistic, C_{NOHE} also has a *classical* output $\mathbf{s}_0 \in \{0, 1\}^{N-\log N-1}$, which collects them; formally, when during the application of C_{NOHE} on the input $|\Xi\rangle$ we obtain the measurement outcomes \mathbf{s}_0 , we write the output as $C_{\text{NOHE}}^{(\mathbf{s}_0)}|\Xi\rangle$. In summary, this operation implements a map of the form

$$C_{\text{NOHE}}^{(\mathbf{s}_0)} : \mathcal{H}_{\mathcal{D}} \longrightarrow \mathcal{H}_{\mathcal{P}} \otimes \mathcal{H}_{\mathcal{F}}. \quad (21)$$

Here, \mathcal{D} is the set of qubits which supports the input, and has size $|\mathcal{D}| = N - 1$; the qubits in \mathcal{P} , with $|\mathcal{P}| = 2(N - \log N - 1)$, are those which will then be subjected to the adaptive SQPMs; finally, \mathcal{F} collects the $|\mathcal{F}| = \log N$ qubits which will support the output.

The final sequence of adaptive SQPMs is performed

by leveraging standard techniques of the stabiliser formalism: measurement outcomes different from +1 can always be accounted for by propagating virtual Pauli byproducts through the Clifford circuit, and thereby updating subsequent SQPM bases. The number of rounds of parallel SQPMs equals exactly the number of circuit-layers of U_{NOHE} : measurements clearly correspond to gadgets, and the measurement outcomes corresponding to each gadget only influence the measurement basis of subsequent gadgets. This can therefore be summarised as follows: given any arbitrary state $|\Xi\rangle \in U_{\text{NOHE}}(\mathcal{H}^{(\log N)})$, then there exists a sequence of adaptive SQPMs that implements the transformation

$$C_{\text{NOHE}}^{(\mathbf{s}_0)} |\Xi\rangle \xrightarrow{\text{SQPMs}} U_{\text{NOHE}}^{-1} |\Xi\rangle, \quad (22)$$

upon the application of a final Pauli correction; moreover, the protocol is always completed in $T_f = 2 \log N - 3$ measurement rounds.

RS based implementation. This same protocol for inverting U_{NOHE} can as well be executed with the aid of a resource-state of the form

$$|\Phi^{(2)}\rangle = \frac{1}{2^{N-1}} \sum_{\mathbf{Y}, \mathbf{Z}} (-)^{\mathbf{Y} \cdot \mathbf{Z}} |\mathbf{Y}\rangle_{\mathcal{D}'} \otimes C_{\text{NOHE}} |\mathbf{Z}\rangle_{\mathcal{P} \cup \mathcal{F}}, \quad (23)$$

where the indexes run over $\mathbf{Y}, \mathbf{Z} \in \{0, 1\}^{N-1}$ and $|\mathcal{D}'| = N - 1$. Therein we omit the classical output of $C_{\text{NOHE}}^{(\mathbf{s}_0)}$ and simply write C_{NOHE} because manifestly any \mathbf{s}_0 is equally well-suited. This state can thus be assembled by first preparing $N - 1$ Bell pairs, and then applying $C_{\text{NOHE}}^{(\mathbf{s}_0)}$ to one half with any arbitrary \mathbf{s}_0 . For the inversion, we employ the scheme in Fig. 6(d): we first teleport the input state in the resource state via BMs between the input qubits and \mathcal{D}' , collecting the measurement outcomes in a binary vector \mathbf{s}_{-1} ; then, we perform SQPMs on \mathcal{P} similarly to what discussed above, but now also accounting for \mathbf{s}_{-1} . Again, this is allowed by the fact that C_{NOHE} is Clifford, implying that $|\Phi^{(2)}\rangle$ is a *stabiliser* state.

Compact (linearised) resource state. The definition of $|\Phi^{(2)}\rangle$ used so far can be drastically optimized via standard Clifford methods. We first discuss the simple case of $N = 2$, where we show that $|\Phi^{(2)}\rangle$ can be reduced to a *linear* graph-state. Before the X measurement on qubit 5, the state is characterised by the following stabilisers: $X_1 Z_4$, $X_4 Z_1 Z_7$, $X_5 Z_2 Z_8$, $X_7 Z_4 Z_8$, $X_8 Z_5 Z_7$, $X_2 Z_5 Z_6$, $X_3 Z_6$ and $X_6 Z_3 X_5$. Measuring X_6 substitutes the last three stabilisers with $X_2 X_3 Z_5$, $\pm X_6$ and $\pm X_5 Z_6$ respectively, with the sign set by the measurement outcome. Thus, a $X_6 = -1$ outcome is accounted for by applying X_3 . Importantly, we note the emergence of a *linear* graph state according to the order $1 - 4 - 7 - 8 - 5 - 2 - 3$, up to a Hadamard H_3 on qubit 3. More precisely, if we apply H_3 , then the stabiliser group on the unmeasured qubits is generated by $X_1 Z_4$,

$Z_1 X_4 Z_7$, $Z_4 X_7 Z_8$, $Z_7 X_8 Z_5$, $Z_8 X_5 Z_2$, $Z_5 X_2 Z_3$, $Z_2 X_3$. Therefore, $|\Phi^{(2)}\rangle$ can be prepared with a measurement-free approach with a 1D circuit, which corresponds to Fig. 2(c) in the main text.

By iterating this, for any N $|\Phi^{(2)}\rangle$ is prepared via simple Clifford operations which merge linear *cluster states* - in fact preparing a RS for the execution of a circuit in standard measurement-based quantum computation (MBQC). However, crucially for the processing the SQPMs bases remain adaptive. This is in sharp contrast with standard MBQC with cluster states, where Clifford circuits are executed in $\mathcal{O}(1)$ time by measuring all Pauli operators in a single round [40, 41]. Differently, here, while still the RS is equivalent to a cluster state, and while also the measurement bases are Pauli, still they are adaptive - highlighting the non-Cliffordness of the operation we are inverting. This traces back to the fact that here the adaptive basis is chosen between two orthogonal bases, X and Z .

QRAM resource-state

Formally, $|\Phi\rangle$ is specified in Fig. 7: we prepare the RSs $|\Phi^{(1)}\rangle$ and $|\Phi^{(2)}\rangle$ defined in Eqs. (16) and (23) respectively, and perform (partial) BMs. Specifically, referring to the notation in Eq. (16), we only measure the first $N - 1$ qubits of \mathcal{D} . After this, we finally apply a Pauli correction to $\mathcal{P} \cup \mathcal{F}$, conditioned on the measurement outcomes. Despite the BMs rendering the circuit stochastic, the Pauli correction can be chosen to make it deterministic (see the section below); for now, we formally define $|\Phi\rangle$ as the output of this circuit when all measurement outcomes are +1, and no correction is applied. Thus,

$$|\Phi\rangle = B \left[|\Phi^{(1)}\rangle \otimes |\Phi^{(2)}\rangle \right], \quad (24)$$

where we defined the contraction $B : \mathcal{H}^{(3N-2)} \rightarrow \mathcal{H}^{(N)}$ as the linear map

$$B = \sum_{\mathbf{x}} \sum_{\mathbf{j}, \mathbf{k}} (-)^{\mathbf{j} \cdot \mathbf{k}} D(\mathbf{x}, \mathbf{j}) |\mathbf{x}\rangle_{\mathcal{L}} \langle \mathbf{j} |_{\mathcal{D}} \langle \mathbf{k} |_{\mathcal{D}'}. \quad (25)$$

Therein, $\mathbf{x} \in \{0, 1\}^N$ indexes the computational basis on \mathcal{L} , while $\mathbf{j}, \mathbf{k} \in \{0, 1\}^{2N-1}$ label the computational basis on \mathcal{D} and \mathcal{D}' respectively; moreover, the term $D(\mathbf{x}, \mathbf{j}) \equiv \prod_{\alpha=0}^{N-1} \delta_{x_\alpha, j_{N-1+\alpha}}$ forces a correspondence between \mathbf{x} and the last N components of \mathbf{j} . The action of B is also schematized in the top inset of Fig. 7.

Virtual and physical pictures. When we execute the query, $|\Phi\rangle$ is already prepared; it has support on a set of qubits \mathcal{A} of dimension $|\mathcal{A}| = 5N - 3$, and belongs to the Hilbert space $\mathcal{H}_{\mathcal{A}} \cong \mathbb{C}^{2^{|\mathcal{A}|}}$. The construction in Fig. 7 suggests to partition \mathcal{A} in disjoint subsets as $\mathcal{A} = \mathcal{I} \cup \mathcal{L} \cup \mathcal{P} \cup \mathcal{F}$, of sizes $|\mathcal{I}| = \log N$, $|\mathcal{L}| = N$,

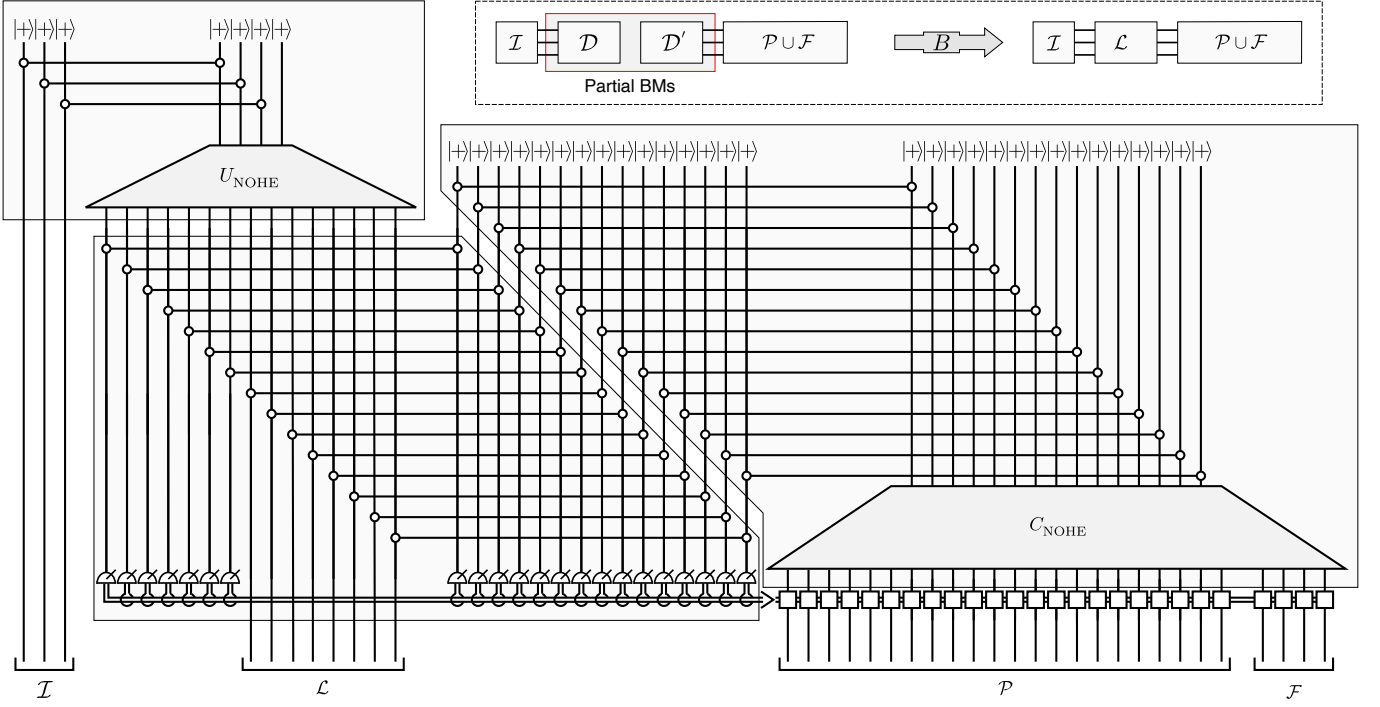


FIG. 7. **Circuit for the resource-state.** The resource-state $|\Phi\rangle$ can be understood as emerging from a ‘synthesis’ of the previously introduced states $|\Phi^{(1)}\rangle$ and $|\Phi^{(2)}\rangle$. Here, we display a circuit which defines it formally. In the main figure, the top-left and right panels highlights the preparation of $|\Phi^{(1)}\rangle$ and $|\Phi^{(2)}\rangle$ respectively; the bottom-left panel contains a ‘partial’ Bell measurement, where not all the qubits are projected. This is also summarised in the scheme above, which highlights the action of the contraction B ; therein, horizontal informally represent the presence of entanglement between sets of qubits.

$|\mathcal{P}| = 2(2N - \log N - 2)$ and $|\mathcal{F}| = \log N + 1$; the ancillary Hilbert space is thus partitioned as

$$\mathcal{H}_A = \mathcal{H}_I \otimes \mathcal{H}_L \otimes \mathcal{H}_P \otimes \mathcal{H}_F. \quad (26)$$

We will refer to this as the ‘physical’ Hilbert space, as it describes the quantum state of the qubits \mathcal{A} , which are physically present on hardware during the query. Formally, $|\Phi\rangle$ can be written in the computational basis as $|\Phi\rangle = \sum_{i_0, \dots, i_Q} \Phi_{i_0, \dots, i_Q} |i_0, \dots, i_Q\rangle$, where $Q \equiv |\mathcal{A}| - 1$ and we set the tensor entries as

$$\Phi_{i_0, \dots, i_Q} = \sum_{\mathbf{j}, \mathbf{k}} (-)^{j \cdot \mathbf{k}} D(\mathbf{x}, \mathbf{j}) \Phi_{i_0, \dots, i_M; \mathbf{j}}^{(1)} \Phi_{\mathbf{k}; i_{M+N+1}, \dots, i_Q}^{(2)}; \quad (27)$$

therein, we also set $M = \log N - 1$ and we identify $\mathbf{x} \equiv (i_{M+1}, \dots, i_{M+N})$. We find it useful to associate the contracted mute indexes (\mathbf{j}, \mathbf{k}) with *virtual* degrees of freedom; these belong to the virtual Hilbert space $\mathcal{H}_D \otimes \mathcal{H}_{D'}$, which is not associated to physical qubits. The interplay between the physical picture and the virtual one is then mediated by the map $B : \mathcal{H}_D \otimes \mathcal{H}_{D'} \rightarrow \mathcal{H}_L$; many aspects of the query will be most easily understood in the virtual picture.

Deterministic resource-state preparation. This formal definition of $|\Phi\rangle$ is apparently non-deterministic due to the BMs. Importantly, we can always efficiently cope with this randomness by adding a Pauli correction

at the end, making the output deterministic. This is allowed by the fact that one of the two states we are ‘merging’ via BMs, namely $|\Phi^{(2)}\rangle$, is a stabiliser state; thus, by implementing standard propagation of Pauli operators to the right-side of the circuit in Fig. 7, we eventually end up with a simple Pauli byproduct on \mathcal{F} .

Query protocol: details

Our proposed query proceeds in three steps, which can be put in correspondence with those highlighted in Fig. 5(f). However, in our implementation these are executed ‘virtually’ with the aid of $|\Phi\rangle$ by employing the techniques introduced above. Specifically, it is convenient to use the abstract map B in Eq. (25) to connect the physical operations to a virtual-space dynamics, whose steps are more explicit. For what follows, it is useful to refer to Fig. 8 for keeping track of this correspondence.

The query begins as follows. The address-state $|\psi\rangle = \sum_{\mathbf{x}} \psi_{\mathbf{x}} |\mathbf{x}\rangle$ is initially supported on the $\log N$ qubits composing the QPU register \mathcal{R} ; the resource-state $|\Phi\rangle$ is already assembled and stored on qubits \mathcal{A} .

For step (i), we perform BMs between corresponding qubits in \mathcal{R} and \mathcal{I} . The resulting state has the form $|\Psi_{\mathbf{m}}\rangle |\Phi_{\mathbf{m}}(\psi)\rangle = \mathbb{P}^{(\mathbf{m})} |\psi\rangle |\Phi\rangle$, where $\mathbb{P}^{(\mathbf{m})}$ is a projector describing the action of the BMs, $|\Psi_{\mathbf{m}}\rangle$ is the projected

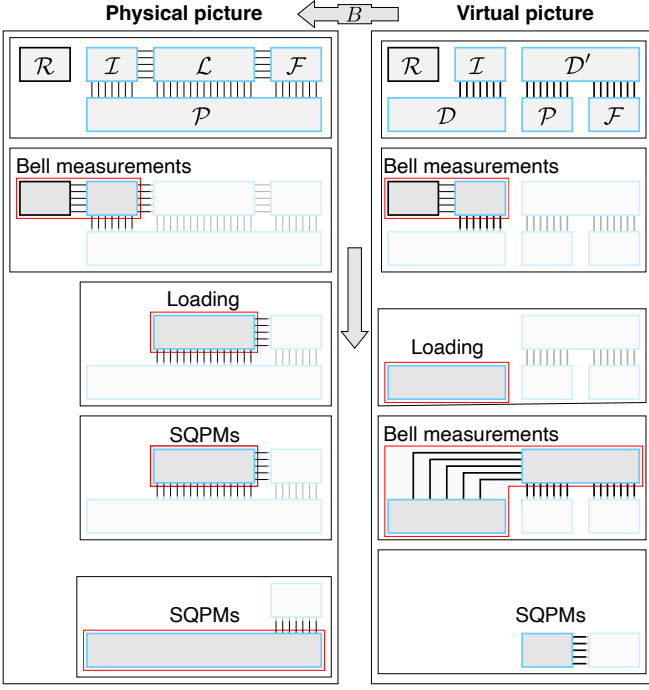


FIG. 8. **Sketch of the query protocol.** To the left, we schematise the induced evolution in the physical Hilbert space $\mathcal{H}_{\mathcal{R}} \otimes \mathcal{H}_{\mathcal{A}}$, where $\mathcal{A} = \mathcal{I} \cup \mathcal{L} \cup \mathcal{P} \cup \mathcal{F}$; to the right, we show the corresponding evolution in virtual space. Here boxes represent sets of qubits (either physical or virtual), and bonds between them denote the presence of entanglement. The two pictures are connected by the action of the contractive map $\mathcal{P} : \mathcal{H}_{\mathcal{D}} \otimes \mathcal{H}_{\mathcal{D}'} \rightarrow \mathcal{H}_{\mathcal{L}}$, detailed in Fig. 7, which essentially implements a partial Bell measurement between \mathcal{D} and \mathcal{D}' . The right panel also traces the steps of the ‘prototypical Clifford query protocol’.

state of Bell pairs on $\mathcal{R} \cup \mathcal{I}$, and $|\Phi_{\mathbf{m}}(\psi)\rangle$ is the conditional state on $\mathcal{L} \cup \mathcal{P} \cup \mathcal{F}$. By propagating $\mathbb{P}^{(\mathbf{m})}$ through B , we can rewrite the nontrivial part of the resulting state as

$$|\Phi_{\mathbf{m}}(\psi)\rangle = B \left[|\Phi_{\mathbf{m}}^{(1)}\rangle \otimes |\Phi^{(2)}\rangle \right], \quad (28)$$

where $|\Phi_{\mathbf{m}}^{(1)}(\psi)\rangle \in \mathcal{H}_{\mathcal{D}}$ is supported on the virtual qubits \mathcal{D} . From GT, this has the form

$$|\Phi_{\mathbf{m}}^{(1)}(\psi)\rangle = VP_{\mathbf{m}} |\psi\rangle |0\rangle; \quad (29)$$

thus, to all effects we have implemented in virtual space the first step of the rewriting in Eq. (15).

For step (ii), we now proceed by loading the data. This is achieved via the *loading* operation $W_D(\mathbf{m})$ on \mathcal{L} :

$$W_D(\mathbf{m}) = \bigotimes_{l=0}^{N-1} Z_l^{D_{b \oplus \mu^{-1}(l)}}, \quad (30)$$

where, as before, we indicated by $l \in \mathcal{L}$ the qubits in $\mathcal{L} \subset \mathcal{A}$. By applying this, in the real picture we obtain the

state $|\Phi_{\mathbf{m}}(\psi|D)\rangle = W_D(\mathbf{m}) |\Phi_{\mathbf{m}}(\psi)\rangle$; by propagating $W_D(\mathbf{m})$ through B , we can write it as

$$|\Phi_{\mathbf{m}}(\psi|D)\rangle = B \left[|\Phi_{\mathbf{m}}^{(1)}(\psi|D)\rangle \otimes |\Phi^{(2)}\rangle \right]; \quad (31)$$

herein, also $|\Phi_{\mathbf{m}}^{(1)}(\psi|D)\rangle \in \mathcal{H}_{\mathcal{D}}$ is supported on the virtual qubits \mathcal{D} , and reads

$$|\Phi_{\mathbf{m}}^{(1)}(\psi|D)\rangle = W_D(\mathbf{m}) VP_{\mathbf{m}} |\psi\rangle |0\rangle. \quad (32)$$

Therefore, we realized step (ii) of Eq. (15) in virtual space.

For step (iii), we complete our protocol by inverting the virtual NOHE. We first measure all the qubits in \mathcal{L} in the X basis, collecting the measurement outcomes \mathbf{M} ; crucially, the resulting conditional state reads

$$\mathbb{P}_{\mathcal{L}}^{(\mathbf{M})} |\Phi_{\mathbf{m}}(\psi|D)\rangle = C_{\text{NOHE}}^{(\mathbf{M}')} |\Phi_{\mathbf{m}}^{(1)}(\psi|D)\rangle, \quad (33)$$

where $\mathbb{P}_{\mathcal{L}}^{(\mathbf{M})}$ is a projector acting on \mathcal{L} which describes these measurements. Here, \mathbf{M}' is calculated efficiently by simply propagating Pauli operators through the Clifford circuit. This equation must be read as follows: the state $|\Phi_{\mathbf{m}}(\psi|D)\rangle$ has support on qubits $\mathcal{L} \cup \mathcal{P} \cup \mathcal{F}$ as defined in Eq. (31); the state $|\Phi_{\mathbf{m}}^{(1)}(\psi|D)\rangle$ belongs to the virtual space $\mathcal{H}_{\mathcal{D}}$ as specified by Eq. (32); the operation C_{NOHE} acting on it executes a map from virtual to physical space of the form $\mathcal{H}_{\mathcal{D}} \rightarrow \mathcal{H}_{\mathcal{P} \cup \mathcal{F}}$.

Further, from Eq. (32) we note that we always have $|\Phi^{(1)}(\psi|D)\rangle \in U_{\text{NOHE}}(\mathcal{H}^{(\log N+1)})$. Thus, the same concept of Eq. (22) holds here as well: we can design a sequence of SQPMs on \mathcal{P} such that, upon the application of a final Pauli operation, we get

$$\mathbb{P}_{\mathcal{L}}^{(\mathbf{M})} |\Phi_{\mathbf{m}}(\psi|D)\rangle \xrightarrow{\text{SQPMs}} U_{\text{NOHE}}^{-1} |\Phi_{\mathbf{m}}^{(1)}(\psi|D)\rangle. \quad (34)$$

The right-hand side state in the equation above is supported on the remaining unmeasured physical qubits \mathcal{F} . In particular, from Eq. (32), it follows that we can retrieve the correct output of the QRAM query, i.e. $|\psi_D\rangle$, by simply applying the Pauli operator $P_{\mathbf{m}}^{-1}$ to the first $\log N$ qubits of \mathcal{F} , and a Hadamard H , which is Clifford, to the last qubit.

Built-in noise-resilience

Here, we discuss the impact of errors and noises in our QRAM module, explaining its built-in noise-resilience and analysing our numerical results concerning it.

Background. The *query fidelity* F_{QRAM} of a QRAM call is defined as follows. Given a dataset D and a quantum address $|\psi\rangle$, let the (potentially faulty) output

of the QRAM module be the density matrix $\rho_D(\psi)$; here we also trace out any ancillary qubit. Then,

$$F_{\text{QRAM}} = \frac{1}{2^N} \sum_D \int d\psi \langle \psi_D | \rho_D(\psi) | \psi_D \rangle, \quad (35)$$

where $2^{-N} \sum_D$ and $\int d\psi$ average uniformly over all possible memory configurations, and over all (normalized) inputs, respectively.

For generic QRAM protocols, this scales as $F_{\text{QRAM}} \sim \exp\{-\text{poly}N\}$, because errors at any of the $\mathcal{O}(N)$ space-time events are detrimental. In contrast, Giovannetti and colleagues introduced a protocol [3], dubbed as *bucket-brigade*, which was conjectured to drastically suppress query errors. After this remained a conjecture for many years, recently Hann et al. proved [37] that specific versions of the bucket-brigade have an error-rate

$$1 - F_{\text{QRAM}} \lesssim \text{polylog}N. \quad (36)$$

For achieving this, one must design a query circuit where error propagation is strongly constrained [37].

Noise suppression mechanism. In our scheme, the noise-resilience of the bucket-brigade method is incorporated in the whole QRAM procedure. Similarly to Ref. [37], our analysis is based on the following concept. Here, for simplicity we will ignore the averaging over D (which is included in the numerical calculations). Considering a generic Kraus map $\rho_D(\psi) = \sum_j K_j |\psi\rangle \langle \psi| K_j^\dagger$, and assuming for simplicity that errors are unitary (i.e., $K_j^\dagger K_j = p_j \mathbb{1}$ with $\sum_k p_k = 1$), one can prove that

$$F_{\text{QRAM}} \geq 4 \left[\frac{1}{N} \sum_j p_j |\mathcal{G}_j| - \frac{1}{2} \right]^2, \quad (37)$$

where $\mathcal{G}_j \subseteq \{0, 1\}^{\log N}$ is a family of classical addresses of the form (informal definition)

$$\mathcal{G}_j = \{ \mathbf{x} \text{ such that } K_j |\mathbf{x}\rangle = \sqrt{p_j} |\mathbf{x}\rangle |D_{\mathbf{x}}\rangle |A_j\rangle \} \quad (38)$$

for a certain state $|A_j\rangle$ on the ancillas. In the SM we give a rigorous definition; in essence, \mathcal{G}_j is a subset of classical addresses, which can be queried coherently together.

Crucially, in the footsteps of the bucket-brigade protocol [3, 37], our NOHE procedure is designed in such a way that

$$\sum_j p_j |\mathcal{G}_j| \simeq N - C\varepsilon N \log^\alpha N - \mathcal{O}(\varepsilon^2), \quad (39)$$

where ε is an error rate specified in the Kraus map. The coefficient C and the exponent α depend on the error model. Thus, for small error rates, one gets a favorable polylogarithmic scaling of the infidelity,

$$1 - F_{\text{QRAM}} \leq 8C\varepsilon \log^\alpha N + \mathcal{O}(\varepsilon^2). \quad (40)$$

In the SM we provide a rigorous analysis.

Error models and numerical analysis. We certify this expected performance via numerical calculations. Despite the dimension of the Hilbert space scaling as $2^{\mathcal{O}(N)}$, we employ specialised techniques [37] to simulate QRAM queries for memory sizes up to $N \simeq 10^4$. More precisely, we note that the basic operations of QRAM only map computational basis states in computational basis states; thus, since the input state is on $\log N$ qubits, even though the dimension of the Hilbert space grows up to 2^{2N-1} during the query, we can always efficiently represent the state via $\mathcal{O}(N)$ variables.

Our simulations take in consideration several error models listed below. We performed numerical calculations via standard quantum Monte Carlo techniques, implementing the random application of Pauli errors. Results are displayed in Figs. 4(c-e) in the main text; there, we certify the expected scaling and estimate the dominating exponents α by interpolating the results in a log-log plot.

The first error model assumes a continuous depolarisation (CD) of all the qubits, both active and idle. More precisely, at each time step, all the qubits undergo a random Pauli error with probability ε . Within this model, we estimate that $\alpha_{\text{CD}} \simeq 3.8$.

The second error model assumes operational Pauli (OP) errors; this is similar to the first, with the difference that here we only consider errors during the gates. Specifically, any time a qubit enters a gate, it undergoes a random Pauli error with probability ε .

The third model assumes that a Z error occurs with probability ε to a qubit, when it undergoes a gate. This is strongly motivated by the capability, demonstrated e.g. in neutral atoms [17, 51], to erasure-convert (EC) two-qubit errors to Z errors [52–54]. In this case, the Z bias reduces significantly the impact of errors, because with Z errors only, the classical addresses are always queried correctly, only leaving errors in the coherence of the query. Specifically, this results in a quadratic fidelity enhancement, compatible with out interpolation leading to $\alpha_{\text{EC}} \simeq 1.9$.

Quantum error-corrected QRAM

Previous literature has long been concerned on whether QEC can scale-up a QRAM module [37, 38, 46]. Concerns are motivated as follows. First, employing $\mathcal{O}(N)$ ancillary qubits suggests that the error-rate to be addressed via QEC scales exponentially in $\mathcal{O}(N)$, making QRAM not error-correctable in practice. Second, the non-Cliffordness of V demands unbearable resources for FT implementations, as $\mathcal{O}(N)$ non-Clifford gates need to be applied *during* the query. Below, we show how our QRAM design overcomes these challenges. Before entering the details, we review two cardinal concepts in QEC: fault-tolerant QC and transversal gates.

Fault-tolerant computation. In a ‘fault-tolerant

quantum computation’ (FTQC) the processor operates on *logical qubits*, and implements standard QEC between the logical gates [1, 61]. The necessary condition for QEC to be effective in these schemes is that errors on physical qubits never propagate inside the logical blocks; if this holds for any logical operation, including syndrome-extraction and error-correction, then QEC can arbitrarily suppress the logical error rate.

Transversal gates. A logical single-qubit gate U_L is transversal if it can be executed by applying one single-qubit gate to each physical qubit in a block; an analogous definition holds for two-qubit gates. Transversal gates are intrinsically FT [1]; however, no QEC code exists with a universal set of transversal gates (Eastin-Knill theorem [62]). It is a common fact for typical QEC codes, that gates from the Clifford group are transversal: for instance, this is true for Calderbank-Shor-Steane (CSS) codes [63, 64], for 2D color codes [65], and for the toric and surface codes [66]. For standard QEC schemes, Clifford gates are thus much simpler, and drastically less resource-consuming, than non-Clifford gates; the latter require more costly techniques, e.g. ‘magic-state injection’ [42]. The hardness of implementing non-Clifford gates with standard QEC has so far left fundamental concerns on the very possibility of error-correcting a QRAM query, since previous proposals needed $\mathcal{O}(N)$ such gates to be implemented online during the execution of the algorithm.

Main concept. Within our QRAM design, two key aspects allow to directly integrate QEC. First, as discussed above, F_{QRAM} scales as $\text{polylog}N$, implying that QEC is possible to begin with. Second, the query is *entirely* Clifford: thus, with standard QEC codes any operation within the query can be implemented by transversal gates only. Specifically, we note that for the query to be entirely transversal, it is sufficient that the following operations are transversal for the specific code considered: Pauli gates, single-qubit Pauli measurements (SQPMs), and a Clifford two-qubit gate enabling Bell measurements (e.g., the controlled-not or the controlled-phase gate). In the following, we assume these simple conditions to hold, and we analyze the various steps and of our QRAM design in the spirit of FTQC.

Resource-state preparation. Preparing the RS $|\Phi\rangle$ is the most demanding part, both with and without QEC. Indeed, any remarkable complexity associated with QRAM, in this work is outsourced to this step. Our approach has two main advantages. The first is that now any demanding operation does not directly impact the online query: once the main algorithm is running, any highly complex protocol is already executed, and the query is fast and simple. Thus, $|\Phi\rangle$ can be interpreted as a resource furnished to the processor. Second, we no longer need to apply the unitary U_{NOHE} to an *arbitrary* input state: rather, we need to prepare a *specific*, known

state, which has no connection with any detail of the algorithm nor the memory. This is generally a much simpler task: for instance, one can employ post-selected methods, as nothing is lost if the preparation fails.

The cost of the preparation of $|\Phi\rangle$ can be evaluated in several ways. For instance, the number of Toffoli gates employed in the circuit-level decomposition of Fig. 7 is $2N - \log N - 2$ (SM). We note that since the only non-Clifford gate which is needed is the Toffoli gate, a sound strategy is to directly distill ad-hoc RSs [67, 68], resulting in a minimal number of ‘magic-state factories’ (MSFs). Alternatively, the standard paradigm is to distill T states [69, 70], for which several decompositions of the Toffoli are possible. Since the preparation of $|\Phi\rangle$ does not impact the runtime of the principal algorithm, it might be convenient to sacrifice circuit-depth for lowering the number of needed MSFs; thus, decompositions of the Toffoli gate in four T gates are optimal [49].

Crucially, as stated in the main text and discussed below, (i) the query is entirely Clifford, and (ii) the times T_{query} and T_{Φ} needed respectively for a query and for assembling $|\Phi\rangle$ are practically, equal, $T_{\Phi} \simeq T_{\text{query}}$. It follows that the QRAM factory can operate *in parallel* with the query, assembling a new copy of $|\Phi\rangle$ while an old copy is consumed. Most importantly, since the query has no T cost, the QRAM factory can employ all the MSFs which are present on the processor.

Resource-state storage. The RS is stored statically in the QRAM zone until the query begins. Since no logical gates are applied, error rates are much lower here. In addition, as shown above, our QRAM query can tolerate even significant errors in the RS; consequently, syndrome extraction can be performed at low rates. Importantly, errors which are detected during the storage time, do *not* need to be corrected in real time, and not even before the query starts. Instead, one can simply calculate the propagation of detected errors through the query in classical processing, and only correct them at the end of the query on the final $\log N + 1$ qubits. Eventually, this means that only very limited resources are required for storing the RS, and no heavy parallel classical computation is needed for fast syndrome processing.

Fault-tolerant query. To exploit at best our proposed query protocol, which is mostly based on SQPMs, measurement-based approaches [55] to QEC can be beneficial. To this end, the paradigmatic recipe is to pre-assemble a 3D stabiliser states which ‘foliates’ the desired QEC code [56]. Modern approaches allow to also ‘grow’ this resource while the computation proceeds in a ‘fusion-based’ scheme [54, 57]; we note that, importantly, within the latter approach also methods have been studied, specific to neutral-atoms, which allow to preserve the bias in the noise [54], thereby allowing for the quadratic fidelity enhancement discussed in the main text and above to be exploited.

For the query we only need transversal operations,

namely a first layer of parallel BMs on $\log N$ pairs of logical qubits, and $\mathcal{O}(\log N)$ rounds of SQPMs on $\mathcal{O}(N)$ logical qubits. Since all these operations are transversal, there is no T cost associated with the query, and no MSF is needed.

To further understand the advantage of our query scheme in FTQC, we start by remarking the following important fact. Throughout common FTQCs, one needs to continuously extract the syndrome, which allows to identify the location of errors and consequently correct them. Typically, this is achieved by implementing repeated *stabiliser measurements*: these consist of the measurement of particular correlations between Pauli operators, that do not project the logical state, but allow to detect deviations from the logical space. For measuring the stabilisers fault-tolerantly, one usually needs to employ resource-consuming protocols [1, 58, 61, 71], with the introduction of a large number of ancillary qubits and many rounds of ‘ancilla-state verification’; moreover, commonly the whole stabiliser measurement needs to be repeated several times, in order to mitigate measurement errors [71]. Importantly, none of these techniques are necessary during our query scheme. This is because almost the whole procedure only contains *projective measurements* of the logical qubits in the Pauli basis. Since Pauli operators are transversal, these projections can be executed by simply measuring all the *physical* qubits in a block, and is automatically fault-tolerant; indeed, the obtained outcomes then not only contain the result of the desired logical measurement, but also the needed syndrome information. Furthermore, the only operation which does not consist of a trivial SQPM is the initial GT, which also requires to apply entangling gates for executing the Bell measurements. However, again we do not need mid-circuit syndrome extraction: as was shown by Knill in its seminal work [58], by executing the GT we also *directly* get the syndrome. In summary, the Clifford and intrinsically measurement-based character of the query allows us to execute it fault-tolerantly with transversal operations only, without injecting magic states, and without the need of mid-circuit stabiliser measurements and physical error-correction.

Neutral atom blueprint and QRAM factory

Here, we outline a detailed QRAM blueprint based on the concepts above, which is specifically designed for state-of-the-art neutral-atom processors.

Processor overview. We refer to reconfigurable processors as described in Refs.[9–11]. Specifically, atoms are trapped individually in an array of optical tweezers generated by a spatial light modulator (SLM). Physical qubits are encoded in electronic or nuclear levels of single atoms, with high-fidelity two-qubit gates [17, 18, 72] realised via Rydberg interactions at typical distances of few μm , and the possibility

of single-atom mid-circuit readout [9, 17, 73–76]. An additional tweezer array, generated by an acousto-optical deflector (AOD), can be employed to coherently *shuttle* selected atoms [43] across regions spanning hundreds of μm . Modern neutral atom processors use a ‘zoned’ design, with separate entangling and readout zones [9–11], allowing for remarkable flexibility of the system layout, and fueling recent QEC demonstrations [9, 10].

Neutral atom QRAM. We envision a realization of our QRAM module as in Fig. 1(d). The qubits \mathcal{A} supporting the RS $|\Phi\rangle$ are stored statically in SLM tweezer-traps, realising a ‘QRAM storage zone’. Between queries, low-rate syndrome extraction is performed to detect errors on $|\Phi\rangle$ due to decoherence, but error-correction is not needed as discussed above.

When the query starts, we interface the $\log N$ qubits in $\mathcal{I} \subset \mathcal{A}$ with the $\log N$ address QPU qubits; for this, we can employ coherent atom transport, or leverage pre-distilled Bell pairs for entanglement swapping, and perform BMs. As discussed above, this directly provides all the needed syndrome information to correct errors during the gates and the transport (via ‘Knill QEC’ [58]); remarkably, this also allows to detect loss errors during the transport as erasures. The rest of the query protocol can be implemented by means of local, highly parallelized operations only on the remaining *physical single atoms* in \mathcal{A} . Specifically, we can use developed techniques for single-qubit gates and measurements such as SLM-induced light shifts. For the measurements, (at least) two approaches are possible: (i) As shown in recent experiments with alkaline-earth atoms, specific atomic structures can be leveraged to implement single-qubit non-destructive measurements [17, 74–76]; (ii) Otherwise, coherent transport to a ‘readout zone’ can be used for collective, destructive readout of subsets of qubits, as was implemented in large-scale QC demonstrations with alkali atoms [9, 11].

Finally, we extract the remained $\log N + 1$ qubits in $\mathcal{F} \subset \mathcal{A}$, and feed them back to the QPU; for this, again we can use coherent transport, or pre-assembled Bell pairs. We note that the latter operation can also be performed at any time in advance to the start of the query, or in parallel with any previous step. This completes an end-to-end query.

QRAM factory. Central to our QRAM design is the preparation of $|\Phi\rangle$, which is carried out independently. For implementing U_{NOHE} as in Fig. 5, the major challenge is the non-local connectivity. Importantly, on a locally-connected processor, it cannot be coped with efficiently, as any method (including chains of swaps or teleportation) would jeopardize the fundamental error-resilience of the query (see the SM). Here, we leverage coherent atom transport to artificially build the needed connectivity while preserving the error-resilience; however, at the hardware level there are several stringent requirements, for this to be achieved efficiently. Below

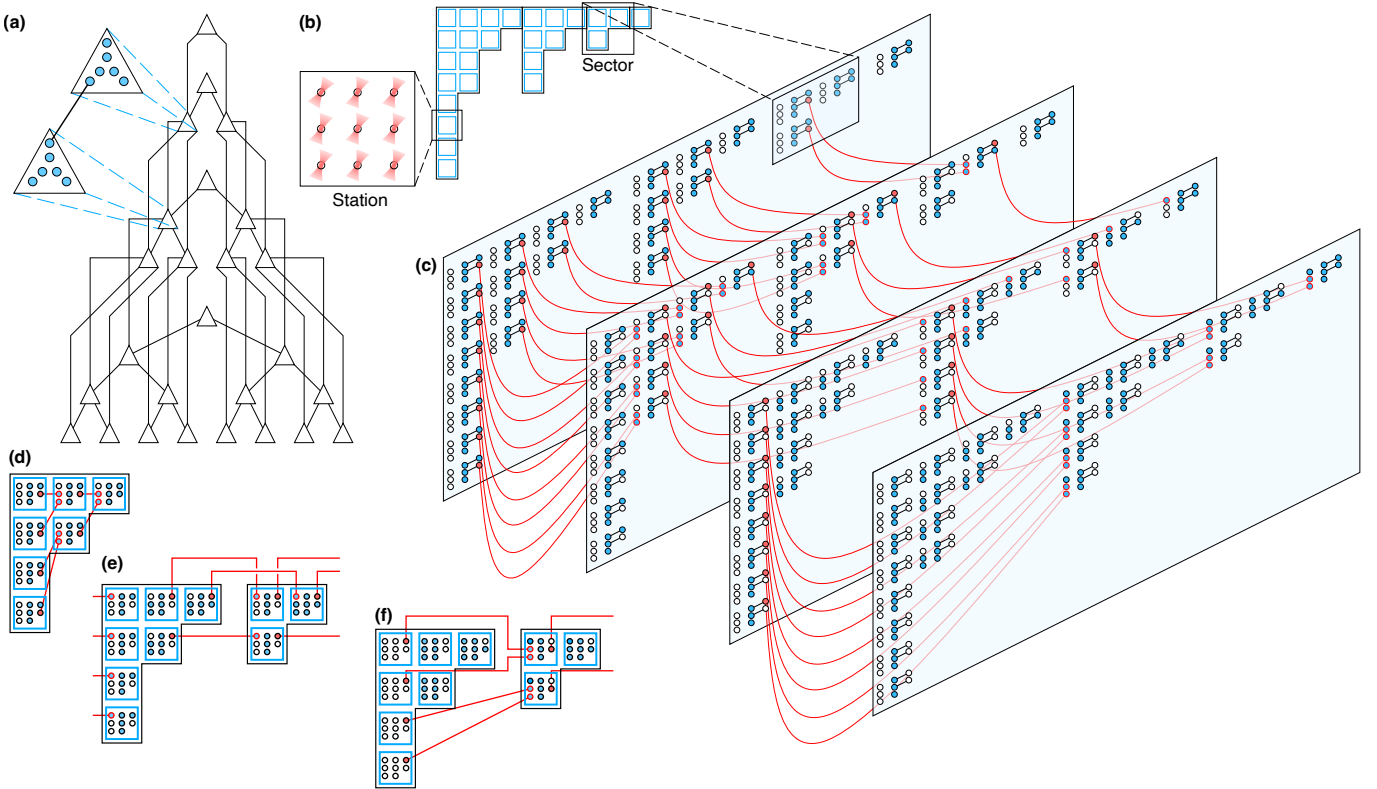


FIG. 9. **Rearrangement subroutine.** (a) The Bell-pair distribution described as a nested one-hot encoding bifurcation graph. (b) The grouping of SLM traps employed for describing the rearrangement protocol. (c) Depiction of the rearrangement. (d,e,f) Details of the rearrangement.

we first outline a generic scheme for preparing $|\Phi\rangle$ starting from a series of Bell pairs; then we present an end-to-end rearrangement protocol, whose output is the desired distribution of Bell pairs, positioned in space so to effectively reproduce the needed connectivity. Finally, we show that within our proposed QRAM factory prepares high fidelity RSs at the desired rates.

QRAM factory: preparation scheme. Any quantum circuit can be implemented via local operations on a set of suitably distributed Bell pairs (Bell-pair distribution, BPD), where the spatial distribution of the pairs depends on the connectivity required by the circuit; this is achieved by simply employing standard teleportation to shuttle the qubit information, and interfacing qubits locally. We now first focus on this paradigm for preparing $|\Phi\rangle$, and then elaborate on the preparation of the BPD in the paragraph below. This can be understood in two parts: first, we prepare $|\Phi^{(1)}\rangle$ and $|\Phi^{(2)}\rangle$; second, we implement B via partial BMs to assemble $|\Phi\rangle$. Importantly, the BPD for $|\Phi^{(1)}\rangle$ and $|\Phi^{(2)}\rangle$ is the same, allowing for efficient preparation.

As detailed in the SM, the needed BPD can be understood in terms of the ‘nested bifurcation graph’ (NBG) displayed in Fig. 9(a). Therein, as shown in the insets, triangles represent ‘stations’ where qubits are stored; links represent the presence of a Bell pair shared

between the triangles. For preparing $|\Phi^{(1)}\rangle$ and $|\Phi^{(2)}\rangle$, we simply iterate the application of the three-qubit gadgets displayed in Figs. 5(d) and 6(b) respectively; correspondingly, each station contains six qubits (three to support the teleported-in input, and three to teleport-out the output). Once the BPD is prepared according to the NBG, preparing $|\Phi\rangle$ is straightforward; remarkably, while $|\Phi^{(1)}\rangle$ needs $\mathcal{O}(\log N)$ steps to be prepared, instead $|\Phi^{(2)}\rangle$, thanks to its stabiliserness, is prepared with a *single* layer of parallel operations. The only nontrivial part that remains to be discussed is the preparation of the BPD, which we outline below.

QRAM factory: rearrangement subroutine. We now detail the rearrangement subroutine which allows us to efficiently prepare the BPD needed for assembling $|\Phi\rangle$. This is divided in exactly three rearrangement steps, independently on N . Remarkably, each step fully respects state-of-the-art constraints on parallel coherent transport with acousto-optical deflectors (AODs); namely, that columns and rows are transported rigidly.

As an underlying structure, we consider $8(2N - \log N - 2)$ static traps generated by a spatial-light modulator (SLM), spatially arranged as shown in Fig. 9(b). Specifically, we employ a hierarchy of two groupings: First, we divide the traps in $\log N$ main

sectors, labeled by $K = 0, 1, \dots, \log N - 1$; each sector K is further divided in $K + 1$ columns, labeled by $C = 0, 1, \dots, K$; moreover, column C in sector K is divided in 2^C stations, labeled by $S = 0, 1, \dots, 2^C - 1$. For each station, we consider 8 traps, which are arranged in a 3×3 checkerboard (with a defect in the right-bottom spot); we can thus label the traps within a station by two integers (x, y) , so that the right-bottom defect spot is $(1, 3)$. Together, the five labels (K, C, S, x, y) identify unambiguously one static trap. If we impose integer cartesian coordinates (X, Y) on the 2D plane, these are related with the adopted labeling as $X = x + 3C + 3K(K + 1)/2$ and $Y = y + 3S$.

To start, we position $5(2N - \log N - 2)$ qubits in the traps, such that 5 traps are occupied per station; precisely, we leave empty the leftmost column of each station, i.e. the traps $(3, y)$. This can be visualised in the first panel of Fig. 9(c). In each station, the qubits are initialised in the following configuration: the one in trap $(2, 3)$ is simply in the $|0\rangle$ state, while the others are divided in two entangled pairs of the form $\sum_{i,j} (-)^{ij} |i, j\rangle$, which is a two-qubit cluster state; for common language, we will refer to the involved qubits as 'Bell pairs', as they are locally equivalent. The pairs are such that $(1, 1)$ and $(1, 2)$ are entangled with $(2, 1)$ and $(2, 2)$ respectively; thus, the 'entanglement bonds' are horizontal as shown in Fig. 9(c). These pairs are prepared simultaneously in $\mathcal{O}(1)$ time by first initializing the involved qubits in the $|+\rangle$ state, and then moving them to the entangling zone to apply a CZ gate. After this, we proceed with three subsequent layers of rearrangements. We recall that the goal of this rearrangement is to spread the Bell pairs among the stations to realize the needed BPD, namely the one specified by the NBG in Fig. 9(a).

The first layer of rearrangements couples stations within the same sector as shown in Fig. 9(d); this is also displayed in the first transition of Fig. 9(c). Specifically, for each station (except the rightmost ones of each sector) we pick with the acousto-optical deflector (AOD) beams the qubit in trap $(1, 2)$, and we move it to a trap of a different station of the neighboring column. Precisely, depending on the starting basis, the arrival trap is either $(1, 2)$ or $(1, 3)$; we can write this rearrangement as

$$(K, C, S, 1, 2) \longrightarrow \left(K, C - 1, \left\lfloor \frac{S + 1}{2} \right\rfloor, 3, 2 + \lfloor S/2 \rfloor \right) \quad (41)$$

for $C > 0$ and $K > 0$. Crucially, note that across the whole construction (i.e., even considering all the sectors together), moved qubits starting with the same vertical coordinate end up with the same vertical coordinate, as well as qubits starting with the same horizontal coordinate end up with the same horizontal coordinate; thus, we can perform this rearrangement with a single AOD step.

The second layer of rearrangements couples neighboring sectors as shown in Fig. 9(e); this is also highlighted

in Fig. 9(c). Specifically, for all the stations in sector K (except those in the leftmost column), we pick the qubit in trap $(1, 1)$, and we move it to trap $(3, 1)$ of a corresponding station in the neighboring sector \mathcal{S}_{K-1} . Thus, the rearrangement reads

$$(K, C, S, 1, 1) \longrightarrow (K - 1, C, S, 3, 1) \quad (42)$$

for $C < K$ and $K > 0$. Again, a crucial feature is that moved qubits starting with the same vertical (horizontal) coordinate end up with the same vertical (horizontal) coordinate; thus, again we can execute this with a single AOD step.

The last layer of rearrangements couples the leftmost columns of each sector. Specifically, for each station in the leftmost column of sector K we pick the qubit in trap $(1, 3)$, and we move it to a station in the leftmost column of sector $K - 1$, as shown in Fig. 9(f) - and as also highlighted in Fig. 9(c); depending on the starting station, the arrival trap is either $(3, 2)$ or $(3, 3)$. Specifically, we perform the rearrangement

$$(K, C, S, 1, 1) \longrightarrow \left(K - 1, C - 1, \left\lfloor \frac{S + 1}{2} \right\rfloor, 3, 2 + \lfloor S/2 \rfloor \right) \quad (43)$$

for $K > 0$. Also in this third case, again motions are uniform in the vertical (horizontal) coordinates, such that this final layer of rearrangements can be executed in a single AOD step as well.

QRAM factory: optimized rearrangement. The rearrangement subroutine outlined above can be improved by compacting the main columns, so that the 2^C stations in column C are arranged in a 2D geometry. This has the main advantage that now the largest distance has a quadratic improvement, becoming of order $\mathcal{O}(\sqrt{N})$ instead of $\mathcal{O}(N)$; this will have an important impact on the time needed for the rearrangement.

QRAM factory: preparation rate. Here, we study the rate of synthesis of the RS $|\Phi\rangle$ in the QRAM factory. From the scheme above, it is manifest that three main components enter the count:

$$T_\Phi = T_g + T_m + T_r, \quad (44)$$

concerning the time employed for performing the gates (T_g), the measurements (T_m) and the atom rearrangement (T_r). We now estimate these one by one.

After the BPD is prepared via the rearrangement subroutine, we need to implement a circuit of depth $\mathcal{O}(\log N)$; moreover, circuit layers are interleaved by measurements for teleporting the qubits across the BPD. Thus, both T_g and T_m scale as $\mathcal{O}(\log N)$. Since in neutral-atom experiments [43] the typical gate time ($\tau_g \sim 100\text{ns}$) is much smaller than the typical readout time ($\tau \sim 500\mu\text{s}$), it follows that $T_m \gg T_g$, so that to all effects we can neglect T_g in our estimation. More precisely, for the measurement time we find that $T_m = 2\tau \log N$.

The most crucial estimation concerns T_r , i.e. the rearrangement time during the preparation of the BPD. For this, we follow the analysis in Refs. [43, 77], and assume that the time needed for moving an atom across a distance d grows like $T(d) = T_0\sqrt{d/d_0}$, where $T_0 \simeq 200\mu\text{s}$ is the time for moving an atom across a distance of $d_0 = 110\mu\text{m}$. For concreteness, let now l be the minimal distance between tweezers in the processor. In our rearrangement scheme, we have shown that only three main rearrangements are necessary; it can be easily seen that

the largest motion can never exceed a distance $3Nl/2$, which allows us to estimate $T_r \leq 3\sqrt{3N/2}T$, where $T = T_0\sqrt{l/d_0}$. With realistic numbers (e.g., $l = 3\mu\text{m}$ [9, 43]), one gets $T \simeq 35\mu\text{s}$.

An analogue concept applies if we adopt the optimized rearrangement mentioned above, with the difference that now the number of needed steps becomes 6, and the maximal traveled distance at each step becomes $3\sqrt{N}l/2$; it follows that now $T_r \leq 3\sqrt{6}TN^{1/4}$, as stated in the main text.

Supplemental material for Fast and error-correctable quantum RAM

Francesco Cesa,^{1,2,3,4,*} Hannes Bernien,^{1,5,6} and Hannes Pichler^{1,2,†}

¹*Institute for Quantum Optics and Quantum Information of the Austrian Academy of Sciences, 6020 Innsbruck, Austria*

²*Institute for Theoretical Physics, University of Innsbruck, 6020 Innsbruck, Austria*

³*Department of Physics, University of Trieste, Strada Costiera 11, 34151 Trieste, Italy*

⁴*Istituto Nazionale di Fisica Nucleare, Trieste Section, Via Valerio 2, 34127 Trieste, Italy*

⁵*Institute for Experimental Physics, University of Innsbruck, 6020 Innsbruck, Austria*

⁶*Pritzker School of Molecular Engineering, University of Chicago, Chicago, IL 60637, USA*

CONTENTS

I. Non-Cliffordness of the QRAM operation	1
A. Clifford hierarchy: basics	2
B. Non-Cliffordness of the QRAM operations	2
II. Nested one-hot encoding: supplemental details	3
A. Main idea of nested one-hot encoding	3
B. Formality: circuit decomposition	5
C. Graphical intuition: the nested bifurcation graph	9
III. Gate teleportation and Bell measurement conventions	9
A. Bell measurements	9
B. Gate teleportation: details	10
C. Comment	11
IV. QRAM factory Toffoli and T-gate cost	11
V. Noise resilience	11
A. Main setting	11
B. Unitary error models and conditional fidelity	12
C. Bounding the conditional fidelity	12
D. Error models	14
1. Continuous depolarisation errors	14
2. Operational Pauli errors	14
3. Operational phase-biased errors and erasure-conversion in neutral atom platforms	15
E. Mathematical details	15
1. Uniform distribution over the Hilbert space	15
2. Bounding the erroneously queried portion of the wavefunction	16
3. Bounding the conditional query fidelity	17
4. Statistics of the first n amplitudes	17
5. Distribution of the overlap	18
6. Calculating some nontrivial averages	19

I. NON-CLIFFORDNESS OF THE QRAM OPERATION

Here, we investigate the non-Cliffordness of the main building blocks of QRAM. For this, we first introduce the concept of Clifford hierarchy, and then show that the QRAM operation, in general, requires to implement circuits which are at deep layers in the hierarchy.

* francesco.cesa@uibk.ac.at

† hannes.pichler@uibk.ac.at

A. Clifford hierarchy: basics

Recall that the Clifford hierarchy

$$\mathcal{C}_0 \subset \mathcal{C}_1 \subset \mathcal{C}_2 \subset \mathcal{C}_3 \subset \dots \quad (1)$$

is defined as follows. First, \mathcal{C}_0 is set to be the Pauli group - that is, the group of all operators that can be written as a tensor product of Pauli operators X, Y, Z , possibly up to phases ± 1 and $\pm i$. Next, the K -th layer of the Clifford hierarchy is defined such that it maps Pauli operators to the Clifford layer below. That is,

$$\mathcal{C}_K = \{U \text{ such that } UPU^\dagger \in \mathcal{C}_{K-1} \ \forall \ P \in \mathcal{C}_0\}. \quad (2)$$

We note that, formally, $U \in \mathcal{C}_K$ for some K implies that $U \in \mathcal{C}_{K'}$ for any $K' \geq K$. Typically, we are interested in the *lowest* layer an operation U belongs to. For instance, if $U \in \mathcal{C}_K$ but $U \notin \mathcal{C}_{K-1}$, we say that U belongs to the layer K of the Clifford hierarchy.

With this definition, \mathcal{C}_1 is said to be the Clifford group; it contains important operations such as the Hadamard gate H , and the controlled-not CX and controlled-phase CZ gates. This can be easily proved to have all the features of a group. However, for $K \geq 2$, \mathcal{C}_K is not closed anymore: for instance, \mathcal{C}_2 is already universal for quantum computation, implying that in principle any operation $U \in \mathcal{C}_K$ belonging to any Clifford layer can be implemented to arbitrary precision by combining elements from \mathcal{C}_2 . For this reason, gates from \mathcal{C}_2 , such as the T-gate $T = e^{-iZ\pi/8}$ or the Toffoli gate $CCX = \mathbb{1} - 2|11-\rangle\langle 11-|$, are often referred to as ‘magic gates’, where the phrasing ‘quantum magic’ is frequently used for the notion of ‘non-Cliffordness’.

In general, given an operator U , it might not be evident what Clifford layer it falls in. However, there are specific classes of operators which are simple to analyze. One first instance are multi-controlled phase gates, of the form $C_n Z = \mathbb{1} - 2|1\rangle\langle 1|^{\otimes n+1}$. This is a gate acting on $n+1$ qubits, where n ‘control’ qubits trigger a conditional Z gate on the last ‘target’ qubit. It can be easily shown that with this definition, one has

$$C_n Z \notin \mathcal{C}_{n-1} \quad \text{and} \quad C_n Z \in \mathcal{C}_n, \quad (3)$$

meaning that $C_n Z$ belongs to layer n of the Clifford hierarchy. This can be seen very easily by induction, by noting that $(C_n Z)X(C_n) = X(C_{n-1}Z)$, where X acts on any of the $n+1$ involved qubits, and that $C_0 Z = Z$. We note that $C_2 Z$ equivalent to the Toffoli gate up to a Hadamard rotation, and in general $C_n Z$ is equivalent to the multi-controlled-not gate with n controls (up to a H on the target).

A second class of operators whose Clifford layer can be easily understood is given by the single-qubit operators of the form $T_n = e^{-iZ\pi/2^n}$, for which one can easily see that

$$T_n \notin \mathcal{C}_{n-1} \quad \text{and} \quad T_n \in \mathcal{C}_n. \quad (4)$$

Again, this can be seen by induction, as $T_n X T_n^\dagger = T_{n-1}$, and $T_0 = -iZ \in \mathcal{C}_0$. Note that $T_2 = T$ is the T gate, one of the most used ‘magic gates’ for fault-tolerant quantum computation.

B. Non-Cliffordness of the QRAM operations

We now discuss the generic non-Cliffordness of U_{QRAM} for a memory of size N . We note that in general the Clifford layer of U_{QRAM} depends on how the memory is composed. For instance, if we had $D_{\mathbf{x}} = 0$ for all memory locations, then $W_D = \mathbb{1}$, implying that also $U_{\text{QRAM}} = VW_D V^{-1} = \mathbb{1}$ is the identity. However, the composition of the memory only enters the loading operation, and it is simple to see that

$$W_D \in \mathcal{C}_0 \quad \forall \ D, \quad (5)$$

as it is always defined as a tensor product of Z operations and identities. Thus, in general all the non-Cliffordness of QRAM is captured by V , which does not depend on the dataset D . We now prove that for a memory of size N one must necessarily have

$$V \in \mathcal{C}_{\log N+1}. \quad (6)$$

To see this, recall that we defined the QRAM operation such that

$$U_{\text{QRAM}} |\mathbf{x}\rangle |0\rangle = |\mathbf{x}\rangle |D_{\mathbf{x}}\rangle. \quad (7)$$

Now, from the fact that, manifestly, one has $U_{\text{QRAM}}^2 = \mathbb{1}$, we immediately see that if $D_{\mathbf{x}} = 1$ for a specific \mathbf{x} , then one also has $U_{\text{QRAM}} |\mathbf{x}\rangle |1\rangle = |\mathbf{x}\rangle |0\rangle$. Now, let us choose the dataset as follows:

$$D_{\mathbf{x}} = \begin{cases} 0 & \text{if } \mathbf{x} = \mathbf{1} \equiv (1, 1, 1, \dots, 1) \\ 1 & \text{otherwise} \end{cases} \quad (8)$$

It follows now that $U_{\text{QRAM}} |\mathbf{x} \neq \mathbf{1}\rangle |1\rangle = |\mathbf{x} \neq \mathbf{1}\rangle |0\rangle$, while for unitarity we also must have $U_{\text{QRAM}} |\mathbf{1}\rangle |1\rangle = \pm |\mathbf{1}\rangle |1\rangle$, where at most one sign is undecided. More generally, with this choice we can write

$$U_{\text{QRAM}} |\mathbf{x}\rangle |B\rangle = (\pm)^{B\delta_{\mathbf{x},\mathbf{1}}} |\mathbf{x}\rangle |B \oplus \delta_{\mathbf{x},\mathbf{1}} \oplus 1\rangle. \quad (9)$$

We now envision the following protocol: (i) First, we apply U_{QRAM} ; (ii) Second, we apply $-Z$ to the bus qubit; (iii) We apply U_{QRAM} again. On the computational basis, this results in

$$-U_{\text{QRAM}} Z_{\text{bus}} U_{\text{QRAM}} |\mathbf{x}\rangle |B\rangle = (-)^{B+\delta_{\mathbf{x},\mathbf{1}}} |\mathbf{x}\rangle |B\rangle. \quad (10)$$

Also recalling that $U_{\text{QRAM}} = U_{\text{QRAM}}^\dagger$, this directly implies

$$U_{\text{QRAM}} Z_{\text{bus}} U_{\text{QRAM}}^{-1} = -Z_{\text{bus}} C_{\log N-1} Z. \quad (11)$$

Now, from the section above, it is simple to recognize that the operator to the right-hand side belongs to layer $\log N - 1$ of the Clifford hierarchy. This implies that, *with this choice of the memory D* , one has

$$U_{\text{QRAM}} \in \mathcal{C}_{\log N} \quad (\text{specific case of memory}). \quad (12)$$

However, as we noted above, while the entire operation U_{QRAM} depends on D , and specifically its Cliffordness depends on it, on the other hand V is independent on D . Thus, since by definition $U_{\text{QRAM}} = VW_D V^{-1}$ where $W_D \in \mathcal{C}_0$ always, from $U_{\text{QRAM}} \in \mathcal{C}_{\log N}$ it follows directly that $V \in \mathcal{C}_{\log N+1}$, as we wanted to prove.

II. NESTED ONE-HOT ENCODING: SUPPLEMENTAL DETAILS

Here, we present an extended discussion of the nested one-hot encoding defined in the main text and in the Methods, together with several explicit examples. This concept is borrowed from classical computer science and machine learning, and it allows us to capture the principal aspects of existing proposals for realizing a *fast* quantum RAM in a unified framework. Most importantly, we introduce the notion of *nested* one-hot encoding (NOHE), which enables intrinsic *error-resilience* - a fundamental requirement for a QRAM, both for near-term implementations and for quantum error-corrected modules.

This supplemental section is structured as follows. First, we provide an intuitive discussion of our nested OHE, where we also qualitatively explain its circuit decomposition. Next, we give detailed account for the circuit decomposition, showing how the claimed NOHE emerges. Finally, we present a graphical description of this discussion, which will be useful for understanding the rearrangement in the QRAM factory.

A. Main idea of nested one-hot encoding

We start by giving the intuition on the NOHE used in our work. To this end, let us consider an arbitrary bitstring $\mathbf{x} = (x_0, \dots, x_{\log N-1})$ consisting of $\log N$ bits. As mentioned in methods, within the standard OHE framework this is represented via a string of N bits, such that all are set to 0, except a ‘hot’ pointer bit, at position $\mu(\mathbf{x}) = \sum_K 2^K x_K$, which is set to 1. Specifically,

$$\mathbf{ohe}(\mathbf{x}) = (0, 0, \dots, 1, \dots, 0, 0), \quad (13)$$

where the 1 is at position $\mu(\mathbf{x})$. Note that $\mu(\mathbf{x})$ is nothing more than the integer whose binary representation is given by \mathbf{x} ; it thus establishes a one-to-one correspondence, and can be inverted on its image. For our quantum OHE, we are interested in encoding the computational basis states $|\mathbf{x}\rangle$ via

$$|\text{OHE}(\mathbf{x})\rangle = |0, 0, \dots, +, \dots, 0, 0\rangle, \quad (14)$$

where now the $|+\rangle$ state is at position $\mu(\mathbf{x})$, in fact playing the role of a quantum pointer. Importantly, note that in general $\langle \text{OHE}(\mathbf{x}) | \text{OHE}(\mathbf{y}) \rangle = (1 + \delta_{\mathbf{x},\mathbf{y}})/2$; that is, two states $|\text{OHE}(\mathbf{x})\rangle$ and $|\text{OHE}(\mathbf{y})\rangle$, corresponding to the OHEs

of orthogonal states $|\mathbf{x}\rangle$ and $|\mathbf{y}\rangle$, are *not* orthogonal. This highlights that we cannot design a quantum operation that deterministically *just* maps $|\psi\rangle \rightarrow |\text{OHE}(\psi)\rangle$ for any input state $|\psi\rangle$, as it would violate the distinguishability of orthogonal quantum states. In practice, the additional term $|\text{NOHE}(\mathbf{x})\rangle$ appearing can be understood as a necessary byproduct of the OHE operation, which guarantees reversibility.

Most importantly, the exact structure of $|\text{NOHE}(\mathbf{x})\rangle$ originates from a carefully designed protocol, which has crucial features in terms of noise-resilience. In essence, it constrains the propagation of errors in such a way that the resulting infidelity scales as $\mathcal{O}(\text{polylog}N)$, even though the space-time resources for employed are at best $\mathcal{O}(N \log N)$.

We postpone the discussion on the noise-resilience of our protocol to Section V. Here, we aim at explaining where the structure of $|\text{NOHE}(\mathbf{x})\rangle$ claimed in Methods originates from in practice. For this, we now intuitively sketch a protocol for implementing the map $|\psi\rangle \rightarrow |\text{OHE}(\psi)\rangle$; our circuit decomposition in Methods, which we discuss rigorously below, is nothing more than the mathematical formalization of this protocol.

Intuitive protocol. For simplicity, consider a classical address $|\mathbf{x}\rangle = |x_0, x_1, \dots, x_{\log N-1}\rangle$; all that follows generalizes by linearity to an arbitrary superposition state $|\psi\rangle = \sum_{\mathbf{x}} \psi_{\mathbf{x}} |\mathbf{x}\rangle$. We start by considering $\log N + 1$ sets of qubits, labeled by $K = 0, \dots, \log N$, such that sector K contains 2^K qubits. Now, qubit K of the address (i.e., the one supporting $|x_K\rangle$) is identified with the first qubit of sector K ; the first qubit of the last sector ($K = \log N$) is set to $|+\rangle$; all other qubits are initially set to zero. Thus, the initial configuration is of the form

$$\left[|x_0\rangle \right] \left[|x_1\rangle, |0\rangle \right] \left[|x_2\rangle |0\rangle^{\otimes 3} \right] \left[|x_3\rangle |0\rangle^{\otimes 7} \right] \left[|x_4\rangle |0\rangle^{\otimes 15} \right] \dots \left[|x_{\log N-1}\rangle |0\rangle^{\otimes N/2-1} \right] \left[|+\rangle |0\rangle^{\otimes N-1} \right], \quad (15)$$

where we used the parenthesis to highlight the sectors. We now proceed as follows.

First (step $t = 0$), we take the first qubit (the only one in sector $K_c = 0$), and we use it as control for a Friedkin gate targeting the first two qubits of each sector $K \geq 1$. That is, if $x_0 = 0$ nothing changes, while if $x_0 = 1$ the first two qubits of each sector are swapped. Precisely, assuming $x_0 = 1$, we get the state

$$\left[|x_0 = 1\rangle \right] \left[|0\rangle |x_1\rangle \right] \left[|0\rangle |x_2\rangle |0\rangle^{\otimes 2} \right] \left[|0\rangle |x_3\rangle |0\rangle^{\otimes 6} \right] \dots \left[|0\rangle |x_{\log N-1}\rangle |0\rangle^{\otimes N/2-2} \right] \left[|0\rangle |+\rangle |0\rangle^{\otimes N-2} \right]. \quad (16)$$

Second (step $t = 1$), we now use the first qubit of sector $K_c = 1$, and use it as control for Friedkin gates between the first and the third qubit of each sector $K \geq 2$; moreover, the second qubit of $K_c = 1$ acts as control of Friedkin gates targeting the second and the fourth qubit of each $K \geq 2$. Again, if $x_2 = 0$, nothing changes, while if $x_1 = 1$ we are in fact shifting by 2 sites the only nontrivial qubit in each sector. More precisely, if we previously had $x_0 = 0$ and now $x_1 = 1$, we would get the state

$$\left[|x_0 = 0\rangle \right] \left[|x_1 = 1\rangle |0\rangle \right] \left[|0\rangle^{\otimes 2} |x_2\rangle |0\rangle \right] \left[|0\rangle^{\otimes 2} |x_3\rangle |0\rangle^{\otimes 5} \right] \dots \left[|0\rangle^{\otimes 2} |x_{\log N-1}\rangle |0\rangle^{\otimes N/2-3} \right] \left[|0\rangle^{\otimes 2} |+\rangle |0\rangle^{\otimes N-3} \right], \quad (17)$$

while if we had $x_0 = 1$ and now $x_1 = 1$, instead we would get

$$\left[|x_0 = 1\rangle \right] \left[|0\rangle |x_1 = 1\rangle \right] \left[|0\rangle^{\otimes 3} |x_2\rangle \right] \left[|0\rangle^{\otimes 3} |x_3\rangle |0\rangle^{\otimes 4} \right] \dots \left[|0\rangle^{\otimes 3} |x_{\log N-1}\rangle |0\rangle^{\otimes N/2-4} \right] \left[|0\rangle^{\otimes 3} |+\rangle |0\rangle^{\otimes N-4} \right]. \quad (18)$$

This can be understood as follows: for $K \geq 2$, the only nontrivial (hot) qubit is shifted to position $\mu(x_0, x_1) = x_0 + 2x_1$; moreover, note that in sectors $K = 0, 1$ we have to all effects prepared $\mathbf{oh}e^{(0)}(\mathbf{x})$ and $\mathbf{oh}e^{(1)}(\mathbf{x})$ respectively.

This intuitive protocol for preparing $|\text{OHE}(\mathbf{x})\rangle$ continues by iterating this procedure: at each step (say, step t), we pick all the qubits in sector $K_c = t$, and use them as controls for Friedkin gates in the sectors $K \geq K_c + 1$. More precisely, qubit k in sector K_c controls the Friedkin gates targeting qubits k and $k + 2^{K_c}$ in each sector $K \geq K_c + 1$. After this step, all sectors $K = 0, 1, \dots, K_c + 1$ will be supporting $\mathbf{oh}e^{(K)}(\mathbf{x})$; all the others, i.e. for $K \geq K_c + 2$ on, will display the only nontrivial qubit, hosting the state $|x_K\rangle$ (or $|+\rangle$ for $K = \log N$), at position $\sum_{J=0}^{K_c} 2^J x_J$. For instance, after step $t = 4$, we get a state of the form

$$|x_0\rangle \left| \mathbf{oh}e^{(1)}(\mathbf{x}) \right\rangle \dots \left| \mathbf{oh}e^{(5)}(\mathbf{x}) \right\rangle \left[|0\rangle^{\otimes \mu-1} |x_6\rangle |0\rangle^{\otimes 2^6-\mu} \right] \left[|0\rangle^{\otimes \mu-1} |x_7\rangle |0\rangle^{\otimes 2^7-\mu} \right] \dots \left[|0\rangle^{\otimes \mu-1} |+\rangle |0\rangle^{\otimes N-\mu} \right], \quad (19)$$

where we set $\mu = \sum_{J=0}^4 2^J x_J$ for simplicity.

It follows that after step $t = \log N - 1$, the state is exactly the following: all sectors $K = 0, 1, \dots, \log N - 1$ display the state $\left| \mathbf{oh}e^{(K)}(\mathbf{x}) \right\rangle$; the last state the desired $|\text{OHE}(\mathbf{x})\rangle$. That is, we end up with

$$\begin{aligned} |\text{NOHE}(\mathbf{x}, +)\rangle &= \left| \mathbf{oh}e^{(0)}(\mathbf{x}) \right\rangle \left| \mathbf{oh}e^{(1)}(\mathbf{x}) \right\rangle \dots \left| \mathbf{oh}e^{(\log N-1)}(\mathbf{x}) \right\rangle |\text{OHE}(\mathbf{x})\rangle = \\ &= |\text{NOHE}(\mathbf{x})\rangle |\text{OHE}(\mathbf{x})\rangle, \end{aligned} \quad (20)$$

which is what we claimed.

B. Formality: circuit decomposition

Here, we discuss circuit decompositions of the nested one-hot encoding (NOHE) operation. In essence, the following is a formal analysis of the section above.

Formalities. We introduce an operation implementing the NOHE, i.e. acting on any state $|\psi\rangle$ on $\log N$ qubits as $|\psi\rangle \rightarrow |\text{NOHE}(\psi)\rangle$. Since this maps a Hilbert space of dimension N to one of dimension 2^{N-1} , so far this can be understood as an isometry. To write it as a unitary U_{NOHE} , we can introduce $N - 1 - \log N$ ancillary qubits, and first specify the action when these are all initialized in the $|0\rangle$ state:

$$U_{\text{NOHE}}^{(N)} |\psi\rangle \otimes |0\rangle^{\otimes N-1-\log N} = |\text{NOHE}(\psi)\rangle; \quad (21)$$

the complete unitary rotation remains undefined, and will be fixed e.g. by specifying the circuit decomposition. As in Methods, here the superscript N indicates the dimension of the input Hilbert space of the isometry, and we will omit it when it is clear from the context. Moreover, we will frequently just write $U_{\text{NOHE}} |\psi\rangle = |\text{NOHE}(\psi)\rangle$ when the dimensions are clear from the context. Specifically, when introducing a bus qubit, we might simply write

$$U_{\text{NOHE}}^{(2N)} |\psi\rangle |+\rangle = |\text{NOHE}(\psi, +)\rangle, \quad (22)$$

subtending that the input contains $2N - 2 - \log N$ ancillas initialized in the $|0\rangle$ state.

Unitary decomposition. We now formalize the concept above; that is, we discuss the decomposition of U_{NOHE} in basic gates stated in the Methods section,

$$U_{\text{NOHE}}^{(N)} = \left[\prod_{K=0}^{\log N-2} \prod_{J=K+1}^{\log N-1} \overline{CS}(K|J) \right] \left[\prod_{K=2}^{\log N-1} S_{K,2^{K-1}} \right], \quad (23)$$

that we introduced in Methods. Recall that here $S_{b,c} \equiv (\mathbb{1}_{b,c} + X_b X_c + Y_b Y_c + Z_b Z_c) / 2$ implements a swap of the qubits $b \leftrightarrow c$, i.e. $S_{b,c} |\psi_b\rangle \otimes |\phi_c\rangle = |\phi_b\rangle \otimes |\psi_c\rangle$ for any factorized state, and for $K < J$ we defined

$$\overline{CS}(K|J) = \prod_{\alpha=2^{K-1}}^{2^{(2^K-1)}} CS(\alpha|\alpha + 2^J - 2^K, \alpha + 2^J), \quad (24)$$

where

$$CS(a|b, c) = |0\rangle_a \langle 0| \otimes \mathbb{1}_{b,c} + |1\rangle_a \langle 1| \otimes S_{b,c}, \quad (25)$$

is the Friedkin gate (controlled-swap). Moreover, recall that we use the ordering convention that $\prod_{k=k_{\min}}^{k_{\max}} U_k = U_{k_{\max}} U_{k_{\max}-1} \dots U_{k_{\min}}$.

Unitary decomposition: formal proof. To show that the proposed decomposition indeed acts as desired, i.e. as

$$\left[\prod_{K=0}^{\log N-2} \prod_{J=K+1}^{\log N-1} \overline{CS}(K|J) \right] \left[\prod_{K=2}^{\log N-1} S_{K,2^{K-1}} \right] |\psi\rangle |0\rangle^{N-1-\log N} = |\text{NOHE}(\psi)\rangle \quad (\text{Claim 1}) \quad (26)$$

for any state $|\psi\rangle$ on $\log N$ qubits, by linearity it is sufficient to prove it when $|\psi\rangle$ is an arbitrary computational basis state $|\mathbf{x}\rangle$. We recall here that $|\text{NOHE}(\psi)\rangle$ is defined as follows:

$$\text{NOHE}(\mathbf{x}) = \left(\mathbf{oh}e^{(0)}(\mathbf{x}), \dots, \mathbf{oh}e^{(\log N-1)}(\mathbf{x}) \right), \quad (27)$$

where $\mathbf{oh}e_{\alpha}^{(K)}(\mathbf{x}) = x_K \delta_{\alpha, \mu(x_0, \dots, x_{K-1})}$ and $\mu(\mathbf{z}) = \sum_J x_J 2^J$ (see Methods).

For proving the circuit decomposition above, we proceed as follows. We start by rewriting the decomposition above as

$$\left[\prod_{K=0}^{\log N-2} \prod_{J=K+1}^{\log N-1} \overline{CS}(K|J) \right] \left[\prod_{K=2}^{\log N-1} S_{K,2^{K-1}} \right] = \left[\prod_{J=1}^{\log N-1} U^{(J \rightarrow J+1)} \right] \left[\prod_{K=2}^{\log N-1} S_{K,2^{K-1}} \right], \quad (28)$$

where we isolated the part $U^{(J \rightarrow J+1)} = \prod_{K=0}^{J-1} \overline{CS}(K|J)$ for $J \geq 1$. This can be seen straightforwardly by putting together the following two observations. First, that

$$\left[\overline{CS}(K|J), \overline{CS}(K'|J') \right] = 0 \quad \text{whenever} \quad J \neq J', \quad (29)$$

and independently on K and K' . Second, that on the left-hand side of Eq. (28) the operations $\overline{CS}(K|J)$ are ordered for increasing J (specifically, with smaller J to the right, i.e. acting first). With these considerations, it is simple to see that the gates in the product can be recollected as above.

We are now interested in proving the following preliminary claim:

$$U^{(J \rightarrow J+1)} |\text{NOHE}(x_0, x_1, \dots, x_{J-1})\rangle |x_J\rangle |0\rangle^{\otimes 2^J - 1} = |\text{NOHE}(x_0, x_1, \dots, x_J)\rangle \quad (\text{Claim 2}). \quad (30)$$

For this, we directly prove the stronger claim that for $J' \leq J$ we always have

$$\prod_{K=0}^{J'-1} \overline{CS}(K|J) |\text{NOHE}(x_0, \dots, x_{J-1})\rangle |x_J\rangle |0\rangle^{\otimes 2^J - 1} = |\text{NOHE}(x_0, \dots, x_{J-1})\rangle |x_J \mathbf{oh}e(x_0, x_1, \dots, x_{J'-1})\rangle |0\rangle^{\otimes 2^J - 2^{J'}}, \quad (31)$$

which reduces to our Claim 2 in Eq. (30) when $J' = J$. To prove Eq. (31), we proceed by induction on $1 \leq J' \leq J$. First, we can straightforwardly check that it holds for $J' = 1$, as

$$\overline{CS}(0|J) |\text{NOHE}(x_0, \dots, x_{J-1})\rangle |x_J\rangle |0\rangle^{\otimes 2^J - 1} = |\text{NOHE}(x_0, \dots, x_{J-1})\rangle \left[(1 - x_0) |0, 0\rangle + x_0 |0, x_J\rangle \right] |0\rangle^{\otimes 2^J - 2}, \quad (32)$$

where we used the definition (24), and it is easy to recognize that

$$(1 - x_0) |0, 0\rangle + x_0 |0, x_J\rangle = (1 - x_J) |0, 0\rangle + x_J \left[(1 - x_0) |0, 0\rangle + x_0 |0, 1\rangle \right] = x_J |\mathbf{oh}e(x_0)\rangle. \quad (33)$$

Next, we move to the inductive step $J' \rightarrow J' + 1$. Noting that $\prod_{K=0}^{J'} \overline{CS}(K|J) = \overline{CS}(J'|J) \prod_{K=0}^{J'-1} \overline{CS}(K|J)$, we use the inductive hypothesis to get

$$\begin{aligned} & \overline{CS}(J'|J) \prod_{K=0}^{J'-1} \overline{CS}(K|J) |\text{NOHE}(x_0, \dots, x_{J-1})\rangle |x_J\rangle |0\rangle^{\otimes 2^J - 1} = \\ & \stackrel{(1)}{=} \overline{CS}(J'|J) |\text{NOHE}(x_0, \dots, x_{J-1})\rangle |x_J \mathbf{oh}e(x_0, x_1, \dots, x_{J'-1})\rangle |0\rangle^{\otimes 2^J - 2^{J'}} = \\ & \stackrel{(2)}{=} \overline{CS}(J'|J) |\text{NOHE}(x_0, \dots, x_{J-1})\rangle \left[(1 - x_J) |0\rangle^{2^{\otimes J'}} + x_J |\mathbf{oh}e(x_0, x_1, \dots, x_{J'-1})\rangle \right] |0\rangle^{\otimes 2^J - 2^{J'}} = \\ & \stackrel{(3)}{=} |\text{NOHE}(x_0, \dots, x_{J-1})\rangle \left[(1 - x_J) |0\rangle^{\otimes 2^{J'+1}} + x_J |\mathbf{oh}e(x_0, x_1, \dots, x_{J'})\rangle \right] |0\rangle^{\otimes 2^J - 2^{J'+1}} = \\ & \stackrel{(4)}{=} |\text{NOHE}(x_0, \dots, x_{J-1})\rangle |x_J \mathbf{oh}e(x_0, x_1, \dots, x_{J'})\rangle |0\rangle^{\otimes 2^J - 2^{J'+1}}. \end{aligned} \quad (34)$$

In the chain of equalities above, we proceeded as follows. For (1) we explicitly used the inductive hypothesis. For (2) we just conveniently rewrite the expression in the parenthesis. For (3), we note that for any state $|\Psi_c\rangle$ on $2^J - 1$ qubits, we always have $\overline{CS}(J'|J) |\Psi_c\rangle |0\rangle^{\otimes 2^{J'+1}} = |\Psi_c\rangle |0\rangle^{\otimes 2^{J'+1}}$, and that moreover

$$\begin{aligned} & \overline{CS}(J'|J) |\text{NOHE}(x_0, \dots, x_{J-1})\rangle |\mathbf{oh}e(x_0, x_1, \dots, x_{J'-1})\rangle |0\rangle^{\otimes 2^{J'}} = \\ & \stackrel{(3a)}{=} |\text{NOHE}(x_0, \dots, x_{J-1})\rangle \left[(1 - x_{J'}) |\mathbf{oh}e(x_0, x_1, \dots, x_{J'-1})\rangle |0\rangle^{\otimes 2^{J'}} + x_{J'} |0\rangle^{\otimes 2^{J'}} |\mathbf{oh}e(x_0, x_1, \dots, x_{J'-1})\rangle \right] = \\ & \stackrel{(3b)}{=} |\text{NOHE}(x_0, \dots, x_{J-1})\rangle |\mathbf{oh}e(x_0, x_1, \dots, x_{J'})\rangle. \end{aligned} \quad (35)$$

Herein, for equality (3a) we make explicit use of the definition (24), and of the NOHE structure in Eq. (27). Specifically, from Eq. (24) we see that $\overline{CS}(J'|J)$ is an operation where qubits $\{2^{J'} - 1, \dots, 2(2^{J'} - 1)\}$ act as controls; from

Eq. (27) we see that among these qubits, we can only have a $|1\rangle$ state anywhere if $x_{J'} = 1$; thus, we infer the first part of the equality, that if $x_{J'} = 0$ the target qubits are unaffected. For the second part of the equality, again from Eq. (27) we see that if instead $x_{J'} = 1$, then among the control qubits of $\overline{CS}(J'|J)$, we have one, and only one $|1\rangle$ state at position $2^{J'-1} - 1 + \mu_{J'}(x_0, \dots, x_{J'-1})$; moreover, from Eq. (24), we see that this corresponds exactly to the one control, whose first target is the pointer of $|\mathbf{ohc}(x_0, \dots, x_{J'-1})\rangle$: this therefore shifts the pointer by $2^{J'}$ positions, resulting in step (3a) above. Finally, for step (3b) we simply rewrite the standard OHE. Together, these equalities thus result in step (3) of Eqs. (34). The proof of Eqs. (34) is thus completed by noting that in step (4) we just rewrite the standard OHE as before. In summary, this therefore proves the inductive step, and thus Claim 2 in Eq. (30).

We now use this result to prove Claim 1 in Eq. (26). For this, we use the form in Eq. (28), and we first note that the first part of the decomposition, i.e. the swap gates, has the effect of reordering the input as

$$\left[\prod_{K=2}^{\log N-1} S_{K,2^k-1} \right] |\mathbf{x}\rangle |0\rangle^{\otimes N-\log N-1} = \bigotimes_{J=0}^{\log N-1} \left[|x_J\rangle |0\rangle^{2^J-1} \right], \quad (36)$$

where again by linearity we only focus on computational-basis states as inputs. Thus, our goal for proving Claim 1 in Eq. (26) is now reduced to showing that

$$\left[\prod_{J=1}^{\log N-1} U^{(J \rightarrow J+1)} \right] \left[\bigotimes_{J=0}^{\log N-1} |x_J\rangle |0\rangle^{2^J-1} \right] = |\text{NOHE}(\mathbf{x})\rangle. \quad (37)$$

For this, it is sufficient to make direct use of Claim 2 in Eq. (30). Specifically, we can now prove that for any $2 \leq J' \leq \log N$ the following holds:

$$\left[\prod_{J=1}^{J'-1} U^{(J \rightarrow J+1)} \right] \left[\bigotimes_{J=0}^{\log N-1} |x_J\rangle |0\rangle^{2^J-1} \right] = |\text{NOHE}(x_0, \dots, x_{J'-1})\rangle \left[\bigotimes_{J=J'}^{\log N-1} |x_J\rangle |0\rangle^{2^J-1} \right]. \quad (38)$$

Again, to see this we proceed by induction on $2 \leq J' \leq \log N$. First, for $J' = 2$ we can check that

$$\begin{aligned} & U^{(1 \rightarrow 2)} \left[\bigotimes_{J=0}^{\log N-1} |x_J\rangle |0\rangle^{2^J-1} \right] = \\ &= \left[U^{(1 \rightarrow 2)} |\text{NOHE}(x_0)\rangle |x_1\rangle |0\rangle \right] \left[\bigotimes_{J=2}^{\log N-1} |x_J\rangle |0\rangle^{2^J-1} \right] = \\ &= |\text{NOHE}(x_0, x_1)\rangle \left[\bigotimes_{J=2}^{\log N-1} |x_J\rangle |0\rangle^{2^J-1} \right], \end{aligned} \quad (39)$$

where we made explicit use of Eq. (30) for the case $J = 1$. Finally, for the inductive step $J' \rightarrow J' + 1$, we can use the straightforward rewriting

$$\prod_{J=1}^{J'} U^{(J \rightarrow J+1)} = U^{(J' \rightarrow J'+1)} \prod_{J=1}^{J'-1} U^{(J \rightarrow J+1)} \quad (40)$$

to recognize that the following chain of equalities holds true:

$$\begin{aligned} & U^{(J' \rightarrow J'+1)} \prod_{J=1}^{J'-1} U^{(J \rightarrow J+1)} \left[\bigotimes_{J=0}^{\log N-1} |x_J\rangle |0\rangle^{2^J-1} \right] = \\ & \stackrel{(1)}{=} U^{(J' \rightarrow J'+1)} |\text{NOHE}(x_0, \dots, x_{J'-1})\rangle \left[\bigotimes_{J=J'}^{\log N-1} |x_J\rangle |0\rangle^{2^J-1} \right] = \\ & \stackrel{(2)}{=} \left[U^{(J' \rightarrow J'+1)} |\text{NOHE}(x_0, \dots, x_{J'-1})\rangle |x_{J'}\rangle |0\rangle^{\otimes 2^{J'}-1} \right] \left[\bigotimes_{J=J'+1}^{\log N-1} |x_J\rangle |0\rangle^{2^J-1} \right] = \\ & \stackrel{(3)}{=} |\text{NOHE}(x_0, \dots, x_{J'})\rangle \left[\bigotimes_{J=J'+1}^{\log N-1} |x_J\rangle |0\rangle^{2^J-1} \right]. \end{aligned} \quad (41)$$

Specifically: For equality (1) we explicitly use the inductive hypothesis; For (2) we simply recollected part of the product; For (3) we used Claim 2 in Eq. (30). Altogether, this proves by induction that Eq. (37), thereby directly proving the desired Claim 1 in Eq. (26).

Parallelization. By naively counting from the decomposition in Eq. (23), it seems that a (realistic) circuit implementing $U_{\text{NOHE}}^{(N)}$ requires $\mathcal{O}(\log^2 N)$ logical steps. This is due to the following fact: even though all the gates in the inner product over J commute, and thus *might* be executed in parallel, nevertheless they are manifestly non local: for any fixed K , we have 2^K control qubits, each acting on $\log N - K - 2$ targets; thus, we cannot assume that all those gates are executed in parallel on a real device, even though they commute.

Intuitively, this can also be understood by recalling the scheme introduced in Section II A. Therein, for implementing $U_{\text{NOHE}}^{(2N)}$, we proceeded with ‘main steps’ labeled by $t = 1, 2, \dots, \log N - 1$. However, during step t each qubit in sector $K_c = t$ was used as a control-qubit for $\log N - t$ Friedkin gates - those involving sectors $K = K_c + 1, K_c + 2, \dots, \log N$. Even though they commute, these cannot be realistically executed in parallel, as they share a common control qubit; thus, step t involves $\log N - t$. It follows that the total runtime of the protocol for $U_{\text{NOHE}}^{(2N)}$ is proportional to $\sum_{t=0}^{\log N - 1} (\log N - t) = \log N (\log N + 1)/2$. Consequently, for implementing $U_{\text{NOHE}}^{(N)}$ via the decomposition in Eq. (23) the runtime is $\log N (\log N - 1)/2 = \mathcal{O}(\log^2 N)$.

In contrast, as mentioned in the main text and in Methods, here we show that $U_{\text{NOHE}}^{(N)}$ can be parallelized to a circuit of depth $\mathcal{O}(\log N)$. Specifically, we now show that the decomposition in Eq. (23) can be rearranged as

$$U_{\text{NOHE}}^{(N)} = \left[\prod_{T=1}^{T_f} \prod_{K=0}^{D_T} \overline{CS}(K_T - K | J_T + K) \right] \left[\prod_{K=2}^{\log N - 1} S_{K, 2^{K-1}} \right], \quad (42)$$

where the final step is $T_f = 2 \log N - 3$ and we set the indexes $K_T = \lfloor \frac{T-1}{2} \rfloor$, $J_T = \min \{T, \log N - 1\}$ and $D_T = K_T - \max \{0, T - \log N + 1\}$. Importantly, for a fixed $1 \leq T \leq T_f$ one always has

$$\left[\overline{CS}(K_T - K | J_T + K), \overline{CS}(K'_T - K' | J_T + K') \right] = 0 \quad (43)$$

for $0 \leq K, K' \leq D_T$; moreover, for a fixed T , the gates contained in the product over K are such that any qubit (be it a control or a target) only appears once, so that the product over K can be performed locally and in parallel for any T . From these two considerations, it follows that all the operations in the product over K can be performed in parallel on a real processor; this therefore results in exactly $2(\log N - 1)$ parallel circuit steps (also accounting for the initial swaps).

To prove Eq. (42), it is sufficient to recall the main intuition behind our protocol, and modify as follows. Specifically, below we modify the steps in Section II A in such a way that the protocol eventually has duration $\mathcal{O}(\log N)$. Note that below we use the variable t' to identify steps of runtime $\mathcal{O}(1)$.

For steps $t' = 0$ and $t' = 1$, we proceed as in the previous scheme: we use the only one qubit of sector $K_c = 0$ as the control of Friedkin gates in sectors $K = 1$ and $K = 2$ respectively.

During step $t' = 2$, we use again the qubit of sector $K_c = 0$, now as control of a Friedkin gate between the first two qubits in sector $K = 3$; but crucially, in parallel we can also use the qubits in sector $K_c = 1$ as controls of Friedkin gates in sector $K = 2$.

For step $t' = 3$ we proceed similarly: the qubit of sector $K_c = 0$ controls Friedkin gates in sector $K = 4$, while in parallel the qubits of sector $K_c = 1$ act as controls for Friedkin gates in sector $K = 3$.

For step $t' = 4$, the qubits in sectors $K_c = 0$ and $K_c = 1$ control, respectively, Friedkin gates in sectors $K = 5$ and $K = 4$. But in parallel, now the qubits in sector $K_c = 2$ can be used as controls for Friedkin gates in sector $K = 3$.

The main idea of our parallelized protocol proceeds by iterating this procedure: the main principle is that we start using qubits in sector K as controls of Friedkin gates, as soon as they do not need to be involved as targets anymore. To calculate the new duration of the protocol, let t'_K be the step at which qubits from sector K start to be employed as controls; thus, for instance we have already seen that $t'_0 = 0$ and $t'_1 = 2$. First, note that at time t'_K sector K is interfaced with sector $K + 1$. Then, one can see that $t'_{K+1} = t'_K + 2$. Indeed, at step t'_K sector K acts as control in Friedkin gates where sector $K + 1$ is involved as target; at step $t'_K + 1$, sector $K + 1$ is ready to be employed as control, but it must wait because sector $K + 2$ is now interfaced with sector K ; finally, at step $t'_K + 2$ sector $K + 2$ is ready to undergo Friedkin gates controlled by qubits in sector $K + 1$. Thus, we get $t'_K = 2K$. For implementing $U_{\text{NOHE}}^{(2N)}$, we know that the largest sector which is employed as control is $K_c = \log N - 1$, which only controls Friedkin gates with qubits in sector $K = \log N$. Thus, the last step occurs exactly at $t'_{\log N - 1} = 2 \log N - 2$; considering that we start counting from $t' = 0$, it follows that the total number of steps is $2 \log N - 1$. Thus, for implementing $U_{\text{NOHE}}^{(N)}$ the runtime is exactly $T_f = 2 \log N - 3$ as claimed.

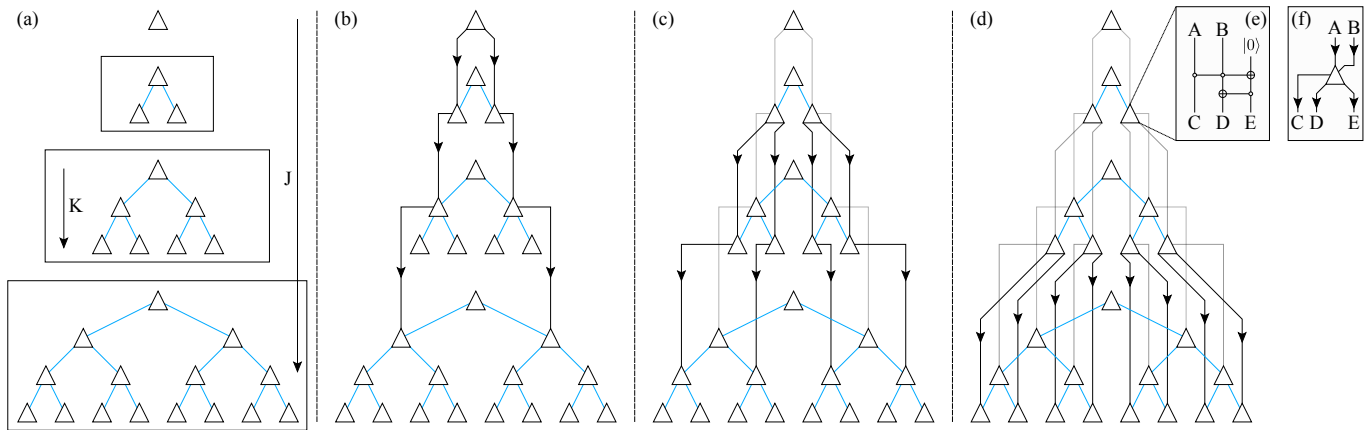


FIG. 1. **Nested bifurcation graph construction.** (a) We start with $\log N$ bifurcation graphs of increasing size; triangles represent vertexes, while blue lines are the edges of the sub-graphs. Here the specific example is with $N = 16$. (b-d) We connect subsequent sub-graphs by adding ‘cascaded’ patterns. Here different shades of black for the edges only help reading the figure. (e) To each vertex in the resulting graph we associate the gadget displayed, which takes as input a two-qubit state and outputs a three-qubit state; specifically, we introduce an additional qubit initialised in the $|0\rangle$ state, and execute a Toffoli gate followed by a controlled-not. (f) Details of how the edges connected to each edge in the graph refer to input and output qubits.

C. Graphical intuition: the nested bifurcation graph

Here, we introduce an understanding of OHE operations in terms of graphs and (classical) logical circuits. This has the threefold purpose of (i) shining light on the circuit decomposition in Eq. (23), (ii) understanding the relation of our NOHE with known QRAM proposals and (iii) preparing for the dynamical rearrangements subroutine that we will employ in the QRAM factory. The following construction proceeds in two steps: First, we define a ‘nested bifurcation graph’ (NBG); Second, we relate this to a logical circuit that characterises the OHE.

The NBG is constructed as shown in Fig. 1. We start by drawing an array of binary tree graphs of increasing depth $J = 1, 2, \dots, \log N$ as in Fig. 1(a); we label the sub-graphs by J , so that sub-graph J features $2^J - 1$ vertexes. The edges of these sub-graphs are depicted in blue, and they are *directed*: we interpret each edge as ‘incoming’ from the top and ‘outgoing’ towards the bottom. As a convention, we count the layers of a sub-graph J as $K = 0, 1, \dots, J - 1$ starting from the top, so that layer K contains 2^K vertexes. Next, we connect the sub-graphs as shown in Figs. 1(b-d); just for clarity, we depict these new edges in different shades of black, and highlight their orientation. In a nutshell, for every sub-graph $J = 1, 2, \dots, \log N - 1$ we consider the vertexes in the last layer (i.e., $K = J - 1$), and for each of these vertexes we start two ‘cascaded’ pattern; these patterns essentially ‘pass through’ layers $K = J$ of each subsequent sub-graph. This eventually results in a graph where bifurcation graphs of increasing size are nested the one with the other.

We now relate the NBG with the NOHE as follows. To each vertex in the NBG we associate the logic gadget displayed in Fig. 1(e): this formally takes two inputs and returns three outputs, and in fact realises a reversible version of the logical AND operation with quantum gates. In Fig. 1(f) we show explicitly how the entries of each vertex in a graph are related to the entries of the gadgets.

III. GATE TELEPORTATION AND BELL MEASUREMENT CONVENTIONS

A. Bell measurements

In this work, we adopt the following conventions. We define the two-qubit Bell basis as

$$|\Psi_{a,b}\rangle = \frac{1}{2} \sum_{i,j} (-1)^{ai+bj+ij} |i,j\rangle, \quad (44)$$

where $(a,b) \in \{0,1\}^2$. For simplicity, we will commonly refer to the first element as $\Psi \equiv \Psi_{0,0}$. It can be easily verified that $\{\Psi_{a,b}\}$ is indeed a complete orthonormal basis, i.e. that $\langle \Psi_{a,b} | \Psi_{a',b'} \rangle = \delta_{a,a'} \delta_{b,b'}$. We note that this is related to another common choice for the Bell basis $|\bar{\Psi}_{a,b}\rangle \equiv 2^{-1/2} \sum_k (-1)^{ak} |k, k \oplus b\rangle$ by the simple transformation

$$\bar{\Psi}_{a,b} = (\mathbb{1} \otimes \mathbb{H}) \Psi_{a,b}.$$

We note that our Bell basis is related to the conventional Z basis as $|\Psi_{a,b}\rangle = \text{CZ} \mathbb{H}^{\otimes 2} |a,b\rangle$. It follows that we can perform BMs, i.e. measurements in the two-qubit Bell basis, by (i) First, applying a controlled-phase gate CZ, and (ii) Second, measuring the X basis of both qubits. We note that for perfect equivalence we should as well (iii) Third, apply a final CZ gate; however, we will typically not be interested in the measured qubits after the measurement, so we will always skip this unnecessary step. Then, measuring $X = \pm 1$ on the first (second) qubit is equivalent to measuring $a = (1 \pm 1)/2$ (and $b = (1 \pm 1)/2$ respectively). In summary, a BM with outcomes (a, b) is described by the ‘projector’

$$\mathbb{P}_{\text{BM}}^{(a,b)} = \frac{1 + (-)^a X}{2} \otimes \frac{1 + (-)^b X}{2} \text{CZ}. \quad (45)$$

Note that this is not formally a projector, as it is not idempotent (that is, $\mathbb{P}^{(a,b)} \mathbb{P}^{(a,b)} \neq \mathbb{P}^{(a,b)}$); in contrast, with this definition $\text{CZ} \mathbb{P}^{(a,b)}$ would technically be a projector.

B. Gate teleportation: details

We now discuss the conventional paradigm of GT. Let $U : \mathcal{H}^{(n)} \rightarrow \mathcal{H}^{(m)}$ be any quantum operation, e.g. a unitary gate, whose input is the Hilbert space of n qubits. Note that for what follows the codomain can be of any size. For instance, in our case we are interested in the GT of V , so that $n = \log N$ (where N is, as usual, the size of the memory) and $m = 2N - 1$. Then, the goal of GT is to apply U to any arbitrary input state $|\psi\rangle \in \mathcal{H}^{(n)}$. For this, it leverages a pre-assembled resource-state (RS) of the form $|\Phi_U\rangle = (\mathbb{1} \otimes U) |\Psi\rangle^{\otimes n}$. That is, we apply U on one partition of n Bell pairs. Explicitly, this therefore reads

$$|\Phi_U\rangle = \frac{1}{2^n} \sum_{\mathbf{y}, \mathbf{z}} (-)^{\mathbf{y} \cdot \mathbf{z}} |\mathbf{y}\rangle_{\mathcal{I}} \otimes U |\mathbf{z}\rangle_{\mathcal{F}}, \quad (46)$$

where we labeled by \mathcal{I} the first partition of the Bell pairs. Note that $|\mathcal{F}| = m$; thus, according to the discussion above, we might have $|\mathcal{F}| \neq |\mathcal{I}|$ in general.

Let the input state $|\psi\rangle$ be supported on \mathcal{R} , with $|\mathcal{R}| = |\mathcal{I}| = n$. Then, GT proceeds by performing Bell measurements between corresponding qubits in \mathcal{R} and \mathcal{I} . Let $\mathbf{m} = (\mathbf{a}, \mathbf{b})$ be the measurement outcomes. It is simple to show that all the measurement outcomes are equiprobable, thus every \mathbf{m} has probability 2^{-2n} . Moreover, the resulting (normalized) conditional state on the unmeasured qubits \mathcal{F} is exactly

$$2^{2n} \mathbb{P}_{\text{BM}}^{(a,b)} \left[|\psi\rangle_{\mathcal{R}} |\Phi_U\rangle_{\mathcal{I} \cup \mathcal{F}} \right] = U P_{\mathbf{m}} |\psi\rangle, \quad (47)$$

where the Pauli operator $P_{\mathbf{m}} \in \mathcal{C}_0$ takes the form

$$P_{\mathbf{m}} = X^{\otimes \mathbf{b}} Z^{\otimes \mathbf{a}}. \quad (48)$$

Up to this point, GT only needed Clifford operations (namely, n parallel Bell measurements) to be implemented - once the RS $|\Phi_U\rangle$ is given.

Crucially, note that the Pauli correction $P_{\mathbf{m}}$ acts on $|\psi\rangle$ *prior* to the application of the desired operation U . Thus, to complete our protocol, in the standard GT paradigm we need to apply the *byproduct* correction $U P_{\mathbf{m}} U^{-1}$: it is easy to see that after this, the obtained state is exactly the desired $U |\psi\rangle$.

Unfortunately, in general this strategy is only efficient when U is relatively simple. This can be understood elegantly in terms of the Clifford hierarchy: note indeed that if $U \in \mathcal{C}_K$ belongs to a certain level of the Clifford hierarchy, then the byproduct generally is just one layer below. More precisely,

$$U \in \mathcal{C}_K \quad \implies \quad U P_{\mathbf{m}} U^{-1} \in \mathcal{C}_{K-1} \quad \text{for at least some } \mathbf{m}. \quad (49)$$

Indeed, GT has proved to be a very successful paradigm in fault-tolerant QC, where it allows to implement simple non-Clifford gates from \mathcal{C}_2 , e.g. the T gate, via Clifford operations only. Specifically, this is a crucial building-block of many QEC schemes, which employ GT to inject T gates. However, when U is very deep in the Clifford hierarchy, GT is not advantageous: in practice, even though the Clifford complexity is lowered by one layer via GT, the fact that the byproduct correction is random compensates this achievement, as it imposes the application of an unpredictable, deeply non-Clifford gate.

C. Comment

In principle, QRAM seems to clearly fall into the category of operations which do not benefit from GT. Indeed, as we showed $V \in \mathcal{C}_{\log N+1}$ is very deep in the Clifford hierarchy, and in general correcting for any byproduct is extremely hard, specially on a fault-tolerant processor. One of our most important results in this work is realising that the byproduct does *not* need to be corrected: instead, we can accept *any* random outcome VP_m from the GT, and still continue with the query.

IV. QRAM FACTORY TOFFOLI AND T-GATE COST

In a fault-tolerant implementation, the cost is evaluated in terms of basic non-Clifford gates. We note that the only non-Clifford subroutine in our QRAM design is the preparation of the part of the RS related to $|\Phi^{(1)}\rangle$, which can be implemented e.g. via U_{NOHE} in Eq. (23). Here, one can immediately recognize that the native non-Clifford gate is the Toffoli gate; the Toffoli count for implementing $U_{\text{NOHE}}^{(N)}$ is given by

$$\sum_{K=0}^{\log N - 2} \sum_{J=K+1}^{\log N - 1} 2^K = N - \log N - 1, \quad (50)$$

where we used the fact that $\sum_{K=0}^n K 2^K = (n-1)2^{n+1} + 2$. For querying a memory of size N , we need to implement $U_{\text{NOHE}}^{(2N)}$, implying a Toffoli count

$$n_{\text{Toffoli}} = 2N - \log N - 2. \quad (51)$$

In principle, each Toffoli gate can be implemented fault-tolerantly with an ad-hoc distillation procedure.

We note that standard paradigms often rely on the injection of T gates, and thus employ distillation of T states. In this respect, the Toffoli gate can be decomposed in the Clifford + T setting in several ways, depending on the figure of merit that is more convenient to optimize. Importantly, in our setting any non-Clifford gate is implemented offline, in the QRAM factory. This suggests that it might be convenient to sacrifice circuit-depth, to minimize the T cost. In this spirit, decomposition of the Toffoli in 4 gates of the T type, plus Clifford operations might be favorable.

V. NOISE RESILIENCE

Here, we discuss the noise-resilience of our proposed QRAM implementation. We first provide an analytical analysis. Then, we discuss the error models our numerical analysis is based on.

This supplemental section is organised as follows. First, we introduce the main setting and notation. Then, we define the error models we are interested in, and the key figures of merit, e.g. the query fidelity F_{QRAM} . Next, we present the main steps in bounding F_{QRAM} ; this section relies on several mathematical results, which are outsourced to a final section. Then, we explicit and justify the error models analysed numerically. Finally, we present the mathematical methods employed in the previous sections.

A. Main setting

Given a dataset $D = \{D_{\mathbf{x}}\} \in \{0,1\}^N$ and an address state $|\psi\rangle = \sum_{\mathbf{x}} \psi_{\mathbf{x}} |\mathbf{x}\rangle$, an ideal answer to the QRAM query is provided by the state

$$|\psi_D\rangle = \sum_{\mathbf{x}} \psi_{\mathbf{x}} |\mathbf{x}\rangle \otimes |D_{\mathbf{x}}\rangle. \quad (52)$$

For each dataset D stored in the memory, let us now consider a generic Kraus map, specified by a set of Kraus operators $\{K_{D,k}\}$, such that $\sum_k K_{D,k}^\dagger K_{D,k} = \mathbb{1}$; we write a faulty query to the memory as

$$|\psi\rangle \xrightarrow{\text{faulty query to } \mathcal{M}} \rho_{\text{out}}(\psi|D) = \sum_k K_{D,k} |\psi\rangle \langle\psi| K_{D,k}^\dagger; \quad (53)$$

thus, we refer to the index k as labeling ‘error configuration’. In general, $K_{D,k}$ also acts on the ancillas, so that the term $K_{D,k} |\psi\rangle \langle \psi| K_{D,k}^\dagger$ also has support on $\mathcal{O}(N)$ ancillas. We are thus interested in the marginal state, when these ancillas are traced out; we therefore define

$$\rho(\psi|D) = \text{Tr}_{\text{rest}} \left[\rho_{\text{out}}(\psi|D) \right], \quad (54)$$

where Tr_{rest} performs the partial trace over any ancillary qubit.

When the dataset D is specified and the address state is $|\psi\rangle$, the fidelity of the query can be defined as the quantity

$$\begin{aligned} F_{\text{QRAM}}(\psi|\mathcal{M}) &= \langle \psi_{\mathcal{M}} | \rho(\psi|\mathcal{M}) | \psi_{\mathcal{M}} \rangle = \\ &= \sum_{\alpha,k} |\langle \psi_{\mathcal{M}}, \alpha | K_{\mathcal{M},k} | \psi \rangle|^2, \end{aligned} \quad (55)$$

where $\{|\alpha\rangle\}$ is any orthonormal basis on the ancillary Hilbert space. To capture the generic reliability of our QRAM architecture, we are interested in evaluating the following query fidelity:

$$F_{\text{QRAM}} = \frac{1}{2^N} \sum_{\mathcal{M}} \int_{\mathcal{H}} d\psi F_{\text{QRAM}}(\psi|\mathcal{M}); \quad (56)$$

therein, we average over all possible memory configurations (the factor 2^{-N} is the related normalization), and also over all possible states in the Hilbert space. We provide formal details on the average $\int_{\mathcal{H}} d\psi$ in Section V E 1.

B. Unitary error models and conditional fidelity

For simplicity, in the following it is convenient to restrict to ‘unitary’ error models; that is, with $K_{D,k}^\dagger K_{D,k} = p_{D,k} \mathbb{1}$ for $p_{D,k} \geq 0$ and $\sum_k p_{D,k} = 1$. This includes e.g. conventional depolarising error models, as well as dephasing channels. Typically, scaling results which hold in this restricted case also extend to more general settings, including e.g. decay and damping errors; but unitary errors are generally simpler to treat analytically. Moreover, for the neutral atom implementation that we discuss more explicitly, these are the error models of most relevance (see the discussion below). In this assumption, it is also useful to perform a discrete stochastic unraveling of the Kraus map, by defining the conditional normalized states $|\psi_{D,k}\rangle = K_{D,k} |\psi\rangle / \sqrt{p_k}$; then, the map reads

$$\rho_{\text{out}}(\psi|D) = \sum_k p_k |\psi_{D,k}\rangle \langle \psi_{D,k}|, \quad (57)$$

and the query fidelity takes the convenient form

$$\begin{aligned} F_{\text{QRAM}} &= \frac{1}{2^N} \sum_D \int_{\mathcal{H}} d\psi \sum_k p_k F_k(\psi|D) = \\ &= \frac{1}{2^N} \sum_D \sum_k p_{D,k} F_k(D), \end{aligned} \quad (58)$$

with the conditional fidelities

$$F_k(\psi|D) = \sum_{\alpha} |\langle \psi_D, \alpha | \psi_{D,k} \rangle|^2 \quad \text{and} \quad F_k(D) = \int_{\mathcal{H}} d\psi F_k(\psi|D); \quad (59)$$

we recall that here $\{|\alpha\rangle\}$ is an arbitrary basis on the ancillary Hilbert space.

C. Bounding the conditional fidelity

We are first interested in bounding the conditional fidelity

$$F_k(\psi|D) = \sum_{\alpha} |\langle \psi_D, \alpha | \psi_{D,k} \rangle|^2; \quad (60)$$

for simplicity, in this section we will drop any index related to the memory D , and consider both the address ψ and the error configuration k to be fixed.

Analogously to previous work, the key technical point in our error-resilience analysis is the following: for each error configuration k , we define a set of *good addresses* $\mathcal{G}_k \subset \{0, 1\}^{\log N}$; intuitively, this comprises all those (classical) addresses $\mathbf{x} \in \{0, 1\}^{\log N}$, which are queried correctly and *coherently* even under error configuration k . More precisely, \mathcal{G}_k is defined in such a way that if the address only contained components from \mathcal{G} , i.e. if it was of the form $|\psi\rangle = \sum_{\mathbf{x} \in \mathcal{G}_k} \psi_{\mathbf{x}} |\mathbf{x}\rangle$, then K_k would act on it equally (or very similarly) to the ideal query to the QRAM. The formal definition of \mathcal{G}_k is given below.

Set of good addresses: definition. First, let $|A\rangle$ be any generic state in the ancillary Hilbert space \mathcal{H}_A ; that is,

$$|A\rangle = \sum_{\alpha} A_{\alpha} |\alpha\rangle \in \mathcal{H}_A. \quad (61)$$

Now, for each $|A\rangle$ we define the following set of classical indexes:

$$\mathcal{G}_{k,|A\rangle} = \left\{ \mathbf{x} \in \{0, 1\}^{\log N} \text{ such that } K_k |\mathbf{x}\rangle = \sqrt{p_k} |\mathbf{x}\rangle |D_{\mathbf{x}}\rangle |A\rangle \right\}. \quad (62)$$

Finally, we pick the state $|A_k^*\rangle \in \mathcal{H}_A$ which maximises the size of $\mathcal{G}_{k,|A\rangle}$, i.e. such that

$$\left| \mathcal{G}_{k,|A_k^*\rangle} \right| = \max \left\{ \left| \mathcal{G}_{k,|A\rangle} \right| \text{ for } |A\rangle \in \mathcal{H}_A \right\}. \quad (63)$$

We then define $\mathcal{G}_k \equiv \mathcal{G}_{k,|A_k^*\rangle}$. We note that in general there will be several disjoint subsets of addresses which can be queried coherently in superposition; thus, *a priori*, there is no reason as to why $|A_k^*\rangle$, and thus \mathcal{G}_k , should be unique. For the following, in case multiple choices are possible, it is sufficient to choose one, with no consequence on our results.

Generic bound. With this, we straightforwardly get the following form for the conditional state:

$$|\psi_k\rangle = \frac{1}{\sqrt{p_k}} \left[\sqrt{p_k} \left(\sum_{\mathbf{x} \in \mathcal{G}_k} \psi_{\mathbf{x}} |\mathbf{x}\rangle |D_{\mathbf{x}}\rangle \right) |A_k\rangle + \sum_{\mathbf{x} \notin \mathcal{G}_k} \psi_{\mathbf{x}} K_k |\mathbf{x}\rangle \right], \quad (64)$$

which allows us to separate the portion which is queried coherently from the faulty one. We can now choose a basis $\{|\alpha\rangle\}$ such that $|A_k\rangle \in \{|\alpha\rangle\}$; it follows that

$$\begin{aligned} F_k(\psi|D) &= \sum_{\alpha} |\langle \psi_D, \alpha | \psi_k \rangle|^2 \geq \\ &\geq |\langle \psi_D, A_k | \psi_k \rangle|^2 = \\ &= \frac{1}{p_k} \left| \sqrt{p_k} \sum_{\mathbf{x} \in \mathcal{G}_k} |\psi_{\mathbf{x}}|^2 + \langle \psi_D, A_k | \sum_{\mathbf{x} \notin \mathcal{G}_k} \psi_{\mathbf{x}} K_k |\mathbf{x}\rangle \right|^2, \end{aligned} \quad (65)$$

where we simply used the positivity of the terms in the sum.

We are now clearly interested in bounding the portion of the wavefunction which is not queried correctly; in Section V E 2, we use simple linear algebra to show that the following bound always holds

$$\left| \langle \psi_D, A_k | \sum_{\mathbf{x} \notin \mathcal{G}_k} \psi_{\mathbf{x}} K_k |\mathbf{x}\rangle \right| \leq \sqrt{p_k} \left[1 - \sum_{\mathbf{x} \in \mathcal{G}_k} |\psi_{\mathbf{x}}|^2 \right]. \quad (66)$$

Using this, we are now ready to bound the conditional query fidelity: combining the bound above with standard inequalities, in Section V E 3 we show that

$$F_k(\psi|D) \geq \left[2 \sum_{\mathbf{x} \in \mathcal{G}_k} |\psi_{\mathbf{x}}|^2 - 1 \right]^2 \Theta \left(\sum_{\mathbf{x} \in \mathcal{G}_k} |\psi_{\mathbf{x}}|^2 - \frac{1}{2} \right). \quad (67)$$

Importantly, note that this bound is only nontrivial when at least one half of the address wavefunction is queried coherently, as highlighted by the Heaviside step function.

We are now interested in performing the averages over the error configurations k , the memory configurations D , and the state ψ . We start from the latter, i.e., from the conditional fidelity

$$F_k(D) = \int_{\mathcal{H}} d\psi F_k(\psi|D). \quad (68)$$

In principle, with the methods developed in the mathematical inserts, we can perform exactly the integration over the right-hand side of the bound given so far. However, more conveniently, we can use the well known variance inequality,

$$\int_{\mathcal{H}} d\psi f^2(\psi) \geq \left(\int_{\mathcal{H}} d\psi f(\psi) \right)^2 \quad (69)$$

to further bound $F_k(D)$. Specifically, also using the fact that the Heaviside function is idempotent, i.e. $\Theta^2(x) = \Theta(x)$, we get the inequality

$$F_k(D) \geq 4 \left[\int_{\mathcal{H}} d\psi \left(\sum_{\mathbf{x} \in \mathcal{G}_k} |\psi_{\mathbf{x}}|^2 - \frac{1}{2} \right) \Theta \left(\sum_{\mathbf{x} \in \mathcal{G}_k} |\psi_{\mathbf{x}}|^2 - \frac{1}{2} \right) \right]^2. \quad (70)$$

Evaluating this is rather technical. With the methods in Sections V E 4, V E 5 and V E 6 we calculate that

$$\int_{\mathcal{H}} d\psi \left(\sum_{\mathbf{x} \in \mathcal{G}_k} |\psi_{\mathbf{x}}|^2 - \frac{1}{2} \right) \Theta \left(\sum_{\mathbf{x} \in \mathcal{G}_k} |\psi_{\mathbf{x}}|^2 - \frac{1}{2} \right) \geq \frac{|\mathcal{G}_k|}{N} - \frac{1}{2}; \quad (71)$$

we note that this bound can be improved by adding a Heaviside function, as one can easily see that the integral must always be positive; however, for our purposes this will be sufficient.

D. Error models

Here, we discuss the details of the various Kraus maps

$$\rho_D(\psi) = \sum_k K_{D,j} |\psi\rangle \langle \psi| K_{D,j}^\dagger \quad (72)$$

that we consider in this work. We also provide heuristic justifications of the observed numerical results.

1. Continuous depolarisation errors

The first error model assumes that all qubits continuously undergo a depolarization channel. This type of error affects *all* the qubits on the platform, regardless on whether they undergo any operation, or they are just idly waiting to be utilized. Specifically, at any time step, each single qubit has a probability ϵ to completely depolarize - i.e., to be substituted with the completely mixed state $\mathbb{1}/2$. This is equivalent to the fact that at any time step, each qubit undergoes (independently) a random Pauli error with probability $3\epsilon/4$, drawn uniformly from the set $\{X, Y, Z\}$. The update rule of the CD model thus reads, for the single qubit,

$$\mathcal{E}(\rho) = \left(1 - \frac{3\epsilon}{4} \right) \rho + \frac{\epsilon}{4} \left(X\rho X + Y\rho Y + Z\rho Z \right). \quad (73)$$

2. Operational Pauli errors

We note that typically current QC platforms are much more prone to errors during gates, then to decoherence of idle qubits. That is, the gate infidelity is much larger than the typical decoherence rate. This is for instance the case of neutral atoms, where typical decoherence times are of order $T_1 =$ and $T_2 =$, while the gate error rates are in the range of $\epsilon \sim$ for typical gate durations of order $\tau_g \simeq 100\text{ns}$. To model this, after any two-qubit gate we insert a depolarization channel affecting the qubits involved in the gate. In other words, we substitute the application of an ideal two-qubit gate U with the map

$$\mathcal{E}_U(\rho) = \left[\mathcal{E} \otimes \mathcal{E} \right] \left(U\rho U^\dagger \right), \quad (74)$$

where the single-qubit depolarization map is defined as above.

3. Operational phase-biased errors and erasure-conversion in neutral atom platforms

The error maps above assume that Pauli errors are essentially equiprobable; in other words, this can be understood as the environment ‘monitoring’ each physical qubit in completely random, unknown bases. For specific systems, one type of error can be much more likely than the others, thereby introducing a strong bias in the error model. An extreme scenario is for instance when only Z errors occur, resulting in a dephasing map of the type

$$\mathcal{E}_{\text{deph}}(\rho) = (1 - \epsilon)\rho + \epsilon Z\rho Z, \quad (75)$$

where only Z errors are considered. Similarly to the OP error model above, for reasons that we explain below, also here we only insert this error map after a qubit has undergone a gate.

In our work, this map is strongly motivated by recent demonstrations of erasure conversion in neutral atoms, which result in an effective error map of this form. More precisely, in these platforms two-qubit gates are performed via the excitation of the atoms to highly excited Rydberg levels. One of the most important sources of errors during these gates are e.g. decays from the Rydberg state to lower lying levels. With recently developed techniques, these decays can be detected, indicating the presence of an error. Importantly, in the paradigmatic two-qubit gate schemes, excitation to the Rydberg level only occurs from one of the two computational basis states (e.g., the $|1\rangle$ state), implying that detecting one such error also reveals the original state of the qubit. This allows to reset the qubit to this computational basis state (that is, to $|1\rangle$ in this case), only leaving a potential phase error. To all effects, this can be described as a strongly Z biased error model, where errors during the two-qubit gates are erasure-converted to phase errors.

E. Mathematical details

Below, we collect the mathematical methods used to prove the bounds above.

1. Uniform distribution over the Hilbert space

Here, we elaborate on the mathematical details concerning the uniform distribution over the (normalized states of the) Hilbert space.

Defining the distribution. Conceptually, $\int_{\mathcal{H}} d\psi f(\psi)$ represents an integral over the uniform distribution of normalized states in the Hilbert space \mathcal{H} , normalized such that $\int_{\mathcal{H}} d\psi = 1$. To be more precise at the mathematical level, we find it useful to parameterize the wavefunction as

$$\psi_{\mathbf{x}} = e^{i\phi_j} \sqrt{z_j} \quad \text{for } j = 1, \dots, N \quad (76)$$

with $\phi_j \in [0, 2\pi]$ and $z_j \in [0, +\infty]$ in general. The relation between \mathbf{x} and the index j can be e.g. simply $j = \mu(\mathbf{x})$. Then, the average of any function $f : \mathcal{H} \rightarrow \mathbb{R}$ takes the form

$$\int_{\mathcal{H}} d\psi f(\psi) = \frac{(N-1)!}{(2\pi)^N} \int_{[0, 2\pi]^N} d^N \phi \int_{[0, +\infty]^N} d^N z \delta(1 - |\mathbf{z}|_1) f(\phi_1, \dots, \phi_N; z_1, \dots, z_N), \quad (77)$$

where $\delta(x)$ is the conventional Dirac delta distribution, and $|\mathbf{z}|_1 = \sum_i |z_i|$ is the l^1 norm. Note that, correctly, this is only meaningful for $N \geq 2$; indeed, if we had $N = 1$, then the only one amplitude would be necessarily set to 1 by the normalization requirement.

In the following, it will be useful to factorize the distribution, separating the phase and squared-amplitude components, as

$$d\psi = (2\pi)^{-N} p(z_1, \dots, z_N) d^N \phi d^N z, \quad (78)$$

with $p(z_1, \dots, z_N) = (N-1)! \delta(1 - |\mathbf{z}|_1)$ being the distribution over the amplitudes.

Intermediate calculation. For the sake of completeness, it is instructive to study the normalization of this distribution, which highlights how the counting factor $(N-1)!$ emerges naturally. To this end, we first introduce the following intermediate result, which will be of great usefulness also later on:

$$f_n(x) = \int_0^{1-x} dz_1 \int_0^{1-(x+z_1)} dz_2 \int_0^{1-(x+z_1+z_2)} dz_3 \cdots \int_0^{1-(x+z_1+\dots+z_{n-1})} dz_n = \frac{(1-x)^n}{n!}. \quad (79)$$

This can be proved straightforwardly by induction. Indeed, one can easily certify that the claimed equality holds true e.g. for $n = 1$ and $n = 2$. Next, for the inductive step, we can write

$$\begin{aligned}
f_{n+1}(x) &= \int_0^{1-x} dz_1 \int_0^{1-(x+z_1)} dz_2 \int_0^{1-(x+z_1+z_2)} dz_3 \cdots \int_0^{1-(x+z_1+\cdots+z_{n-1})} dz_n \int_0^{1-(x+z_1+\cdots+z_n)} dz_{n+1} = \\
&= \int_0^{1-x} dz_1 f_n(x+z_1) = \\
&\stackrel{(*)}{=} \frac{1}{n!} \int_0^{1-x} dz_1 (1-x-z_1)^n = \frac{(1-x)^{n+1}}{(n+1)!}; \tag{80}
\end{aligned}$$

in this chain of equalities, we used the inductive hypothesis for step (*).

Consistency check: normalization. We can now check the correctness of our normalization by evaluating the integral for the constant function $f(\psi) = 1$; using the intermediate result above, we obtain indeed

$$\begin{aligned}
\int_{\mathcal{H}} d\psi &= \frac{(N-1)!}{(2\pi)^N} \int_{[0,2\pi]^N} d^N \phi \int_{[0,+\infty]^N} d^N z \delta(1-|z|_1) = \\
&= (N-1)! \int_{[0,+\infty]^N} d^N z \delta(1-|z|_1) = \\
&= (N-1)! \int_0^1 dz_1 \cdots \int_0^1 dz_N \delta(1-(z_1+\cdots+z_N)) = \\
&\stackrel{(*)}{=} (N-1)! \int_0^1 dz_1 \cdots \int_0^1 dz_{N-1} \Theta(1-(z_1+\cdots+z_{N-1})) = \\
&= (N-1)! \int_0^1 dz_1 \int_0^{1-z_1} dz_2 \int_0^{1-(z_1+z_2)} dz_3 \cdots \int_0^{1-(z_1+\cdots+z_{N-2})} dz_{N-1} = \\
&= (N-1)! f_{N-1}(0) = (N-1)! \frac{1}{(N-1)!} = 1. \tag{81}
\end{aligned}$$

In this chain of equalities, the crucial step is (*), where we used the Dirac delta to write $z_N = 1 - (z_1 + \cdots + z_{N-1})$, and inserted the Heaviside function to ensure that with this substitution the condition $z_N \geq 0$ is preserved.

2. Bounding the erroneously queried portion of the wavefunction

Here, we prove the bound in Eq. (66). This is obtained straightforwardly from the following:

$$\begin{aligned}
\left| \langle \psi_D, A_k | \sum_{\mathbf{x} \notin \mathcal{G}_k} \psi_{\mathbf{x}} K_k | \mathbf{x} \rangle \right| &= \left| \sum_{\mathbf{y} \in \mathcal{G}_k} \sum_{\mathbf{x} \notin \mathcal{G}_k} \psi_{\mathbf{y}}^* \psi_{\mathbf{x}} \langle \mathbf{y}, D_{\mathbf{y}}, A_k | K_k | \mathbf{x} \rangle + \left[\sum_{\mathbf{y} \notin \mathcal{G}_k} \psi_{\mathbf{y}}^* \langle \mathbf{y}, D_{\mathbf{y}}, A_k | \right] \left[\sum_{\mathbf{x} \notin \mathcal{G}_k} \psi_{\mathbf{x}} K_k | \mathbf{x} \rangle \right] \right| = \\
&= \left| \sqrt{p_k} \sum_{\mathbf{y} \in \mathcal{G}_k} \sum_{\mathbf{x} \notin \mathcal{G}_k} \psi_{\mathbf{y}}^* \psi_{\mathbf{x}} \langle \mathbf{y} | K_k^\dagger K_k | \mathbf{x} \rangle + \left[\sum_{\mathbf{y} \notin \mathcal{G}_k} \psi_{\mathbf{y}}^* \langle \mathbf{y}, D_{\mathbf{y}}, A_k | \right] \left[\sum_{\mathbf{x} \notin \mathcal{G}_k} \psi_{\mathbf{x}} K_k | \mathbf{x} \rangle \right] \right| = \\
&= \left| \left[\sum_{\mathbf{y} \notin \mathcal{G}_k} \psi_{\mathbf{y}}^* \langle \mathbf{y}, D_{\mathbf{y}}, A_k | \right] \left[\sum_{\mathbf{x} \notin \mathcal{G}_k} \psi_{\mathbf{x}} K_k | \mathbf{x} \rangle \right] \right| \leq \\
&\stackrel{(*)}{\leq} \sqrt{\sum_{\mathbf{y} \notin \mathcal{G}_k} |\psi_{\mathbf{y}}|^2} \sqrt{p_k \sum_{\mathbf{x} \notin \mathcal{G}_k} |\psi_{\mathbf{x}}|^2} = \sqrt{p_k} \left[1 - \sum_{\mathbf{x} \in \mathcal{G}_k} |\psi_{\mathbf{x}}|^2 \right]. \tag{82}
\end{aligned}$$

In step (*), we simply used the conventional Schwartz inequality.

3. Bounding the conditional query fidelity

Here, we prove our bound to the conditional query fidelity given in Eq. (67). This is based on the following chain of inequalities:

$$\begin{aligned}
F_k(\psi|D) &= \frac{1}{p_k} \left| \sqrt{p_k} \sum_{\mathbf{x} \in \mathcal{G}_k} |\psi_{\mathbf{x}}|^2 + \langle \psi_D, A_k | \sum_{\mathbf{x} \notin \mathcal{G}_k} \psi_{\mathbf{x}} K_k | \mathbf{x} \rangle \right|^2 \geq \\
&\stackrel{(*)}{\geq} \frac{1}{p_k} \left[\sqrt{p_k} \sum_{\mathbf{x} \in \mathcal{G}_k} |\psi_{\mathbf{x}}|^2 - \left| \langle \psi_D, A_k | \sum_{\mathbf{x} \notin \mathcal{G}_k} \psi_{\mathbf{x}} K_k | \mathbf{x} \rangle \right| \right]^2 \geq \\
&\stackrel{(**)}{\geq} \frac{1}{p_k} \left[\sqrt{p_k} \sum_{\mathbf{x} \in \mathcal{G}_k} |\psi_{\mathbf{x}}|^2 - \sqrt{p_k} \left[1 - \sum_{\mathbf{x} \in \mathcal{G}_k} |\psi_{\mathbf{x}}|^2 \right] \right]^2 \Theta \left(\sum_{\mathbf{x} \in \mathcal{G}_k} |\psi_{\mathbf{x}}|^2 - \frac{1}{2} \right) = \\
&= \left[2 \sum_{\mathbf{x} \in \mathcal{G}_k} |\psi_{\mathbf{x}}|^2 - 1 \right]^2 \Theta \left(\sum_{\mathbf{x} \in \mathcal{G}_k} |\psi_{\mathbf{x}}|^2 - \frac{1}{2} \right). \tag{83}
\end{aligned}$$

We now analyze the two crucial steps (*) and (**) one by one.

- **Step (*)**

For this, we simply used the trivial fact that (if $a \in \mathbb{R}$ and $b \in \mathbb{C}$), it is always true that $|a + b|^2 \geq (a - |b|)^2$. The inequality follows from defining $a = \sum_{\mathbf{x} \in \mathcal{G}_k} |\psi_{\mathbf{x}}|^2$ and $b = \langle \psi_D, A_k | \sum_{\mathbf{x} \notin \mathcal{G}_k} \psi_{\mathbf{x}} K_k | \mathbf{x} \rangle / \sqrt{p_k}$.

- **Step (**)**

For this, more care is necessary. For concreteness, let $\lambda = 1 - \sum_{\mathbf{x} \in \mathcal{G}_k} |\psi_{\mathbf{x}}|^2 = 1 - a$; we are interested in lower bounding the quantity $(a - |b|)^2$, by exploiting the fact that $|b| \leq \lambda \leq 1$. In this setting, a meaningful bound can be given as $(a - |b|)^2 \geq (a - \lambda)^2$; importantly, for $\lambda = 1 - a$ as here, this only holds when either $a \geq 1/3$. Indeed, let $f(|b|) = (a - |b|)^2 - (a - \lambda)^2$. Then, it is easy to see that $f(|b|) \geq 0$ if either $|b| \leq a - |a - \lambda|$, or $|b| \geq a + |a - \lambda|$; however, since $a + |a - \lambda| \geq \lambda$, we can already eliminate this option. To further evaluate, let us consider the two cases $a \geq \lambda$ and $a \leq 1/2$ separately. (i) If $a \geq \lambda$, $|b| \leq a - |a - \lambda| = \lambda$, thus we get $f(|b|) \geq 0$ straightforwardly. (ii) If else $a \leq \lambda$, we obtain $|b| \leq 2a - \lambda$; however, since in this case $2a - \lambda \leq \lambda$, this is not guaranteed by our hypothesis $|b| \leq \lambda$. In summary, from $\lambda = 1 - a \geq |b|$, we get $f(|b|) \geq 0$ whenever $a \geq 1/2$. We thus use the Heaviside function to specify that $(a - |b|)^2 \geq (2a - 1)$ if $a \geq 1/2$, and just $a - |b|^2 \geq 0$ otherwise.

4. Statistics of the first n amplitudes

Here, we are interested in the following problem: for $n \leq N$, what is the statistics of the first n squared amplitudes (z_1, \dots, z_n) of a randomly chosen state $|\psi\rangle \in \mathcal{H}$ in the Hilbert space? Note that only for simplicity here we consider ‘the first’ n squared amplitudes, but (since $|\psi\rangle$ is chosen randomly with uniform distribution) the problem is of course invariant on which n squared amplitudes we actually consider. In summary, we are interested in calculating the marginal probability distribution

$$\begin{aligned}
p(z_1, z_2, \dots, z_n) &= \frac{1}{(2\pi)^N} \int_{[0, 2\pi]^N} d^N \phi \int_{[0, +\infty]^{N-n}} dz_{n+1} dz_{n+2} \dots dz_N p(z_1, \dots, z_N) = \\
&= (N-1)! \int_0^1 dz_{n+1} \dots \int_0^1 dz_N \delta(1 - |z|_1), \tag{84}
\end{aligned}$$

where for the last line we simply evaluated the integral over the phases and wrote $p(z_1, \dots, z_N)$ explicitly. To calculate this marginal distribution, it is convenient to immediately introduce $s = z_1 + \dots + z_n$, which is the only term including

the non-mute variables appearing in the integrand; we then evaluate the integral as

$$\begin{aligned}
p(z_1, \dots, z_n) &= (N-1)! \Theta(1-s) \int_0^{1-s} dz_{n+1} \int_0^{1-(s+z_{n+1})} dz_{n+2} \cdots \int_0^{1-(s+z_{n+1}+\dots+z_{N-2})} dz_{N-1} = \\
&= (N-1)! f_{N-n-1}(s) = \\
&= \frac{(N-1)!}{(N-n-1)!} \Theta(1-s)(1-s)^{N-n-1} = n! \binom{N-1}{n} \Theta(1-s)(1-s)^{N-n-1}, \tag{85}
\end{aligned}$$

yielding the marginal distribution

$$p(z_1, \dots, z_n) = n! \binom{N-1}{n} \Theta(1-s)(1-s)^{N-n-1}. \tag{86}$$

To understand this formula, note that it is only meaningful when $N \geq 2$ and $N \geq n \geq 1$. Indeed, for $N = 1$ the only squared amplitude would be deterministically set to $z = 1$ by the normalization requirement. Moreover, one can straightforwardly check that the limit case $n = N$ provides the correct result. It is also instructive to consider e.g. $n = 1$, corresponding to the marginal distribution of one single squared amplitude z_i , for which we get

$$p(z_i) = (N-1) \Theta(1-z_i)(1-z_i)^{N-2}, \tag{87}$$

which again stresses that $N \geq 2$. This allows for instance to calculate the momenta

$$\begin{aligned}
\langle z_i^m \rangle &= \int dz_i p(z_i) z_i^m = \\
&= (N-1) \int_0^1 dz (1-z)^{N-2} z^m = \\
&= (N-1) \mathcal{B}(m+1, N-1) = \\
&= (N-1) \frac{m!(N-2)}{(N+m-1)!} = \frac{1}{\binom{N+m-1}{m}}, \tag{88}
\end{aligned}$$

where we inserted the well-known Beta function

$$\mathcal{B}(a, b) = \int_0^1 dx x^{a-1} (1-x)^{b-1} \tag{89}$$

and we used the fact that when (a, b) are positive integers, one has

$$\mathcal{B}(a, b) = \frac{(a-1)!(b-1)!}{(a+b-1)!}. \tag{90}$$

To check correctness, we note that the first moment reads $\langle z_i \rangle = 1/N$, as one could already infer from the beginning. Moreover, the variance of z_i reads $\langle z_i^2 \rangle = 2/N(N+1)$.

5. Distribution of the overlap

Let \mathbb{P} be a projector onto a subspace of \mathcal{H} of dimension $n \leq N$; that is, \mathbb{P} is hermitian ($\mathbb{P} = \mathbb{P}^\dagger$) and idempotent ($\mathbb{P} = \mathbb{P}^2$), and has trace $\text{Tr}(\mathbb{P}) = n$. The overlap of an arbitrary state $|\psi\rangle \in \mathcal{H}$ with the space identified by \mathbb{P} is given by $\langle \psi | \mathbb{P} | \psi \rangle$. Here, we treat this overlap as a statistical variable, and we are therefore interested in evaluating its momenta

$$\left\langle \langle \psi | \mathbb{P} | \psi \rangle^m \right\rangle = \int_{\mathcal{H}} d\psi \langle \psi | \mathbb{P} | \psi \rangle^m. \tag{91}$$

We can start by choosing a basis on \mathcal{H} such that the subspace defined by \mathbb{P} is spanned by the first n terms, i.e.

$$\mathbb{P} = \sum_{i=1}^n |i\rangle \langle i|. \tag{92}$$

Then, we get

$$\langle \psi | \mathbb{P} | \psi \rangle = \sum_{i=1}^n |\langle i | \psi \rangle|^2 = \sum_{i=1}^n z_i \equiv s(z_1, \dots, z_n), \quad (93)$$

where the coordinates $z_i \geq 0$ are defined as previously explained. In the following, we will drop the dependence of $s = \langle \psi | \mathbb{P} | \psi \rangle$ on \mathbf{z} whenever it is not necessary. With this redefinition, it is straightforward to see that

$$\langle \langle \psi | \mathbb{P} | \psi \rangle^m \rangle = \int_0^1 ds P(s) s^m, \quad (94)$$

where $P(s)$ is the marginal distribution of the overlap, defined as

$$\begin{aligned} P(s) &= (N-1)! \int_0^1 dz_1 \cdots \int_0^1 dz_n \delta(s - (z_1 + \cdots + z_n)) \int_0^1 dz_{n+1} \cdots \int_0^1 dz_N \delta(1 - |z|_1) = \\ &= n! \binom{N-1}{n} \Theta(1-s) (1-s)^{N-n-1} \int_{[0,+\infty]^n} dz_1 \cdots dz_n \delta(s - (z_1 + \cdots + z_n)) = \\ &= n \binom{N-1}{n} \Theta(1-s) (1-s)^{N-n-1} s^{n-1}. \end{aligned} \quad (95)$$

We now use this to evaluate the momenta:

$$\begin{aligned} \langle s^m \rangle &= \int_0^{+\infty} P(s) s^m = \\ &= n \binom{N-1}{n} \mathcal{B}(n+m, N-n) = \frac{\binom{n+m-1}{m}}{\binom{N+m-1}{m}}. \end{aligned} \quad (96)$$

For instance, we note that, correctly, for $m = 1$ we get $\langle s \rangle = n/N$, as could be deduced from the beginning. In general, we remark that the relation

$$\langle s^m \rangle = \binom{n+m-1}{m} \langle z_i^m \rangle \quad (97)$$

holds between the momenta of one single squared amplitude, and the sum of n of them.

6. Calculating some nontrivial averages

We are now interested in evaluating averages of the following form:

$$J_m(\lambda) = \int_{\mathcal{H}} d\psi \Theta(\langle \psi | \mathbb{P} | \psi \rangle - \lambda) \langle \psi | \mathbb{P} | \psi \rangle^m, \quad (98)$$

where again \mathbb{P} is a projector onto a subspace of \mathcal{H} of dimension $n \leq N$; that is, \mathbb{P} is hermitian ($\mathbb{P} = \mathbb{P}^\dagger$) and idempotent ($\mathbb{P} = \mathbb{P}^2$), and has trace $\text{Tr}(\mathbb{P}) = n$. By simple considerations, it is straightforward to see that this can only depend on n and m and N . As above, we start by choosing a basis on \mathcal{H} such that the subspace defined by \mathbb{P} is spanned by the first n terms, i.e. $\mathbb{P} = \sum_{i=1}^n |i\rangle \langle i|$; then, we get

$$\langle \psi | \mathbb{P} | \psi \rangle = \sum_{i=1}^n |\langle i | \psi \rangle|^2 = \sum_{i=1}^n z_i \equiv s(z_1, \dots, z_n), \quad (99)$$

where the coordinates $z_i \geq 0$ are defined as previously explained. In the following, we will drop the dependence of s on \mathbf{z} whenever it is not necessary. With this redefinition, it is straightforward to see that

$$J_m(\lambda) = \int_0^1 ds P(s) \Theta(s - \lambda) s^m, \quad (100)$$

where we used the probability distribution over s calculated previously. For obvious reasons, we only consider $\lambda \leq 1$; then, using the fact that $\Theta(x) = 1 - \Theta(-x)$, it is convenient to rewrite the integral above as

$$\begin{aligned}
J_m(\lambda) &= \int_0^1 ds P(s) s^m - \int_0^1 ds P(s) \Theta(\lambda - s) s^m = \\
&= \langle s^m \rangle - n \binom{N-1}{n} \int_0^\lambda (1-s)^{N-n-1} s^{n+m-1} = \\
&= \langle s^m \rangle - n \binom{N-1}{n} \mathcal{B}(\lambda; n+m, N-n),
\end{aligned} \tag{101}$$

where we introduced the well-known incomplete Beta function $\mathcal{B}(\lambda; a, b) = \int_0^\lambda dx x^{a-1} (1-x)^{b-1}$.